Aus der

Universitätsklinik für Radioonkolgie mit Poliklinik Tübingen

Sektion Biomedizinische Physik

Automatic radiotherapy treatment planning using Particle Swarm Optimization

Inaugural-Dissertation
zur Erlangung des Doktorgrades
der Humanwissenschaften

der Medizinischen Fakultät
der Eberhard Karls Universität
zu Tübingen

vorgelegt von

Künzel, Luise Anna

2021

Dekan:	Prof. Dr. B. Pichler
1. Berichterstatterin:	Professorin Dr. D. Thorwarth
2. Berichterstatter:	Professor Dr. T. Schäffer
Tag der Disputation	12.05.2021

Contents

Figures

Tables

Abbreviations

3D-CRT	3D-conformal radiotherapy
CT	computed tomography
dMLC	dynamic multileaf collimators
DTH	distance to target histogram
DVH	dose-volume-histogram
EUD	equivalent uniform dose
FFF	flattening filter free
GA	genetic algorithm
gEUD	generalized equivalent uniform dose
GI	gastrointestinal
GPU	graphics processing unit
HDR	high dose rate
ICRU	International Commission on Radiation Units
IGRT	image guided radiotherapy
IMRT	intensity modulated radiotherapy
LINAC	linear accelerator
LRPM	lexicographic reference point method
MCO	multicriteria optimization
MLC	multileaf collimator
MRT	magnetic resonance tomography
MU	monitor unit

NTCP	normal tissue complication probability
OAR	organ at risk
PET	positron emission tomography
PSO	particle swarm optimization
PTV	planning target volume
PQS	plan quality score
QUANTEC	Quantitative Analyses of Normal Tissue Effects in the Clinic
ROI	region of interest
RT	radiotherapy
SBRT	stereotactic body radiotherapy
SOP	standard operating procedure
TCP	tumor control probability
TPS	treatment planning system
VMAT	volumetric modulated arc therapy

1 Introduction

Radiotherapy (RT) is an established treatment option for cancer patients, along with chemotherapy and surgery. The aim of RT is to apply a sufficiently high radiation dose to the tumor to kill the cancerogenous cells, while at the same time minimizing the dose burden to the surrounding healthy tissues to preserve their function. Therefore RT offers different forms of treatments such as brachytherapy, where tiny radioactive sources are brought close to the tumor, and external beam RT (teletherapy), where patients are treated with high-energy X-rays (photons), electrons or protons. All these treatments need to be planned on a patient individual basis to ensure that the tumor is irradiated with the prescribed dose, while surrounding healthy tissues are protected from the dose burden. The focus of this work is on external beam RT with high-energy photons, which is for simplicity denoted as RT hereafter.

Patient individual planning in RT is needed due to different anatomies and because modern RT treatment machines offer different options to apply radiation dose. During the planning process the treatment angles, field shapes and field intensities need to be defined. To ensure that a sufficiently high radiation dose is delivered to the tumor and that other structures are spared from the dose burden as much as possible, all these opportunities need to be taken into account when generating patient individual treatment plans. Hence, different treatment options need to be simulated. However time constraints and the experience of the planner may impact the quality of the plan. Finding a balance between the dose administered to the tumor and the dose burden to surrounding tissues is challenging and therefore attention to automatic planning has increased in recent years [1–7].

In this introduction, the current status of RT treatment planning is briefly described, followed by a description of constrained optimization and several so far introduced automatic planning approaches. Then the idea of using particle swarm optimization (PSO) as an automatic RT treatment planning approach is introduced. In the main part of this thesis the implementation of such an approach is described in detail, the quality of the implementation is analyzed and the applicability is shown

for post-operative prostate cancer treatments.

1.1 Radiotherapy treatment planning - an optimization problem

Since the late 1980s, the basis of 3D treatment planning has always been a CT scan, which represents the patient individual anatomy as a 3D density distribution [8]. The physician delineates the region of interest (ROI), i.e. organ at risk (OAR) and tumor on this planning CT scan, see figure 1. In addition to previous diagnostic scans, a planning CT needs to be acquired by standardized protocols. First of all, the patient is immobilized on a flat table top, which is identical to the treatment table at the RT treatment unit (LINAC). Several positioning aids, as can be seen in figure 2, are used to support and enable the patient to hold the treatment position for several minutes. This is important as the patient needs to take exactly the same position for every following treatment fraction. Standardized scanning protocols are also needed to ensure the correct conversion from CT Hounsfield Units to electron densities. The different electron densities of bony structures and soft tissues are later needed to accurately calculate the deposited dose during the planning process. To facilitate the delineation of the structures, other imaging modalities are also used. These includes magnetic resonance tomography (MRT), which is used due to the improved soft tissue contrast compared to CT, and positron emission tomography (PET), which provides additional metabolic information. All additional image information needs to be fused to the CT scan, to ensure that the spatial information matches. Additional planning scans should be preferably acquired in treatment position to facilitate the fusing of different image series.

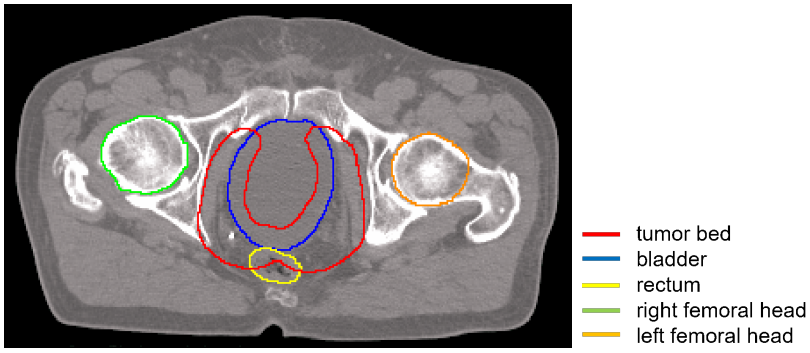

Figure 1: Planning CT scan of a prostate cancer patient in supine position with contoured structures: tumor bed, rectum, bladder and femoral heads.

Figure 2: Medical LINAC with positioning aids on the treatment table which are typically used to comfort a prostate patient in supine position, 1 pillow to rest the head, supportive aid for the knees and 3 fixation to rest the feet.

After delineation, the beam field shapes and intensities need to be defined. In 3D-CRT, the treatment fields are shaped to the outline of the tumor projection. Apertures, wedges and compensators are used to shape the fields and intensity profiles. However, 3D-CRT is unable to account for complex arrangements of target and OAR structures, such as a tumor bending around the spine. The high dose region cannot be conformed precisely to the target outline, see figure 3 a), hence surrounding healthy tissue cannot be properly shielded from dose burden.
In 1988, Brahme pioneered the idea of inverse planning [9], which derives the initial beam profile intensities from the desired dose distribution. This was the theoretical beginning of modern intensity modulated radiotherapy (IMRT) treatments. Nevertheless, in the following years several optimization approaches and technical developments were needed to bring IMRT into clinical practice.
The modulation of a radiation field is reached by the superposition of different segments which are formed by the MLC as is sketched in figure 4. By combining radiation fields from several beam directions, complex and highly conformal dose distributions can be achieved, c.f. figure 3 b). In step and shoot IMRT the first segment is shaped by the multileaf collimator (MLC), then appropriate radiation is applied and after radiation is off, the leafs of the MLC move to form the next segment. During gantry rotation to the next beam direction, the radiation is also turned off. Depending on the total number of segments, treatment time is up to several minutes. The next technical invention is IMRT delivery with dynamic multileaf collimators (dMLC), where the MLC leafs move with varying velocity from one field edge to the opposite while radiation is on. Thereby the intensity is modulated by sliding the leafs through the radiation field. Only during gantry rotation the beam is

turned off. The next step is to leave the beam also on during gantry rotation, which is denoted as volumetric modulated arc therapy (VMAT). Hence VMAT treatments are not restricted to defined beam angles, but make use of the entire 360° of a circle.

a) 3D-CRT **b)** VMAT

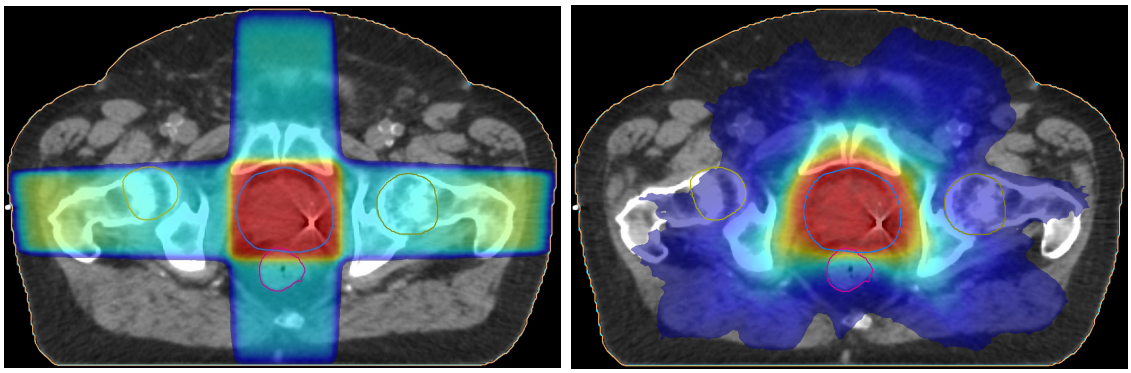

Figure 3: Comparison of 3D-dose distributions for 3D-conformal radiotherapy (3D-CRT) and volumetric modulated arc therapy (VMAT) prostate treatments. In 3D-CRT, fixed beam angles are used and the field is shaped to the projection of the tumor outline, but the intensity in the field is not modulated. In this example, 4 beam angles from 0°, 90°, 180° and 270° result in a rectangular shape the high-dose region (red) around the round prostate (blue line). In contrast, a VMAT treatment uses all beam angles of the 360° circle and modulated intensities and therefore offers better conformance to the shape of the tumor. Nevertheless, the entire surrounding tissue is exposed to low doses (blue), whereas in 3D-CRT less healthy tissue is exposed.

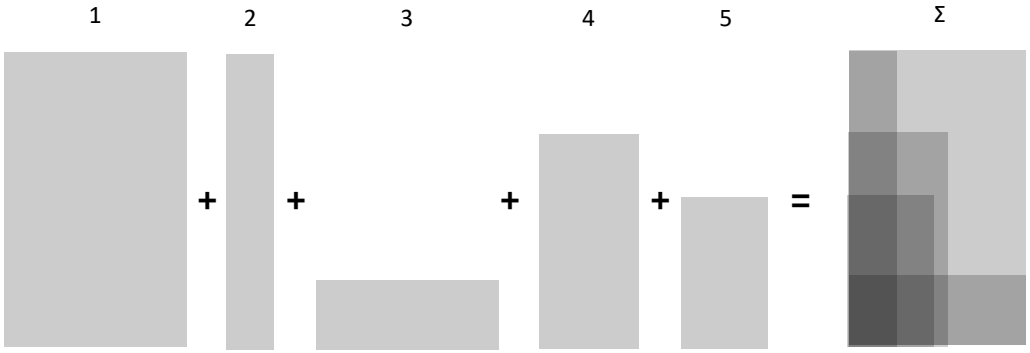

Figure 4: IMRT principle: Intensity modulation reached by the superposition of 5 differently shaped, non-modulated segments.

Considering this technical improvement and also other inventions, such as flattening filter free (FFF) beams, which allow for higher dose rates, the modulation of the dose rate (MU per min), and the integration of imaging modalities such as MRT and PET modern external beam radiotherapy with a state-of the art high-precision

LINAC is able to cover an enormous amount of degrees of freedom. Consequently, highly individualized treatments can be offered to the patients. However, the high amount of steering parameters make treatment planning more complex and challenging. To make use of these opportunities, treatment planning has shifted from forward planning to inverse planning, which means that the desired radiation dose for PTV and maximum tolerated doses for healthy tissues are defined in the form of objectives and constraints and the treatment planning system (TPS) optimizes the needed machine parameters to apply this dose.
In figure 5, some technical steering parameters in addition to the dose objectives and constraints are depicted as a spider net. The figure illustrates that as the net becomes more branched, it also becomes more complicated to predict what will happen if one bifurcation is shifted. Therefore modern RT treatment planning needs to be seen as an optimization problem. We hypothesize that the solution of this optimization problem can be found by applying inverse planning algorithms, producing the appropriate controls for the LINAC. While the solution of the optimization problem may be considered as trivial, the formulation is definitely not. Currently this is typically a time consuming trial and error process, where the planner tries out different combinations of objectives and constraints, i.e. formulations of the patient individual treatment planning problem, until a satisfying treatment plan is founded. Nevertheless, this process is restricted by the time available until a treatment plan needs to be ready and by the planner's experience.

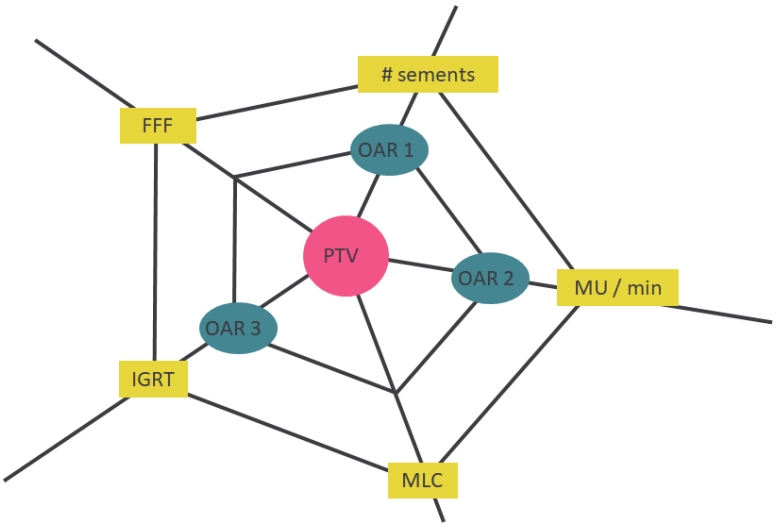

Figure 5: Modern RT treatment planning is an optimization problem with an enormous amount of degrees of freedom. The technical options influence the dose to the PTV and OARs, making the definition of the objectives and constraints crucial for the inverse planning. This system is like a spider web, it will collapse if one cord is pulled too much.
(planning target volume (PTV), organ at risk (OAR), image guided radiotherapy (IGRT), monitor unit (MU), multileaf collimator (MLC), flattening filter free (FFF)).

1.2 Plan quality measures in radiotherapy (RT)

In clinical practice the planner and the physician judge the quality of a treatment plan by visual inspection of the 3D-dose distribution. The 3D-dose distribution is normally inspected in axial, coronal and sagittal views. Figure 7 shows one example for each of the three different view types and a scheme of them. The dose distribution is represented as isodoselines, to all voxels inside the isodoseline a dose as high or higher than the isodose is applied and to voxels outside the isodoseline a lower dose is applied.

3D-dose distributions give detailed information about the applied dose, but it is difficult to compare two dose distributions and to identify key dose information. Therefore dose volume histograms (DVH) were established as standard tools to evaluate dose distributions in RT treatments. A DVH is a histogram where the number of volume elements is plotted as a function of the applied dose. This is also known as differential DVH. A cumulative DVH is generated by integration from the right to the left and is therefore a histogram denominating the number of volume elements which receive at least the defined dose. The volume elements are frequently represented as percentage volume fractions. A differential and a cumulative DVH are presented in figure 6. In RT, cumulative DVHs are generally used and normally denoted as DVH, therefore the term DVH in this work always refers to a cumulative DVH.

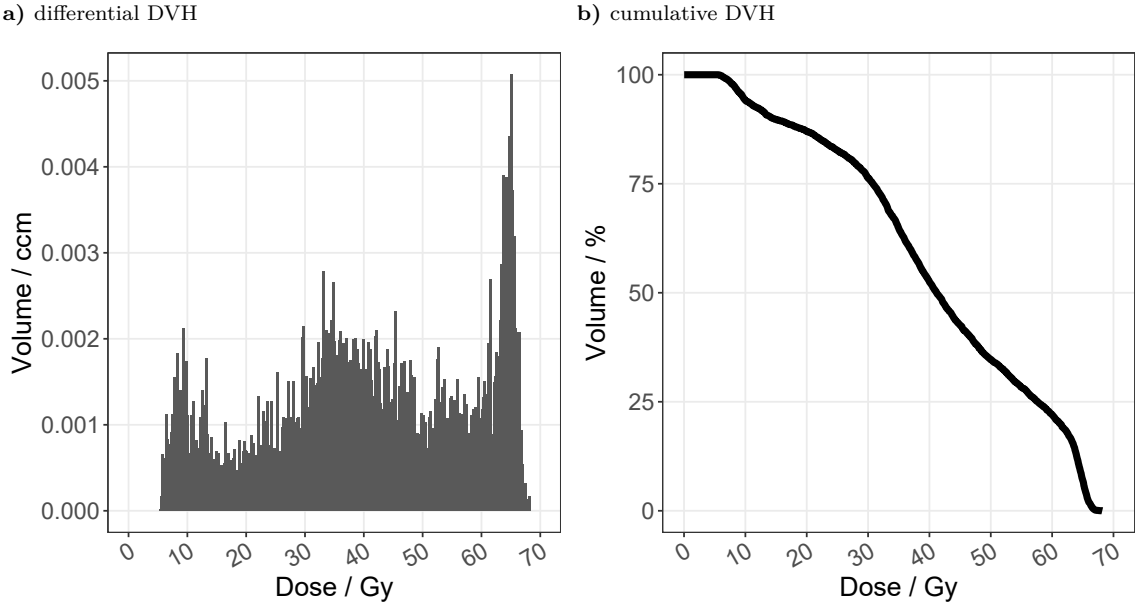

Figure 6: Figure a) presents a differential dose-volume-histogram (DVH), where the number of volume elements receiving a defined dose is plotted. By integration from the left to the right a cumulative DVH is calculated (figure b). Cumulative DVHs therefore represent the volume which receives at least the defined dose.

DVHs are representations of 3D-dose distributions, relatively simple to comprehend and useful to compare different treatment plans. It is easy to assess minimum and maximum doses and therefore the homogeneity of the dose applied to the target and also overdosing (hot spots) received by OARs are easily observed. Therefore DVHs are useful for documentation of important dose parameters including maximum dose D_{max}, minimum dose D_{min}, near maximum dose $D_{2\%}$, near minimum dose $D_{98\%}$ and median dose D_{median} or $D_{50\%}$. Nevertheless, a DVH does not provide spatial information. However, a 3D-dose distribution does. For evaluation, a DVH should therefore always be accompanied by at least representative slices of the spatial 3D-dose distribution [10].

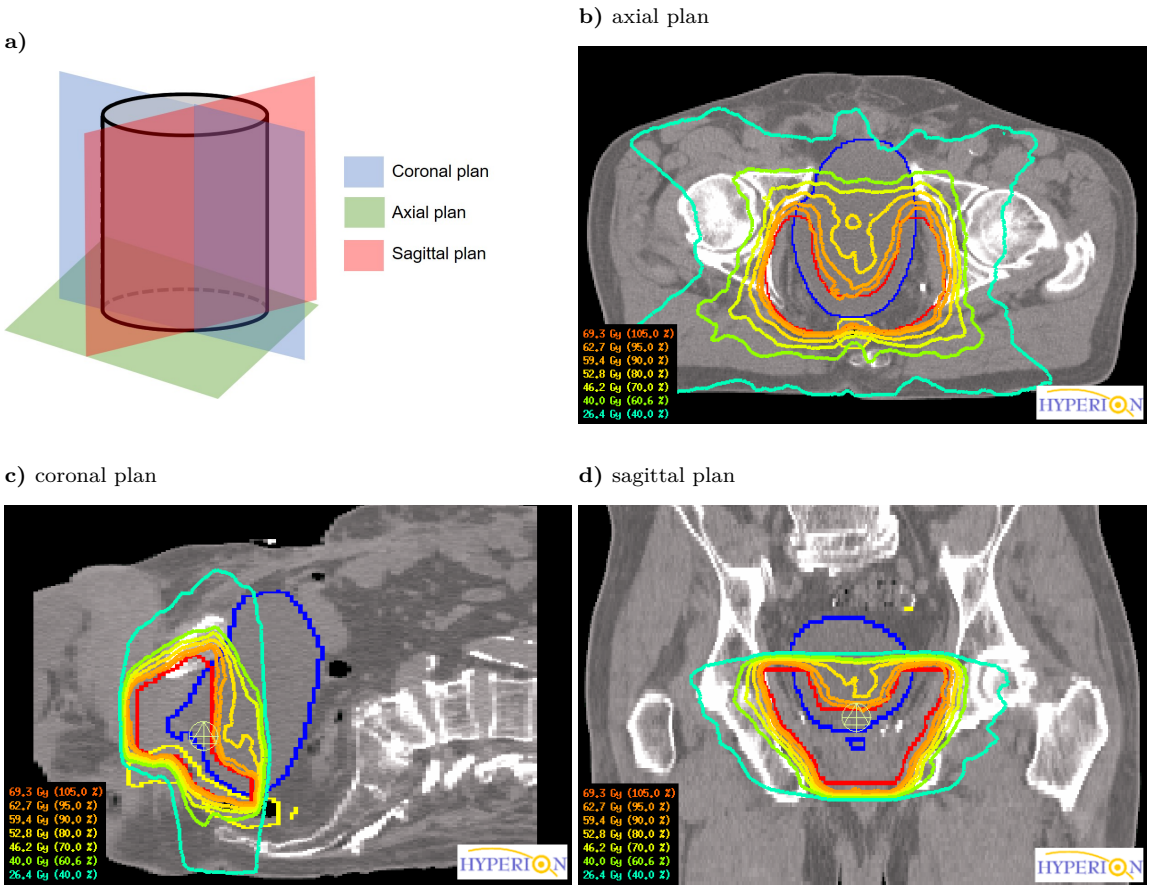

Figure 7: Plan quality is inspected in 3D-dose distributions overlaid on the planning CT. The dose distribution is represented as isodoselines. The dose distribution is depicted in axial, coronal and sagittal views. A sketch of the three view types is provided in a). For each view type a single dose plan is presented in sub-figures b)-d).

1.3 Constrained Optimization in radiotherapy (RT) treatment planning

In modern RT treatment planning optimization is considered essential and the potential of intensity modulation to tailor conformal dose distributions for arbitrary volumes while placing the steepest dose gradient precisely between the target and the most sensitive OAR is recognized [11]. The optimization depends on the precise description of the desired dose distribution, therefore dose objectives and constraints are used. Dose objectives are requirements which should to be met to the extend possible, whereas constraints are mandatory requirements that must be met. In RT planning, a distinction is made between physical and biological constraints and objectives. Therefore described briefly in the following two sections.

1.3.1 Physical objectives and constraints

Physical constraints are constraints which are defined in physical quantities. For RT, dose and volume are particularly important quantities. Another physical constraint which is assumed for every treatment planning optimization is the non-negativity of beam intensities. A well known and often used physical objective is the mean-square deviation between calculated dose distribution and ideal prescription, which is part of a minimization. This objective is also known as least-square optimization, in which it may be hard to balance target and OAR prescriptions adequately. Therefore, least-square optimization is often combined with individual constraints for OARs.

A common constraint is the maximum dose constraint, limiting the maximum dose to an OAR. By definition maximum dose constraints are very strict, which can be difficult to handle for optimization algorithms. Therefore maximum constraints are often combined with penalty factors, which measure the importance of holding a maximum dose constraint. Normally, the penalty factor increases the further the constraint is exceeded, typically with the squared excess beyond the tolerance dose. A graphical representation of maximum constraint with low and high penalty factor is depicted in figure 8. The grey area in the DVH visualizes the area where the penalty is active. With small penalty factors a slight violation of the maximum dose D_{max} is possible, whereas high penalty factors prevent the exceeding of D_{max}. Minimal dose constraints are also used for target structures.

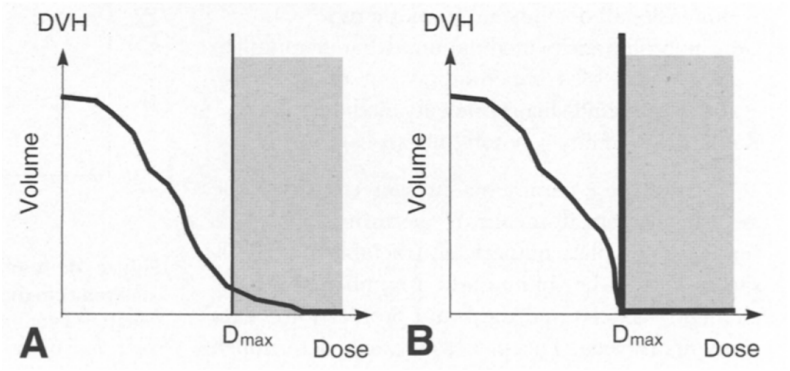

Figure 8: Application of maximal dose constraints in critical structures. (A) The use of a small penalty factor allows for some excess dose beyond the threshold D_{max}. (B) A large penalty factor prevents the delivery of any dose beyond the threshold. *Reprinted from* [11] *with permission from Elsevier.*

With respect to OARs, often not just the maximum dose needs to be controlled, but also distinct dose points referring to a dose given to a certain volume of an OAR. Therefore the so called DVH-constraint is used to limit the volume V_{max} of an OAR receiving a dose D_{max}. The rationale for this approach is, that a structure's tissue may keep its function if a sufficient amount of volume is not exposed to more than the appropriate threshold dose. A graphical representation is given in figure 9. The grey area visualizes the forbidden area of the DVH.

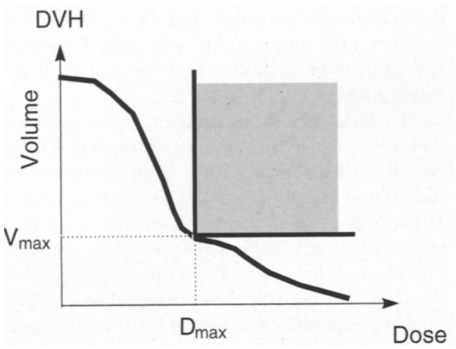

Figure 9: Structures with a large volume effect are more appropriately spared through the application of dose-volume-histogram (DVH) constraints. They prevent the DVH from going above the point (D_{max}, V_{max}). *Reprinted from* [11] *with permission from Elsevier.*

1.3.2 Biological objectives and constraints

Describing dose distributions by physical dose objectives and constraints is straightforward, as physical quantities are well defined and measurable. Nevertheless, the same physical constraint may have different meanings to different ROIs, in terms of biological dose-effect. Therefore constraints and objectives describing dose-effects for structures were proposed for the field of RT planning. To describe dose-effects F to targets or G to OARs mathematically the dose-effect for a volume is defined as the sum over all dose-effects in the voxels of this volume [12]:

$$F = 1/N \sum_{i=1}^{N} f(D_i) \tag{1}$$

$$G = 1/N \sum_{i=1}^{N} g(D_i) \tag{2}$$

Functions $f(D)$ and $g(D)$ are local effect densities and D_i is the dose to the ith volume element. For normal tissues $g(D)$ denominates the damage in a voxel induced by a dose D, therefore $g(D)$ is by definition a continuous and monotonically increasing function. The upper limit is the total damage of the structure. Local effect densities for normal tissues can be mathematically defined as sigmoid function [12]:

$$g(D) = 1/(1 + (D_0/D)^k) \tag{3}$$

D_0 is the maximum accepted dose and hence the inflection point of the sigmoid, parameter k describes the characteristic slope of the dose-effect. With increasing k the sigmoid approaches a step function. A biological description for the tolerance of a structure with respect to radiation dose is given by the volume-effect. The higher the volume-effect of a tissue is, the more $g(D)$ differs from a step function and vice versa.

Structures with high volume-effects, and corresponding small k, will tolerate overdosage in a small sub-volume if an adequate portion is spared from dose. The remaining cells are able to maintain the function of the entire structure. Sometimes this is illustrated as a rope [12], where single-strands will burst, but the rope will not. Structures with high volume-effects are denominated as parallel structures. An ideal dose-constraint for a parallel structure should control doses around the inflection point D_0, see figure 10. Dose values beneath D_0 are uncritical, whereas doses above this limit destroy the cell, but even further escalation will not cause more harm. Therefore small sub-volumes will be exposed to doses higher than D_0 if this will allow for substantial sparing for doses lower than D_0. The parallel constraint

is conceptually equal to the DVH constraint, the difference is that it offers control over a region of the DVH and not only one single point. Organs which are typically seen as parallel organs are lung, liver, kidney and parotid glands.

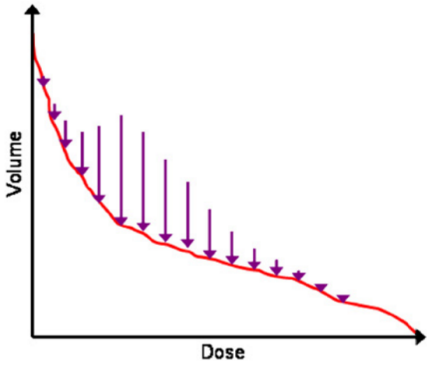

Figure 10: A typical DVH for a parallel organ, e.g. lung. The length of the arrows signifies the control over each dose bin exacted by the parallel Reconstruction Unit (or parallel gEUD) model. Arrow lengths correspond to realistic values for lung with the longest arrow being at 20 Gy. The cost of increasing the high dose bins is relatively low, reflecting the fact that it does not cause any more harm to increase the dose above a certain threshold which is assumed to obliterate organ function. Since the volume receiving at most this threshold dose is most relevant for conserving tissue function, the cost function assigns the greatest weight to the dose bins at this threshold. *Reprinted from* [12] *with permission from Elsevier.*

In contrast, for structures with a small volume-effect the function of a destroyed cell cannot be assumed by the remaining ones, hence the destruction of a single cell causes loss of functionality for the entire structure. Therefore these structures are sensitive to overdosage and a planning-constraint needs to control the maximum dose to the structure. This could be visualized by a chain which collapses if one chain link breaks [12]. An appropriate constraint needs to control the high dose region, as shown in figure 11. Rectum, eyes, brain stem and spinal cord are typical examples for serial behaving organs.

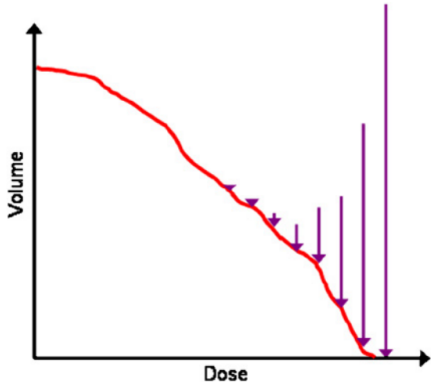

Figure 11: A typical DVH for a serial organ, e.g. rectum. The salient feature of a cost function for dose optimisation in the lo- cal dose-effect measure formalism is the way in which it affects the shape of the DVH. The length of the arrow signifies the con- trol over each dose bin exacted by the serial Reconstruction Unit (or gEUD) model. The last arrow is truncated. Arrow lengths correspond to realistic values for rectum. The cost of increasing the high dose bins outweighs the cost for the lower dose bins by far, so that the volume receiving these high doses is controlled most tightly while the volume receiving low or intermediate doses is not controlled and hence depends on the circumstances of patient geometry. *Reprinted from* [12] *with permission of Elsevier.*

Dose distributions, especially for OARs, are normally not homogeneous. An inhomogeneous dose distribution has an impact on the efficiency of RT, hence it is important to describe this effect mathematically. For comparison of different RT treatment plans, a metric to compare plan efficiency is also beneficial. Therefore the concept of equivalent uniform dose (EUD) was introduced by Niemierko in 1997 [13], where two dose distributions are considered as equivalent if they cause the same biological effect. For tumors biological effect is related to the number of surviving clonogenic cells, while for an OAR the biological effect is related to the function of the structure.

If a tissue volume element receives a homogeneous dose, then the biological effect provoked by this dose is precisely defined by this value. Hence, if two dose distributions are considered to have the same biological effect and one of them is a homogeneous distribution, the inhomogeneous dose can be precisely defined with the dose value for the homogeneous dose distribution which would cause the same effect. This dose is denoted as equivalent uniform dose (EUD), because the biological effect of the inhomogeneous dose equals the effect of homogeneously distributed dose of a certain value. A prerequisite for considering two doses as equivalent is that the same fractional scheme was used, i.e. using the same number of fractions, dose per fraction and total time of treatment.

To apply the concept for OARs, Niemierko also augmented it as generalized equiva-

lent uniform dose (gEUD) in 1999 [14]:

$$gEUD = (\sum_{i=1}^{N} v_i D_i^a)^{\frac{1}{a}} \tag{4}$$

where $\{v_i, D_i\}$ are dose-volume bins from the DVH and a is a tissue specific parameter. For targets, $0 < a < 1$, which tears the gEUD towards the minimum dose, whereas for OARs $a > 1$ with increasing a pushing the gEUD towards the maximum dose. For $a = 1$ the gEUD equals the mean dose D_{mean}. For the same dose distribution in one OAR different EUD values are possible, depending on the clinical endpoint which is evaluated [15]. Nevertheless, EUD values depend on clinical models and thereby the clinical relevance is crucially related to the quality of clinical data [15]. EUD is used to describe serial constraints [12].
The cell survival probability in the target volume can be used as biological objective. Therefore the amount of volumes which do not receive the prescribed dose is evaluated [16]:

$$F = \frac{1}{N} \sum_{i=1}^{N} exp(-\alpha D_i) \tag{5}$$

The objective function assumes a homogeneous cell density inside the target and α is the sensitivity of the cells to radiation damage.

1.3.3 Constrained optimization

In modern radiotherapy treatments, dose-effects to tissues are described as a mathematical function (sections 1.3.1 and 1.3.2). To describe physical dose distributions, these dose-effects are combined as a vector containing the total effect in n target volumes and additionally in m healthy tissues in the (n+m) dimensional space [12]:

$$(F_1, ...F_n, G_1, ...G_m) \in [0, \infty[^{n+m} \tag{6}$$

In the simplest case of only one target and one normal tissue effect, this would be a two dimensional vector. All mathematical combinations of these two effects then span a plane, see figure 12. But not all theoretically possible combinations are physically realizable, which why a boundary is introduced, separating physically realizable plans from un-realizable plans [12]. This boundary is also called the pareto-front or in higher dimensions pareto-surface. This frontier is defined by combinations where it is impossible to reduce one dose-effect without deteriorating the other one. An optimization aims at finding vectors which point at this pareto-surface, and the plans are called pareto-optimal. Plans above the pareto-front are not pareto-optimal and therefore clinically unfavorable whereas plans below this front are physically in-feasible. The pareto-optimal combinations are then calculated by defining a multi-parametric costfunction for the optimization problem. This could be a Lagrange function L [12]:

$$L = \sum_{i=1}^{n} \lambda_i F_i + \sum_{j=1}^{m} \lambda_j G_j \tag{7}$$

By solving this Lagrange function, a pareto-optimal dose-distribution is defined. By altering the Lagrangian multipliers λ, the weighting of the dose-effects is changed and the pareto-front can thereby be navigated. As the dose-effect in the target volume and the normal tissue interact, it is possible to describe the dose-effect to the target volume as function of the dose effect of the normal tissue [12]. Therefore the Lagrangian function L is modified:

$$L = \sum_{i=1}^{n} F_i + \sum_{j=1}^{m} \lambda_j (G_j - C_j) \tag{8}$$

Each normal tissue effect needs to fulfill the constraint $G_j \leqslant C_j$. By setting these constraints for the normal tissue dose-effects, we choose clinically favorable plans out of the infinite number of pareto-optimal plans. Therefore this optimization technique is named constrained optimization. It is important to understand the dif-

ference between a pareto-optimal and a clinical optimal plan. As the aforementioned pareto-optimality means that no dose-effect can be further minimized without deteriorating another dose-effect, a clinically optimal plan is preferably a pareto-optimal plan. As a plan with very strict OAR constraints will cause a poor target coverage, this is obviously not a clinically optimal plan, but it can be a pareto-optimal plan. Furthermore, it should be mentioned that one has to choose appropriate constraints to turn a pareto-optimal plan into a clinically optimal one. The constraints have to reflect the parameters that are evaluated to ensure plan quality, i.e. if the rectum high dose sparing is to be evaluated, definition of a constraint that monitors high doses to the rectum is needed.

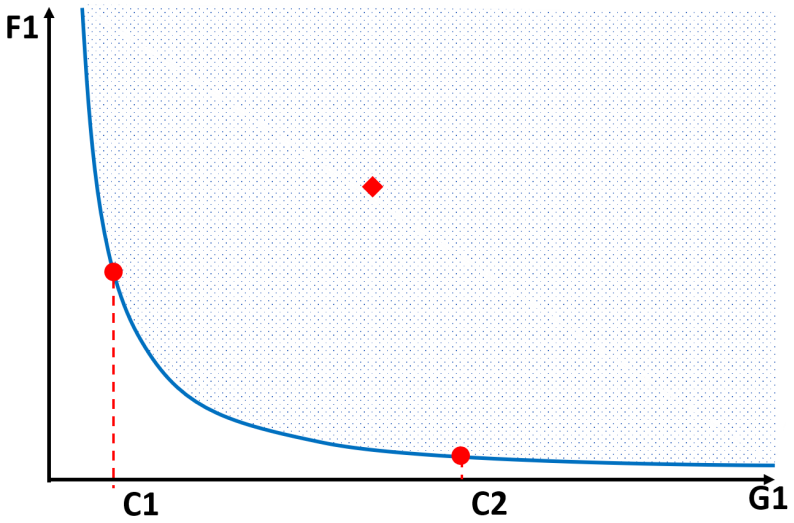

Figure 12: Schematic drawing of a pareto-front ($F1$ target dose-effect, $G1$ OAR dose effect, blue line pareto-front, dotted area physically feasible plan, white physically i n-feasible area, red rhombus non pareto-optimal plan, red points pareto-optimal plans). By choosing an appropriate constraint value C the clinically optimal plan is chosen out of the infinite amount of pareto-optimal plans. $C1$ would represent a plan with poor target dose, but strict OAR sparing, whereas $C2$ represents a plan with good target dose but inferior OAR dose sparing.

1.4 Automatic Treatment planning - current status

As aforementioned, manual planning is time consuming and highly related to the planner's experience and allocated time. To overcome these problems, automatic treatment planning has gained attention in recent years [1–7]. Several concepts have been introduced and some of them are already available in commercial treatment planning systems.

Pinnacle AutoPlanning
In 2003 Cotrutz and Xing introduced a regionally variable penalty scheme to shape IMRT dose distributions [17]. The idea is that a dose distribution could be considered nearly acceptable, but a few subvolumes or regions of the DVH need improvement. As planning objectives normally concern the whole structure it is impossible to control these subvolumes. Therefore, in addition to structure importance factors, Cotrutz and Xing introduced voxel-based importance factors, which are applied to these subvolumes only. Previously these subvolumes were defined manually by the planners by drawing the outlines with a computer mouse or identifying sub-optimal regions of the DVH. Xhaferllari et al. later further developed this approach to a first automatic planning concept by defining these subvolumes automatically by converting isodoselines into structure outlines for these subvolumes [18]. To automatically identify regions which need improvement they use a reference plan, which is automatically chosen from a library of previously treated patients, containing dose distributions and DVH information. This approach is available in the TPS Pinnacle^3 (Philips Medical Systems, Fitchburg, Wisconsin, USA) as AutoPlanning module and has proven clinical applicability for different tumor sites such as head and neck cancer [19–22], Hodgkin lymphoma [23], prostate [24], brain [24] and hepatocellular carcinoma [25].

Erasmus iCylce
A second approach is the so called iCylce, which was introduced by Breedveld et al. [26, 27] at the Erasmus University Rotterdam. iCycle uses the 2-phase ϵ-constraint (2pϵc) optimization method. Therefore a so called wishlist needs to be designed containing prioritized constraints and objectives. This wishlist is a treatment specific template which is used as a class solution and represents a starting point for individual patient planning, but it needs further refinement for individual patients. In the beginning of the optimization, objectives are minimized to reach pre-defined goals, minimizing objectives one after the other, starting with the high-

est priority. Before moving on, the reached objective value is set as an additional constraint for the following minimization of lower priorities. It may be the case that objectives could be further minimized than the specified goal. This is done in a second phase, where all objectives are minimized to their full extent, again moving from the highest to lowest priority levels. This is not done in the first phase as minimizing a higher prioritized objective further than the goal could jeopardize a lower prioritized objective from reaching the goal [27]. iCycle is used as an IMRT optimizer and also selects optimal beam angles [27]. The approach has been successfully tested for head and neck cancer [28, 29] and for prostate patients with metal hip prostheses [30]. Voet et al. showed that by linking iCycle to the TPS Monaco (Elekta, Stockholm, Sweden) it is possible to generate VMAT plans automatically [31]. This showed clinical applicability for several tumor sites: different prostate treatments [1, 32, 33], gastric cancer [4] and cervical cancer [34, 35]. Coupled with the TPS Multiplan® (Accuray, Sunnyvale, USA) iCycle can also calculate treatment plans for non-co-planar treatments with the CyberKnife (Accuray, Sunnyvale, USA) [7]. Nevertheless, there is as risk that the strict execution of the wislist results in an unfavorable position, e.g. a slight relaxation of a higher prioritized constraint could allow for a much better solution for a less prioritized constraint and this better sparing of the lower prioritized organ may outweigh the sparing in the higher prioritized organ. Another problem with the 2pϵc optimization in iCycle is that the number of optimization problems and therefore the computation time is related to the number of constraints, because iCylce solves a consecutive number of optimization's which scale with the number of constraints. To overcome these problems the lexicographic reference point method (LRPM) was introduced [36, 37].

In contrast to the 2pϵc method, the LRPM needs only one single optimization to reach a Pareto-optimal plan. Reference points and global trade-offs serve as input parameters and are treatment intent and site specific. Reference points define goal values for the objectives, whose achievements are considered equally important. The lexicographic ordering introduces multiple reference points and the deflection of these points is then the so called reference path, which steers the optimization. The first priority for the LRPM is to reach the first reference point and then go on to the next until it is impossible to further improve any objective. As this is also the definition of a pareto-optimal plan, this point is the intersection of the pareto-surface and the reference path. But this plan does not necessarily reflect a clinically favorable plan. Therefore a bend to the indifferent curve is introduced. The indifferent curve is a set of points where the optimized overall function takes a certain constant value. By definition these indifferent curves comply to the strict lexicographic ordering.

But by tilting these indifferent curves, one might allow for a small deterioration in a higher prioritized objective which is rewarded by a meaningful gain for a less prioritized objective. This is called a global trade-off and converts the strictly lexicographic ordering to a fuzzy ordering. Van Haveren et al. introduced this method and showed the applicability and superiority of the LRPM in terms of computation time while maintaining plan quality for prostate [36] and head and neck cancer cases [37].

RapidPlan

Another approach, which is based on a model trained on previously treated plans, was introduced by Yuan et al. in 2012. The idea of this approach is to predict the best achievable OAR sparing based on the knowledge and experience of previously treated plans [38]. A training dataset containing these previously treated plans is used to build a support vector regression model, which is then used to map extracted anatomical features of the PTV and OARs to dose-volume features and hence predicts DVHs. To train a good model, high-quality clinical plans are needed to extract anatomical and volumetric features. Volumetric features are OAR and target volumes, overlapping volumes between OAR and PTV, and the OAR volume which is outside the primary treatment fields. The spatial information is provided by a distance to target histogram (DTH), which evaluates the fraction of OAR volume within a maximum distance to the PTV surface. By definition, negative distances are assigned to OAR voxels intersecting the PTV. The models need to be trained site specific and the quality of the training dataset is crucial for the quality of the model. The training dataset needs to reflect the full anatomical variation and also clinical trade-offs. As the approach is able to predict the DVHs, it can be used for automatic planning by extracting OAR constraints from the prediction. Therefore plan quality was shown to be improved in terms of variation among patients, planners' experience, time allocated to the task and complexity [38]. Appenzoller et al. introduced a very similar approach, which also uses a model trained on previous plans to predict achievable OAR DVHs from the individual patient anatomy [39]. They use information from so called sub-DVHs, which means that the OAR is divided in sub-structures that are equally distant from the PTV. Using this information, the spatial and volumetric features are related to dose, and the model can be trained on this data.

In this manner, the software RapidPlan^{TM} for the TPS Eclipse^{TM} (Varian Medical Systems, Palo Alto, CA, USA) was developed as a knowledge based planning tool

and has since then been tested for several treatment sites ranging over different complexities and covering IMRT and VMAT: head and neck [40–42], prostate [43, 44], breast [45, 46] and gastrointestinal treatments [47, 48].

Raystation

In treatment planning the challenge is to find a reasonable compromise between target dose and normal tissue sparing and as this compromise is patient individual, it is difficult for human planners to find this compromise. Craft et al. introduced multicriteria optimization (MCO) into treatment planning to give the planner the opportunity to explore the trade-offs for an individual patient by a real time navigation of the pareto surface [49]. The pareto surface is represented as a linear combination of several pre-calculated plans, this assumes that the underlying optimization problem is convex, because only then the pareto surface is convex and hence the linear combination of two plans leads to a feasible plan. Strictly speaking the linear combination of two pareto optimal plans is just an approximation of the pareto surface, nevertheless if there is a sufficient and well distributed number of pareto optimal plans it is a close approximation. Later this approach was enhanced to non-convex problems like beam angle selection by navigating multiple pareto surfaces [50]. This idea of pareto-front navigation was commercialized in the TPS RayStation (RaySearch Laboratories AB, Stockholm, Sweden). Strictly speaking the pareto-front navigation is not an automatic planning approach, but it gives the human planner the opportunity to explore different trade-offs for individual patients and thereby helps to define the best compromise between PTV and OAR sparing.

Machine learning and Deep learning

Knowledge based planning is used to predict feasible DVH constraints for novel patients using the knowledge about previously treated patients. Afterwards, the predicted DVH constraints are used as planning constraints in the optimization. McIntosh et al. introduced an approach which is based on machine learning and radiomic image features and estimates dose-per-voxel [51–53]. The dose to voxel-feature relationship observed in similar patients is derived from a database of previously treated patients and is used as a basis. Thereby the dose-per-voxel is predicted, which can be used as a spatial dose objective in a voxel-based dose mimicking optimization to convert predicted dose into a treatment plan [52]. This approach needs to learn the relationship between clinical dose distributions and image features characterizing patient geometry. During a second learning phase, a model that is able to select the correct atlas for a novel patient needs to be trained. When the dose for

a novel patient is predicted, it needs to be transferred into a clinical plan. McIntosh et al. proposed to use voxel-based dose mimicking for this purpose [52]. The goal of the dose mimicking is to translate the predicted dose into modulated beams or arcs, which need to adhere to the restrictions from the beam model, e.g. maximum amount of MU, minimal segment size or gantry rotation speed. The dose distributions used in the training phase are used to establish objectives and weights for the dose mimicking. Therefore the original dose distributions are compared to the mimicked dose distributions with different parameter settings. The full pipeline from dose-prediction to treatment plan was tested successfully for 12 head and neck cases [52], whereas the dose-prediction showed its applicability for various treatment sites such as brain, prostate, lung and rectum [53].

Another knowledge-based planning approach was recently introduced by van der Bijl et al., who proposed that a model can be used to predict pareto-fronts of planning parameters on the basis of the planning CT scans and annotated structures [54]. The pareto-fronts of planning parameters are generated by automatic planning of 42 plans for each patient in the training cohort with the iCycle planning approach. The plans are generated using different wishlists reflecting different clinical priorities. The pareto-front is then approximated by fitting a parametrized convex surface to these sample plans. Geometric features are then extracted from the delineated structures and used as input parameters for the model. The model was tested for 23 patients in the validation cohort, and the fit parameters for the pareto-front could be predicted within 1 Gy difference. The proposed approach for prediction of patient individual pareto-fronts is treatment site and technique specific and its principle applicability was demonstrated for simplified prostate cases. Nevertheless it should be mentioned that the proposed super ellipsoid parametrization of the pareto-front is only valid for convex pareto-fronts. This approach does not give a treatable plan, but it provides a human planner with insights regarding the treatment planning trade-offs. The predicted planning parameters, which reflect the favorable trade-off, might than be used in a treatment plan optimization.

Deep learning also recently entered the field of RT treatment planning. In a first step, a prediction of achievable patient individual 3D-dose distributions is needed [55, 56]. Images with delineated targets and OARs of previously planned cases are used as inputs and the related dose maps as outputs of the database. For relatively consistent cases such as prostate treatments, a precise prediction of high-dose regions, especially for the PTV is feasible. But low-dose regions are challenging, because they are highly dependent on patient anatomy and treatment properties, such as beam-angles in step and shoot IMRT [55]. Nevertheless, a predicted 3D-dose dis-

tribution is not yet a treatable plan. To obtain clinically usable RT treatment plans, the voxel-wise 3D-dose distribution might be used for a voxel-wise dose-optimization, as recently proposed by Fan et al. [57].
Prediction of 3D-dose distributions is promising, but one should be aware that such models depend on the quality of the manually optimized dose distributions which are used to train the models. Chen et al. and Fan et al. showed first promising results for step and shoot IMRT [56, 57]. By now these deep learning algorithms are good in predicting the high dose regions, but they have some problems to correctly predict low dose regions. This might be due to the different patient anatomies and treatment properties. The prediction of VMAT treatments also remains challenging.

1.5 Statistical Optimization techniques in RT treatment planning

The optimization algorithms that are currently used in treatment planning normally make use of differential information to steer the optimization in the right direction in the search space and therefore expect convex constrained functions and a single global optimum. Nevertheless, the more complex treatment planning problems get, the more complex the search space might get, and to address this challenge other optimization techniques were developed. Two statistical and nature-analogous techniques which already showed promising results are optimization with genetic algorithm (GA) [58, 59] and PSO [60–64]. Both optimizations rely on the usage of random numbers and therefore explore the search space more or less randomly. This is especially promising if the search space includes several local optima or discontinuities.

Optimization with GA adopts the principle of *survival of the fittest*. Fiandra et al. used a GA to optimize the serial maximum constraints in prostate cases [58]. Therefore pairs of rectum and bladder serial constraints are initialized randomly and the plans are calculated accordingly. Afterwards the plans are compared. The best plan for the optimization round is kept, whereas all other combinations interchange rectum or bladder constraints, respectively. Additionally, constraints might randomly change their constraint value (mutation), employing the nature analogous principle of *survival of the fittest*. This process is repeated several times and in each iteration the best plan is saved. After the optimization is completed, the final best plan is chosen out of all iterations' best plans. The applicability of this concept for different prostate RT treatments was proven by a large multi-center study with 10 different institutions and 100 patient cases [59].

Another nature-analogous, statistical and global optimization technique is particle swarm optimization (PSO), which is based on the idea of the social behavior of swarms of fish or birds. A swarm contains simple individuals which are able to share information and thereby compete for best positions in the search space. The best position is defined by a predefined evaluation function, also called fitness. Further details about PSO can be found in the material and methods sections 2.1.
As PSO is relatively simple to implement and is suitable for large scale non-convex problems due to its statistical nature and global optimization, it quickly gained attention and is applied in many different fields, e.g. truck scheduling [65], design of

an urban transport system [66], determination of nano-particle shapes to determine absorption coefficients [67] and in medical engineering [68]. As inverse RT treatment planning is a large-scale optimization problem, PSO was proposed for planning of external beam RT treatments as well as for brachytherapy.
In IMRT beam angle selection is crucial for plan quality, therefore Li et al. proposed PSO for beam-angle selection in IMRT [60]. Modiri et al. introduced PSO to the field of 4D-conformal lung stereotactic body radiotherapy (SBRT), where the fourth dimension is time with respect to the target respiratory movement [61–63]. PSO is used to set aperture weights for pre-configured apertures. Furthermore Riofrio et al. presented approaches for GammaKnife radiosurgery and high dose rate (HDR) prostate brachytherapy [64]. For radiosurgery PSO determines the positions of the spherical high-dose volumes and the beam-on times, whereas for HDR prostate brachytherapy needle positions and dwell-times need to be optimized. Yang et al. proposed a PSO based planning to automatically set weighting factors in multi-objective optimization [69]. The positions of the particles are determined as sets of weighting factors, thereby each particle represents a plan. The quality of the plans is determined by three evaluation functions which are changed over time. The first evaluation function ensures the target coverage to dose, the second one should minimize high dose to the OAR while keeping the previously established level of PTV dose, and the last evaluation function is then used to reduce low doses. Each evaluation function incorporates key points from the DVH. After evaluation by the appropriate function the weighting factor for each particle is updated using information about the best evaluated plans.
In inverse RT planning, as it is state of art the for all IMRT treatments, many different constraints and objectives need to be balanced. Due to the complexity of the optimization problem it is nearly impossible to predict the impact of a variation of constraints, therefore human planning is trial and error based. With PSO the process will still be trial-and-error, but in difference to a human planner more combinations are examined, unusual combinations get a chance, due to the statistical nature, and by using a clearly defined plan quality measure the comparison of two competing plans is unbiased. Thereby PSO would offer a reliable automatic treatment planning.

1.6 Aims of this thesis

Automatic treatment planning is essential for RT to overcome the problems of time-consuming and ineffective planning. Thus, automatic treatment planning helps to address the dependence between time allocated to the task, the planner's experience, and the quality of the plan. A further advantage is that automatic planning can facilitate a fast and reliable adaption of treatment plans to daily chaining anatomy and setup errors.
Against this background the aim of this thesis is to implement particle swarm optimization (PSO) as an automatic RT planning tool. Thereby the pareto-surface can be efficiently navigated and clinically optimal treatment plans can be generated for individual patients.
The implementation needs to be validated with regard to the convergence ability to the global optimum and effectiveness of covering the search space.
The applicability of this approach is demonstrated with relatively simple post-operative prostate cases. For 10 cases, PSO treatment plans are generated automatically and compared to manual plans. The PSO plans should be as good as or preferable better than the manual plans.

2 Materials and Methods

The methods described in sections 2.1 Particle Swarm Optimization and 2.2 Plan Quality Score are partially published in

> ***Künzel L.A.**, Leibfarth S., Dohm O.S., Müller A.-C., Zips D., Thorwarth D.: "Automatic VMAT planning for post-operative prostate cancer cases using particle swarm optimization: A proof of concept study", Physica Medica, Volume 69, January 2020, pp. 101-109, 2020. DOI: 10.1016/j.ejmp.2019.12.007*

and referenced as [70] *in this thesis.*

2.1 Particle Swarm Optimization

2.1.1 Background

PSO is a nature-analogous optimization technique with collective, iterative and statistical characteristics and is used to solve non-linear problems. It was first introduced by Kennedy and Eberhart in 1995 [71] and is inspired by the behavior of swarms as flocks of birds or schools of fish. Thus relatively simple individuals are able to solve complex problems, such as searching for roosting places or food, if they cooperate and share information in a swam of I individuals. This can be transferred to an optimization problem where the individuals explore a search space for an optimum position and share information about positions in this search space. By comparing information about the best position amongst all particles to the positions it visited, each particle alters its own position in the search space. Particles are attracted to the best position but also try to explore new positions. Thereby the search space is explored by the particles. To adopt this idea for any kind of optimization problem, four prerequisites have to be met:

Position information

The position in the search space for each individual needs to be known and is therefore determined by the vector $x_{i,d}$. Where i is the number of the particle out of $[1, I]$ and d the number of generations out of $[1, D]$. The vector $x_{i,d}$ gets as many entries as the N-dimensional solution space has dimensions.

Quality assessment

Each candidate position has to be evaluated by a function to determine the quality, also known as fitness, to compare competing positions $x_{i,d}$ in the search space.

Memory

Each particle memorizes the best position $p_{best,i}$, which it visited so far in the search space, and the according fitness value. This is a personal attraction point for each particle. Furthermore each particle has to memorize the last position update vector, also called inertia.

Shared information

All particles of a swarm share their personal best position. By comparing these personal best positions, a global best position g_{best} is determined, which is then an attraction point for all particles of the swarm in the subsequent generation.

By combining this shared knowledge, iterative position updates for each particle are calculated, according to equations (9) and (10):

$$x_{i,d} = x_{i,d-1} + \Delta x_{i,d} \tag{9}$$

here $\Delta x_{i,d}$ denominates the relocation vector for each particle i, which is calculated by the sum of three different components, the inertia component T, the cognitive component M and the social component S:

$$\Delta x_{i,d} = T + M + S \tag{10}$$

The first component T is called inertia or nostalgia and is derived from the inertia weight ω and the previous relocation vector $v_{i,d-1}$, c.f. equation (11). The inertia weight was first introduced in 1998 by Shi and Eberhart [72] to control exploration and exploitation abilities of the particle swarm. Exploration here means the ability of the optimization to scout the whole search area or –visually speaking– to leave a local optimum. In contrast, exploitation means the ability to scout a small area more

precisely or –again visually speaking– climbing a founded maximum. The inertia weight determination is a critical part of the PSO implementation, as it affects the ability of the PSO to converge and also the speed of the convergence. A faster convergence is eventually associated with a poor exploration of the search space and hence has the hazard to be trapped in a local optimum, whereas over-exploring might impede the PSO from settling on the optimum. Shi and Eberhart proposed to set a constant inertia weight between 0.9 and 1.2 to balance exploration and exploitation. Based on the idea that the search should start global and settle down to an optimum, the idea of linearly decreasing inertia weights was also proposed [72, 73]. There have also been attempts to use non-linear reduction and even more complex schemes [74]. Adaptive inertia weights were also introduced, where the idea is to monitor the behavior of the swarm and adapt the inertia weight during the PSO [75].

$$T = \omega \cdot v_{i,d-1} \tag{11}$$

The second component M evaluates the distance between the actual position $x_{i,d-1}$ and the particle's own best position $p_{best,i}$ during the whole search history, c.f. (12). As this component is related to the particle's best position, which can be seen as the particle's memory, it is sometimes called the cognitive component.

$$M = c_1 \cdot \zeta \cdot (p_{best,i} - x_{i,d-1}) \tag{12}$$

The third component S is related to the shared information of the swarm and is therefore referred to as the social component. It evaluates the distance between the actual position of the particle $x_{i,d-1}$ and the global best position g_{best} ever seen by a particle of the swarm.

$$S = c_2 \cdot \xi \cdot (g_{best} - x_{i,d-1}) \tag{13}$$

To introduce the statistical nature to the PSO, the cognitive and the social components are weighted by two vectors of random numbers ζ and ξ. Additionally, the cognitive and social components are weighted by optimization constants c_1 and c_2, which should balance the two components. Kennedy and Eberhart proposed to

weight them equally and set them to $c_1 = c_2 = 2$ [71].

When all particles have updated their position once a complete iteration was executed, this is called 'a generation' in PSO. All optimization parameters needed for the PSO are summarized in table 1.

Table 1: Summary of PSO parameter symbols and meanings with related explanations for RT treatment planning and parameter values for the PSO implementation used for post-operative prostate cases. *Reprinted from* [70] *with permission from Elsevier.*

Symbol	**Meaning**	**Explanation**	**Parameter values** postoperative
$\boldsymbol{I}$	Number of particles	A particle is a set of planning constraints, translating to a plan/dose distribution	$I = 30$
$\boldsymbol{N}$	Dimensionality of the solution space	Identical to number of planning constraints	$N = 3$
$\boldsymbol{D}$	Number of generations	Number of PSO iterations	$D_{Max} = 100$
$\boldsymbol{\zeta, \xi}$	Vectors of random numbers	N-dimensional vectors, with components each sampled from the interval [0,1]	[0,1[
$\boldsymbol{c_1, c_2}$	Optimization constants	To balance relocations, these constants are held fixed during the whole optimization process	$c_1 = c_2 = 2$ [71]
$\boldsymbol{\omega}$	inertia weight	Balances exploration and exploitation. This parameter is adapted during optimization process.	$\omega = 1.4$ in generation 0-9, reduced by 0.2 every 10th generation until 0.2 is reached in generation 50
$\boldsymbol{x_{i,d}}$	Current position of particle i in generation d	Vector of planning constraints in the N-dimensional solution space	
$\boldsymbol{v_{i,d}}$	Relocation of particle i in generation d	N-dimensional relocation vector	
$\boldsymbol{p_{best,i}}$	Previously best position of particle i	Position of so far best-scored plan of particle i	
$\boldsymbol{g_{best}}$	Global best position	Best-scored position reached so far over all particles	

2.1.2 Implementation of PSO for RT Treatment Planning

To realize a PSO implementation for RT treatment planning a particle is interpreted as a plan and its position is represented as a vector of N different planning constraints. After initializing the plans randomly, they are calculated by our in-house TPS Hyperion. To judge the quality of competing plans and to determine the best plans, a fitness measure is needed for the implementation, therefore a so called plan quality score (PQS) is introduced, for details see section 2.2. Using this PQS the global and particle's individual best positions g_{best} and $p_{best,i}$ are assessed and the position update is calculated using equations 9 and 10.
The PSO and the manipulation of the TPS Hyperion input files are implemented in separate Python 2.7.3 scripts. A bash-script is used to control the interaction between TPS and PSO, as illustrated in the schematic flowchart in figure 13. The bash-script and the python scripts can be found in Appendix A. The PSO starts with random initialization of the particle positions, i.e. constraint combinations of a plan. This initialization is implemented as separate Python script which also manipulates the constraint values in the respective lines in the TPS Hyperion input file, which formulates the optimization problem. Consequently, all constraint and objective types and values are defined and assigned to the appropriate PTV or OAR. Additionally, this file also contains all other optimization and sequencing parameters such as minimal MU values per segment, minimal segment size, number of arcs and others.
After all plans have been initialized, the constrained optimization for the first particle starts. Once plan calculation is finished, TPS Hyperion automatically saves the dose and DVH files, where for each ROI the DVH information is stored. This DVH is then in a next step accessed by the script *scoring.py*, which calculates the total PQS for the plan. Afterwards, the script *get_pbest.py* compares the actual PQS to the so far reached best PQS of the particle, and the best position is updated if necessary. At this point the first generation for the first particle is finished and the first generation for the second particle starts with the constrained optimization in the TPS Hyperion. After the first plan calculation for all I particles, the swarm's best position is accessed by the script *get_gbest.py* and the position relocation vectors for each particle are calculated according to equations (9) and (10) by Python script *update_velo.py*. This script also manipulates the TPS input file by replacing the constraint values accordingly. At this time point, the first generation of PSO is completed and the following generations are conducted accordingly until the maximum number of generations is achieved.

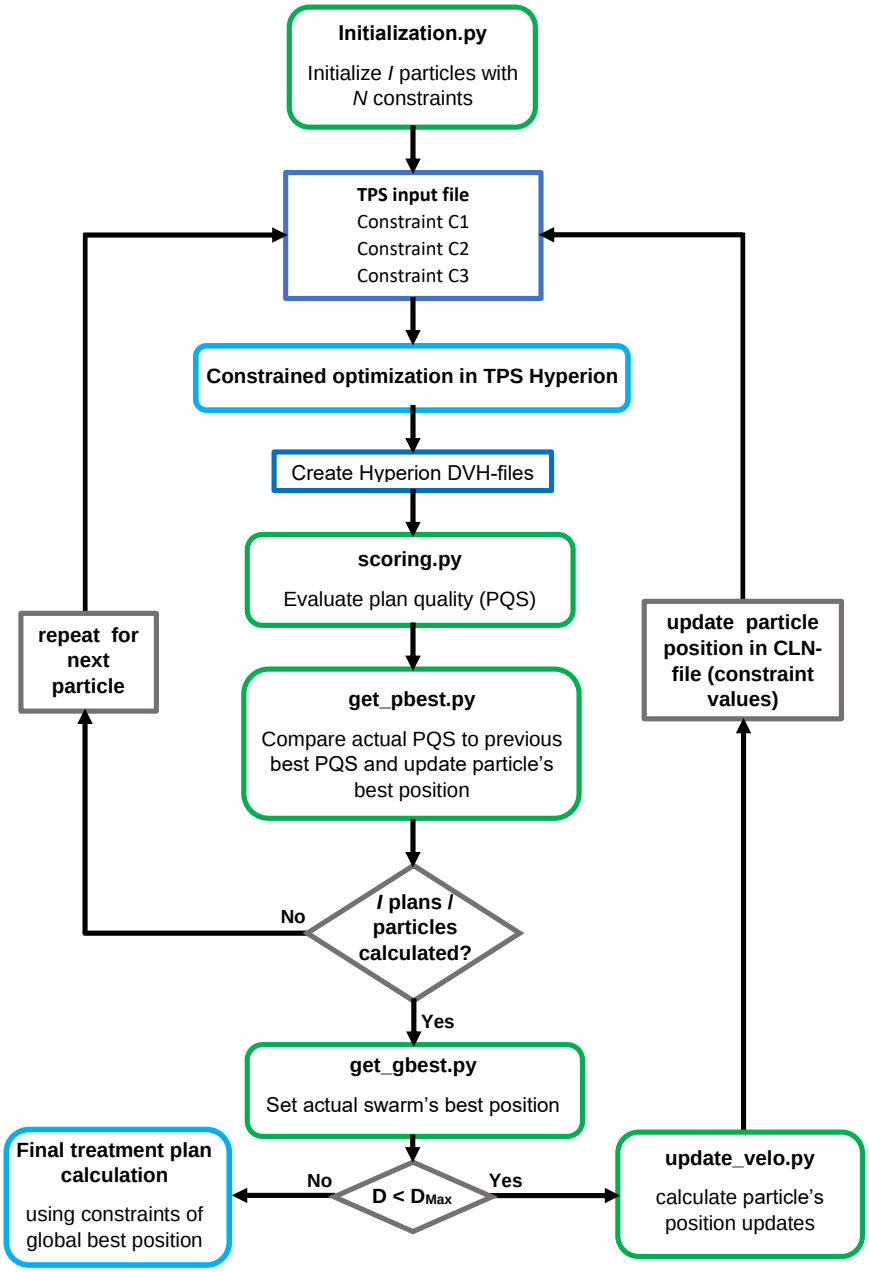

Figure 13: Flowchart of the procedure of the PSO, which is monitored by a bash-script. I number of particles/plans, N number of constraints per plan, D number of generations, PQS plan quality score.

2.1.3 Patient data

To illustrate the applicability of PSO for automatic VMAT planning the procedure was tested on $n = 10$ post-operative prostate cancer cases. All cases were chosen randomly from our clinical database and have clinical manually optimized plans for the same treatment machine. Patient data was pseudonymized as cases PC01 to PC10. The treatment concept included a prescribed EUD of 66 Gy to the PTV and contains rectum and bladder as main OARs. For the OARs, serial constraints taking EUD and an exponent as parameters were used. For details about serial constraints, see section 1.3. In the TPS Hyperion, handling overlap between PTV and OAR structures is possible. Normally, PTV is defined at first in the TPS input file. Thus, by definition voxels belong to the PTV and are ignored for OAR constraints. But it is possible to include compromised voxels to the OAR constraints explicitly if needed. This is especially helpful to control overdosing in the intersection area. For example, in prostate cases rectum and PTV normally overlap as the prostate is in contact with the rectal wall. As the PTV concept considers setup errors, the PTV for the prostate is bigger than the prostate itself and will therefore compromise the rectum. Nevertheless, a slight overdosing, which is in principle accepted for the PTV, should not be in the intersection between PTV and rectum. The first rectum constraint, with exponent $k_{r1} = 12$ and optimizing all voxels, was used to control high doses. A second serial constraint which only applies to voxels of rectum which were not intersected by the PTV, with exponent $k_{r2} = 4$, was used to control middle and low dose regions. For the bladder, a serial constraint optimizing all voxel with exponent $k_b = 8$ was used to control intermediate and high doses. For all serial constraints, the EUD was the parameter to be chosen by the PSO. The exponent was not optimized. The search space for this three serial constraints is 3 dimensional and the position of each particle (plan) is described by a vector taking the three EUD values as entries.

To initialize the particles, a plan with non-binding rectum and bladder constraints ($C_j = 66$ Gy) was calculated to estimate a minimum feasible OAR sparing. Therefore a specific feature in the TPS Hyperion was used, where constraints are minimized further than the defined threshold, as long as this does not harm the PTV objective or other OAR constraints. This is subject to a barrier-penalty multiplier method, which is implemented in TPS Hyperion [76]. The thereby reached dose effects G_j were then used as the center of the initialization space, which spreads out by ± 5 Gy for each dimension. Particles were randomly initialized within this range. The relocation vectors $\Delta x_{i,d}$ were also initialized randomly for each entry from the interval

[-1,1].
The swarm contained $I = 30$ particles (plans) per generation and the termination criterion was set to $D_{Max} = 100$ generations. For a summary of all parameters see table 1.
To generate random numbers during the initialization and also for the weighting vectors ζ and ξ, the Python random module was used. The module is by default initialized by date and time, and gets reinitialized with every call of a python script.

2.2 Plan Quality Score

As PSO requires the identification of global (g_{best}) and local ($p_{best,i}$) best plans, it is necessary to determine criteria for the comparison of treatment plans. This comparison has to be fair, reproducible, needs to identify one plan as the superior one, and related to the corresponding clinical considerations. To measure the particle performance a plan quality score (PQS) was introduced, which was adapted from the DVH parameters defined in our institutional standard operating procedure (SOP). The PQS needs to be redesigned for specific treatment sites and treatment intents. For the post-operative prostate cases a total of eight different DVH parameters were used to evaluate the quality of a treatment plan. A summary of the PQS parameters used for PQS assessment is listed in table 2. The table also contains an explanation for the clinical considerations that were monitored by these parameters. The principle idea was to reward adherence and to penalize violation. For the PTV, three DVH parameters were evaluated for PQS definition concerning EUD, $D_{2\%}$ (near maximum dose) and $D_{98\%}$ (near minimum dose). Schematic drawings illustrating how the achieved dose parameters for the PTV were converted into PQS are provided in figure 14.

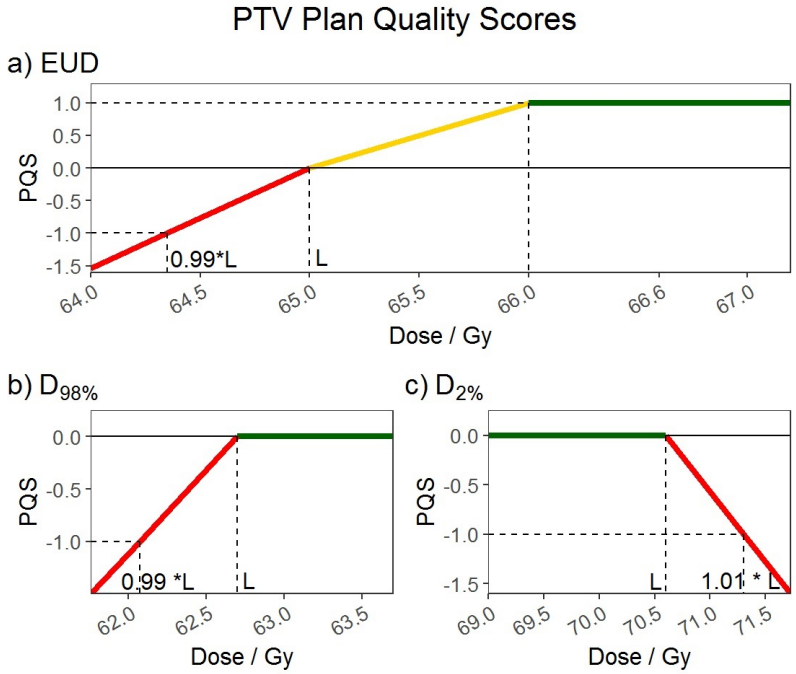

Figure 14: Schematic illustration of the plan quality score (PQS) for PTV parameters equivalent uniform dose (EUD), $D_{98\%}$ near minimum dose, $D_{2\%}$ near maximum dose, L limit defined in standard operating procedure (SOP)). *Reprinted from* [70] *with permission from Elsevier.*

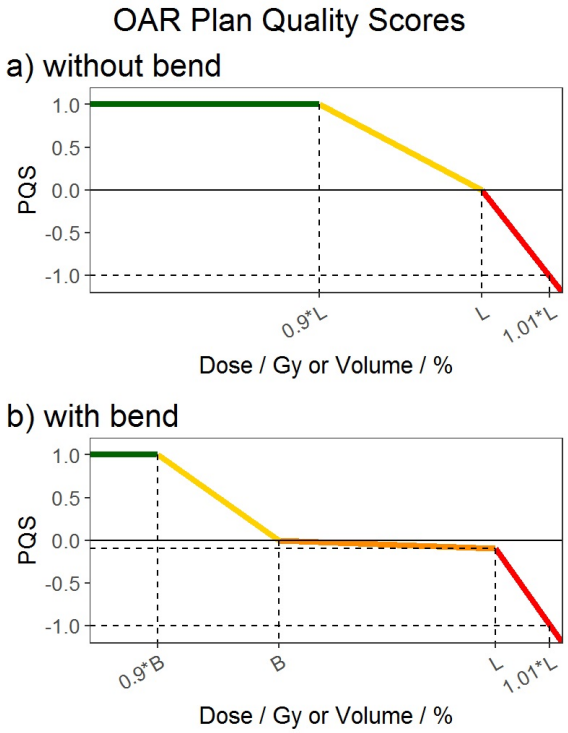

Figure 15: Schematic course of the plan quality score (PQS) related for the OAR parameters. L limit, B bend. *Reprinted from* [70] *with permission from Elsevier.*

Rectum and bladder were identified as main OARs. For the rectum $D_{2\%}, V_{60\text{Gy}}$ and $V_{40\text{Gy}}$, and for bladder $D_{2\%}$ and $V_{60\text{Gy}}$ were evaluated. The associated DVH parameters are summarized in table 2. As the volume constraints $V_{40\text{Gy}}$ and $V_{60\text{Gy}}$ are highly related to the individual patient anatomy, a plan with non-binding OAR constraints ($C_j = 66\text{Gy}$) was calculated beforehand to estimate a minimum possible OAR sparing. The reached dose effects G_j (c.f. equation 7 in section 1.3) were then used to introduce an additional bend in the PQS equaling the reached dose effect G_j, c.f. figure 15. This bend should guide the PSO for optimal OAR sparing by penalizing the exceedance of this bend, nevertheless the penalization is not as strict as the exceedance of the limit defined in the institutional SOP. For plans staying below the bend, the PQS offers a reward by applying positive points.
The maximum reward for each DVH parameter was limited to one scoring point, except for PTV parameters $D_{2\%}$ and $D_{98\%}$ which only penalize violation (c.f. figure 14 b and c). For plans which fulfill all PTV and rectum or bladder goals, an extra reward of 5 points each was applied. Hence a theoretical maximum score of PQS=16 could be reached in this study.

Table 2: Summary of DVH parameters used for plan quality score (PQS) and plan evaluation. All parameters are taken from our institutional SOP (D_P prescribed dose 66 Gy). *Reprinted from* [70] *with permission from Elsevier.*

Structure	**DVH-parameter**	**Limit**	**Explanation**
PTV	EUD	= 66.0 Gy	Dose prescription D_P, minimum requirement EUD = 65 Gy
	$D_{98\%}$	> 62.7 Gy (95% D_P)	adapted from ICRU Reports 62 and 83 [77, 78]
	$D_{2\%}$	< 70.6 Gy (107% of D_P)	
Rectum	$D_{2\%}$	< 66.0 Gy	ICRU 83 [78]
	$V_{40\mathrm{Gy}}$	< 80.0 %	92% of patients without Grade 2+ GI toxicity [79]
	$V_{60\mathrm{Gy}}$	< 40.0 %	To prevent moderate/severe toxicity (any endpoint) [80]
Bladder	$D_{2\%}$	< 66.0 Gy	ICRU 83 [78]
	$V_{60\mathrm{Gy}}$	< 50.0 %	Institutional standard adapted from QUANTEC ($V_{65\%}$ < 50% Grade 3+ toxicity)[81]

2.3 Analysis of convergence

The ability to converge is crucial for a PSO: it means that the entire swarm settles down at a final best position. The convergence of the swarm might also be used as a termination criterion for the optimization. One option to assess the convergence graphically is to plot the mean, minimum and maximum constraint values of each swarm generation over the course of optimization. This could be the actual position of each particle or the personal best position (p_{best}), nevertheless this is a qualitative analysis. For quantitative interpretation, the relative difference of the mean constraint value between two subsequent generations can be calculated:

$$|C_{j,mean}| = 1 - \frac{C_{j,mean}(d)}{C_{j,mean}(d-1)} \tag{14}$$

The mean value stabilizes if all individual particle stabilize. However, this does not necessarily mean that all particles reach the same value. Therefore the gap between maximum and minimum constraint value might be analyzed as a second indicator. As a third indicator for convergence the course of the position update, calculated in equation 10, is analyzed. As described in equation 10, the relocation vector contains three different components: inertia T, the cognitive component M and the social component S. To further analyze the mean contribution $\bar{T}(d)$ of each component to the mean relocation $\Delta\bar{x}(d)$ in each generation d during the course of PSO, the relative contribution of each component in one generation to the absolute mean relocation vector is calculated. Equation (15) defines the calculation of the relative contribution of the inertia component $W_T(d)$. $|\Delta x_{i,d}|$ is the modulus of the relocation vector of particle i in generation d and $|T_{i,d}|$ is the modulus of the inertia component of particle i in generation d, therefore the sign of the components is neglected. I is the number of particles. The relative contributions W_M and W_S of the cognitive and social components are calculated accordingly.

$$W_T(d) = \frac{\bar{T}(d)}{\Delta\bar{x}(d)} \tag{15}$$

$$\Delta\bar{x}(d) = \frac{\sum_{i=0}^{N} |\Delta x_{i,d}|}{I} \tag{16}$$

$$\bar{T}(d) = \frac{\sum_{i=0}^{N} |T_{i,d}|}{I} \tag{17}$$

The different components, especially inertia, are crucial to the exploration and exploitation ability. Inertia describes the effort of the individual particle to keep its own traveling direction. This means that the higher the inertia component is, the less the particle is attracted to the swarm's and its own best position. Therefore a high inertia promotes the exploration of the search space and a good exploration is preferred in the beginning of PSO, whereas during the course of the optimization exploitation should increase. Hence the inertia weight is lowered during the course of PSO to decrease the influence of inertia to the relocation. Therefore it is expected that the contribution of the inertia component to the relocation is high in the beginning and decreases over time.

2.4 Analysis of exploration and exploitation effectiveness

The ability of the swarm to explore the entire search space is crucial for the success of PSO. Exploration means that the entire search space is evaluated and hence visited by at least one particle. As aforementioned, the PSO is tested with relativity simple treatment plans for post-operative prostate cancer cases, where the combination of three serial constraints is optimized. Therefore the search space is 3-dimensional and each constraint can take an EUD value in the interval [10 Gy,66 Gy]. The lower limit was not set to 0 as this would probably cause infeasible constraint combinations, nevertheless a constraint of EUD = 10 Gy may also be too strict. In our study, the upper limit was set to EUD = 66 Gy as this was the prescribed dose to the tumor and an OAR should never be exposed to a higher dose than to the prescribed dose to the tumor.

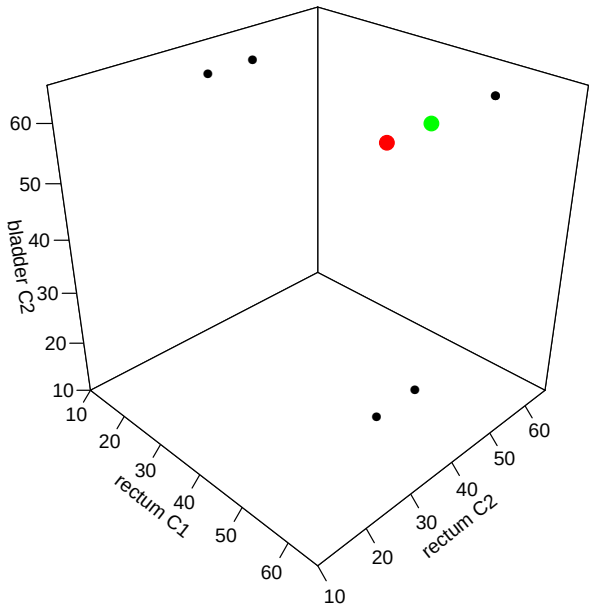

Figure 16: 3D plot of the search space. As 3D plots are difficult to comprehend, the plot can be divided into 2D plots by projecting the third dimension to the boundary of the search space. If we look at the plain representing constraints 1 and 3, one position is obliterated because of the projection. To prevent this, all 3 possible combinations of constraints have to be always taken into account.

To evaluate and get an impression of the constraint combinations, i.e. positions visited during the course of PSO, the search space was visualized. As the search space is three dimensional, 3D-plots were used. But as 3D-plots are hard to evaluate, the positions were additionally projected to the 2D-planes at the boundary of the

search space. This 3D-plot with 2D-projections of the particles' positions is exemplary shown in figure 16. In order to not loose the information of the third dimension all three possible combinations of two constraints were plotted and evaluated.

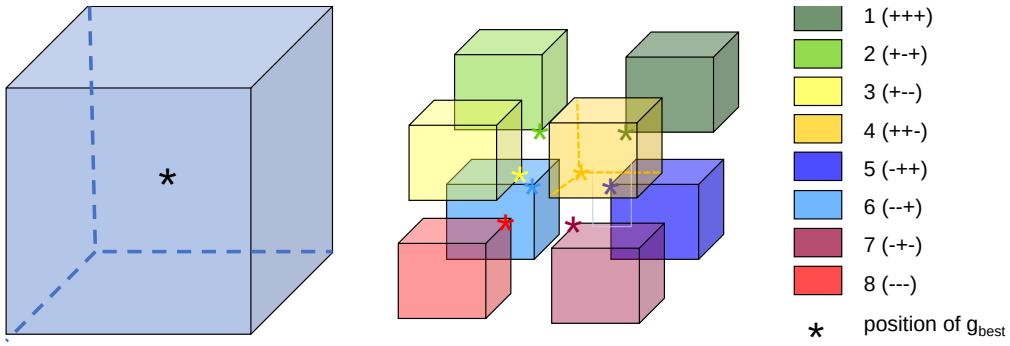

Figure 17: Graphical representation of the 3D-search space divided into eight sub-search spaces, represented as octants. The position of the global best position g_{best} in the corners of the sub-search spaces is marked as asterisk *.

To assess the exploration ability, the distance between the final best position, e.g. the combination of constraints used to calculate the PSO plan, and each position visited during the optimization by a particle is calculated (equation 18). If only distance would be evaluated, the spatial information would be discarded. Therefore the search space was divided in eight sub-search spaces. These octants are defined such that the particle's final best position was in the center, where all eight cubes touch each other. For a graphical representation, see figure 17. Then a frequency polygon of the distance to the final best position is plotted for each sub-search space. Frequency polygons offer the same information as histograms, but are easier and more comprehensible if several polygons are summarized in one plot.

$$|x_{i,d}| = \sqrt{(C1_{i,d} - C1_{g\_best})^2 + (C2_{i,d} - C2_{g\_best})^2 + (C3_{i,d} - C2_{g\_best})^2} \qquad (18)$$

In the beginning of the PSO a good exploration ability is important, whereas with increasing number of generations exploitation ability becomes more important. Exploitation means that the region around the identified global best position should be scanned more precisely, because a slightly better combination can potentially be found nearby. Therefore the distance between the final best position and the actual position was analyzed with respect to the generation number. For this, generations were grouped in blocks of 10 subsequent generations starting with generation 0 to 9. Again, frequency polygons were plotted for evaluation.

2.5 Comparisons of manual and PSO plans

All manual plans in this study were retrospectively taken from the clinical patient database. Patients cases with the same prescription scheme and treatment intend were chosen. No extra time or inputs except from the planning criteria defined in the in-house standard operating procedure (SOP) were used when preparing the manual treatment plan for each patient. The manual plans were not all created by the same physician and planner, as there is a rotation of staff in clinical duties. The PSO plan for each patient was generated as described in section 2.1. In difference to the manual plans, there was no time restriction. The PQS was established in an iterative process. Some of the cases were planned several times to find a PQS definition which ensures planning restrictions according to our in-house SOP. But for all 10 cases, only the PSO plan generated with the PQS described in section 2.2 is presented and compared to the manual plan in this work. Nevertheless PSO is based on the same criteria as defined in the SOP, which were also taken into account during the manual planning process.

2.5.1 Dosimetric comparisons

As for each patient case, a manual and a PSO plan exist, the dosimetric comparison was made between the two plans for each individual case. The dosimetric and volumetric criteria used for comparison are directly related to the plan quality criteria defined in the SOP. The evaluated dosimetric parameters are the same as used for the PQS definition, c.f. table 2, and are presented as boxplots to evaluate the spread over all ten cases via quartiles.

2.5.2 Statistics

A Wilcoxon signed rank test with Bonferroni correction was carried out using the software package R (Version 3.5.1)[82]. Differences between manual and PSO plans resulting in p-values smaller than 0.05 were considered statistically significant. A Wilcoxon signed rank test was deemed appropriate due to the non-normally distributed nature of the tested dosimetric and volumetric parameters and due to the paired test situation, as there was a manual and a PSO plan for each patient case.

Due to the multiple testing for several dosimetric and volumetric criteria, a Bonferroni correction was applied.

2.5.3 Comparisons of dose-volume-histogram (DVH)

DVHs for pairs of manual and PSO plans were compared visually. For a better comprehension of overall differences in DVHs of manual and PSO plans, a DVH spread was plotted. The plot was generated by determining minimum and maximum volume fraction for dose bins over all individual DVH of the respective cohort. Therefore the plotted area contained all individual DVH. A narrow band would indicate a lower inter-patient variability than a broader band.

3 Results

Parts of the results presented in section 3.1 Analysis of convergence ability and section 3.3 comparison of manual and PSO plans are published in

> ***Künzel L.A.**, Leibfarth S., Dohm O.S., Müller A.-C., Zips D., Thorwarth D.: "Automatic VMAT planning for post-operative prostate cancer cases using particle swarm optimization: A proof of concept study", Physica Medica, Volume 69, January 2020, pp. 101-109, 2020. DOI: 10.1016/j.ejmp.2019.12.007*

and referenced as [70] *in this thesis.*

In this thesis, an automatic planning approach based on PSO was successfully implemented and tested for 10 post-operative prostate cancer cases. For 9 out of 10 cases PSO plans reached clinical quality and were comparable to manual plans. In the following results sections the PSO implementation is analyzed concerning the convergence ability and also the balance of exploration and exploitation. Afterwards the automatically planned post-operative prostate cases are presented and compared to the manual plans.

3.1 Analysis of convergence ability

In this study, the termination criterion was set to a maximum of 100 generations. This is the simplest termination criterion, but it may not be the most efficient one. Depending on the case the PSO may find the global optimum earlier or later. In the first case the final generations will not enhance plan quality but waste computation time, in the latter one a better plan may have been found. The ability of the PSO to converge against an optimum is patient specific and also determined by the optimization parameters. To get a better understanding of the convergence of the

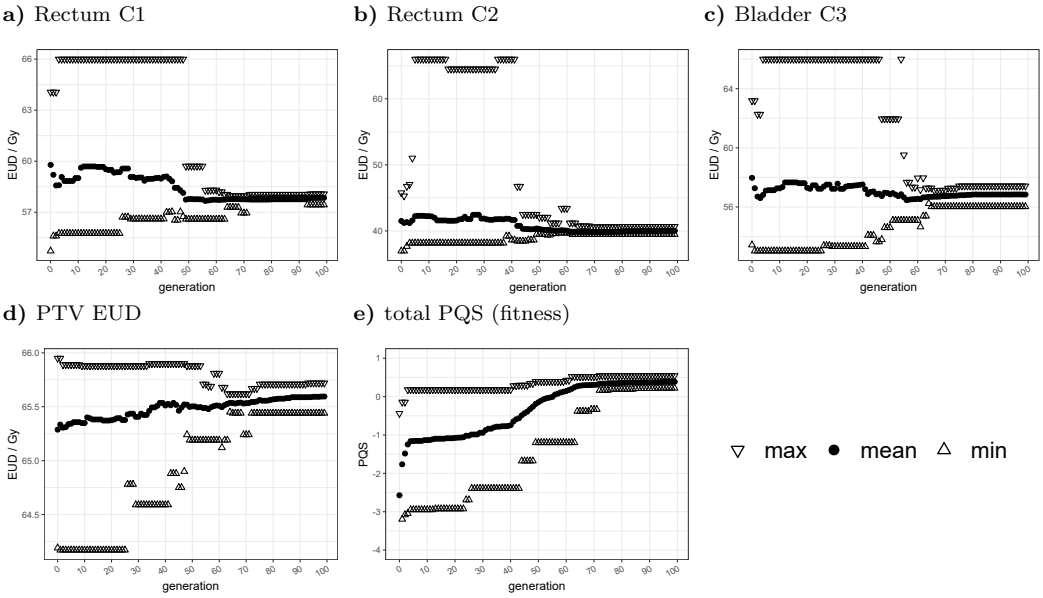

Figure 18: Course of best positions mean, minimum and maximum rectum constraints a) and b), bladder constraint c), PTV EUD c) and total PQS (d) for case PC03, amounted from [70].

PSO for the 10 planned post-operative prostate cases, the convergence ability was further analyzed.

Figure 18 visualizes the evolution of the particles' best positions p_{best} showing mean, maximum and minimum rectum and bladder constraints, PTV EUD and total PQS of the 30 particles for each generation for case PC03. The constraints in figure 18 a) to c) started with a small search space, which was determined by the initialization. Then the search space was explored, which means that the particles explore the entire search space. After generation 50 the particles started exploiting a much narrower part of the search space. They seemed to stabilize after generation 70, which is in line with the stabilization of the total PQS figure 18 e). The PTV EUD which is depicted in figure 18 d) stabilized at 65.6 Gy, which is less than the prescribed EUD of 66 Gy. This reflects a meaningful compromise between PTV dose coverage and OAR dose sparing. The total PQS is intended to converge against a maximum, for the visualized example this was accomplished (figure 18 e) and it appeared to stabilize after generation 80. The update of the global best value (g_{best}) is also visible in the graph as steps in the maximum PQS. But due to the spread between maximum and minimum constraint values, it is also evident that, not all particles are close to the final best position, especially for the bladder constraint.

For further analysis of the convergence ability for all 10 cases, the relative difference in mean constraint values between subsequent generations was calculated. The

criterion was set to a relative difference of less than $\pm 0.1\,\%$ and is visualized in figure 19. For all 10 cases and all constraints the relative difference in mean values stabilized and fulfilled the set criterion. For all cases the rectum $C1$ and bladder $C3$ constraint seem to have stabilized earlier than the second constraint for rectum $C2$. For some cases, the difference criterion for constraint $C3$ was even only fulfilled in the last generations (see figure 19 a), b) and f)) for cases PC01, PC02 and PC06). Also in early generations, the mean value of the global best position can stabilize for a while, this is probably because the best position of the particles was not updated in every generation, especially in the beginning of the PSO, where weak combinations of constraints were also explored. Nevertheless, as was also mentioned for the plot in figure 18, the sole evaluation of difference in mean values does not reflect the distance between minimum and maximum. Therefore the distance between maximum and minimum constraint value can be used as a second criterion. For the rectum constraint $C1$ all cases reached the criterion of a distance less than 1 Gy between minimum and maximum. For the rectum without PTV constraint $C2$, the criterion was violated in all cases. Nevertheless, for some cases like PC01, PC03 and PC06 it was nearly reached (see figure 19 a), c), f)), but for others like PC02 and PC05 it was obviously missed (figure 19 b) and e)). For the bladder constraint $C3$ the criterion was fulfilled in 4 out of 10 cases. For the other cases such as case PC03 in figure 19 c) it was sometimes nearly met, while in others such as cases PC04 and PC09 it was clearly missed. There was no clear connection between the convergence of the different constraints, therefore to access the convergence of the PSO all optimized constraints needed to be evaluated independently. Nevertheless, even if one constraint converges and is stable over several generations, other constraints may need more generations until full convergence is reached.

As described in equation 10 the relocation vector contains three different components: inertia T, the cognitive component M and the social component S. For PC03 the relative contribution of each component to the relocation vector was further analyzed (see figure 20). As expected, the inertia component had the highest relative contribution in the beginning of the PSO, with decreasing importance throughout the optimization. The cognitive and the social component increased during the course of PSO. As the inertia component was the dominating part in the relocation vector in the beginning of PSO and became less important during the course of optimization, the reduction of the inertia weight ω during the PSO gave the expected result for the position updates. During the promotion of inertia in the beginning, the particles also stuck to their movement and were not immediately attracted to the global best

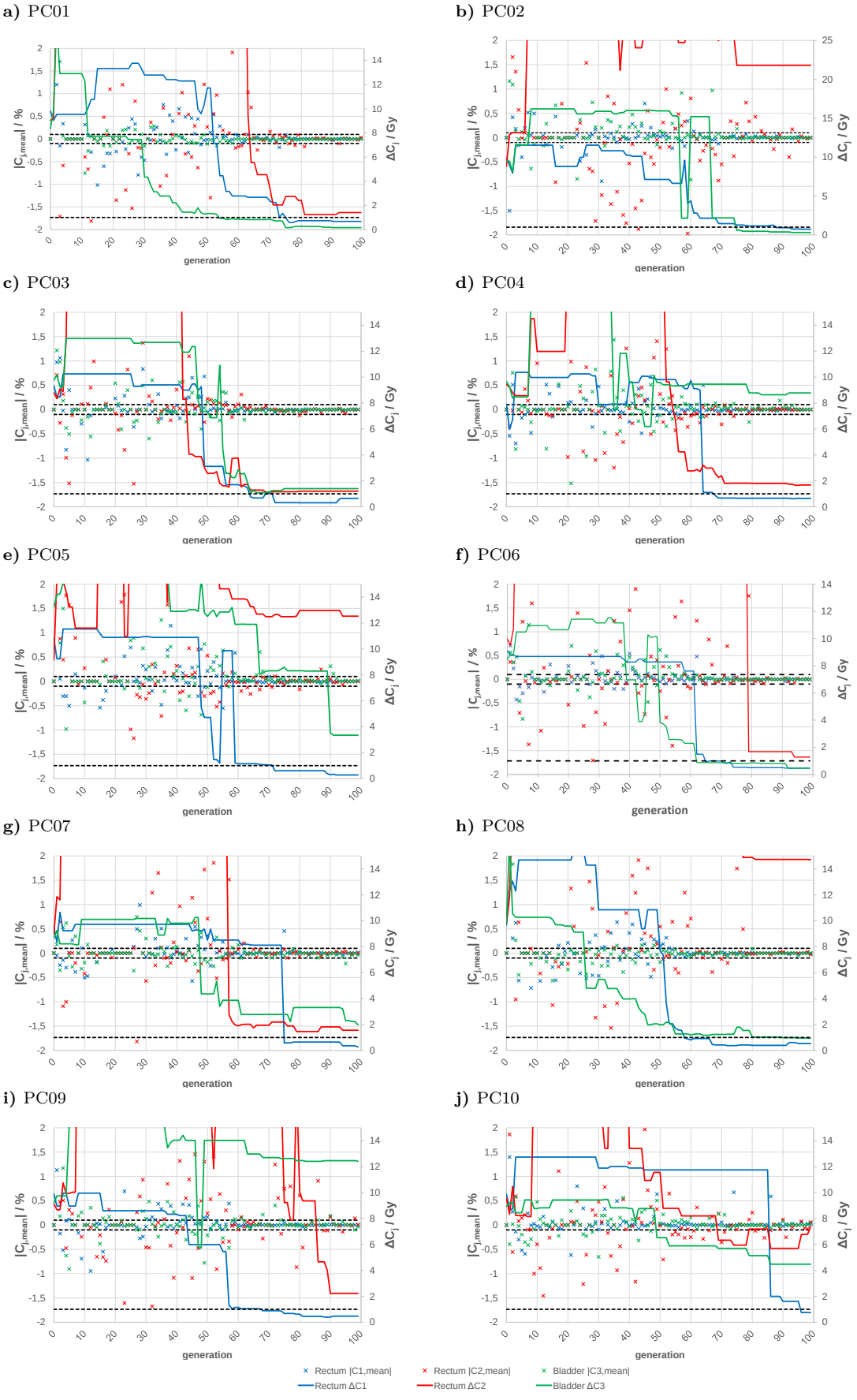

Figure 19: Visualization of termination criteria relative difference of subsequent generations of less than $\pm 0.1\%$ and difference between maximum and minimum constraint less than 1 Gy for all 10 cases (Rectum constraints $C1$ and $C2$, bladder constraint $C3$).

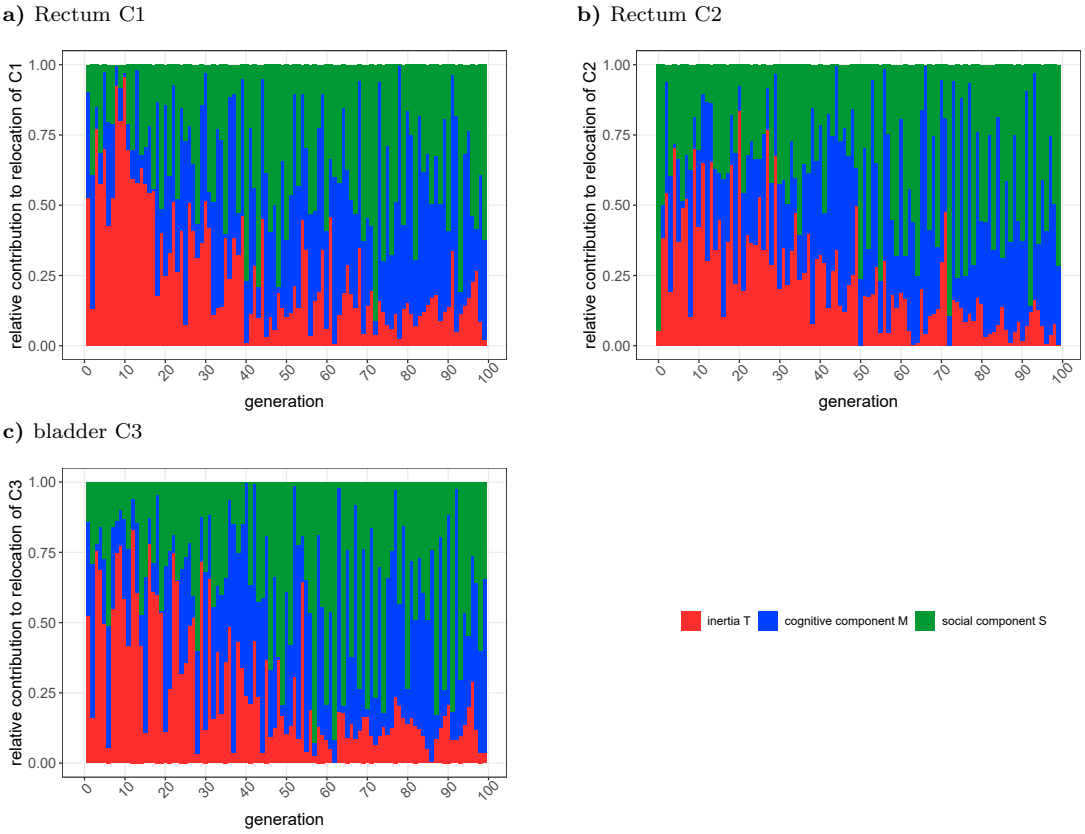

Figure 20: Analysis of relative contribution of the T inertia, M cognitive and S social component to the relocation vectors of the three optimized constraints over the course of PSO for PC03.

position, which is important to guarantee the exploration ability of the swarm. Figure 20 also shows that the cognitive and the social component can outweigh the inertia component. This is probably the case if the actual particle position is already far away from the particle's and swarm's best position. In that case, the large distance between particle and best positions will result in large relocation contributions by the cognitive and social components.

3.2 Analysis of exploration and exploitation ability

For two exemplary cases (PC03 and PC08), all positions visited in the search space during PSO were plotted (figures 21 and 22). The search space seems to be sufficiently explored, as all regions were visited at least once. The upper boundary was visited extremely often, which may be due to the handling of particles which hit the boundary of the search space. A further reason for this observation may be the fact that the final optimum often does not lie in the center of the search space, but is instead frequently located much closer to the upper boundaries. Consequently, the lower boundary was rarely visited, especially for the rectum and bladder high-dose constraints (C1 and C3). Nevertheless it is visible from the PQS that only poorly scored constraint combinations were found in this region, therefore it was not explored more deeply. The mid-dose constraint for the rectum (C2) is expected to take lower EUD values than the high-dose constraint. For that constraint, the lower boundary was also explored more often. The region around the final best-position seems to be most promising and was well exploited for both cases.
As mentioned before, the TPS Hyperion reduces non-binding constraints automatically during plan calculation. Therefore there may be a difference between the position defined by the constraint C_i value and the actual reached dose-effect G_i. This may cause a misinterpretation of the position. To further evaluate this, in figures 21 and 22 e) to h) the particle positions defined by the achieved dose-effects are plotted. Unbinding constraints are expected to occur in the region above the optimum position. By plotting the positions defined by dose-effects, it appears as if this region was never visited, which however is not correct. Consequently, to analyze exploration and exploitation ability, both position definitions are needed. It is noticeable that the lowest scored plans were below the final best position. Above the final best position, plans scored worse than the final best position, but not as bad as the lower ones. Nevertheless, the final best position is clearly visible as the global optimum in the optimization space. In figures 21 and 22 f), where the dose-effects for the two rectum constraints are plotted, the two tails visible in the lower left quadrant seem to be characteristic. They might be explained by the interplay between these two constraints. The C1 constraint is intended to control the high dose region in the rectum, whereas the C2 constraint controls the intermediate dose region. But it is obvious that if the high-dose is heavily restricted, the mid-dose should also be lower. Therefore the combination of a strict high-dose constraint C1 and a loose mid-dose constraint C2 was inherently corrected by reaching a better dose-effect for C2 than requested. This is also applicable vice versa.

In figure 23, the search space is plotted including all positions visited by single particles. The color distinguish particles and again positions are defined by constraints or dose-effects. It is shown that all particles explored the entire search space randomly and that they were not restricted to either exploration or exploitation.

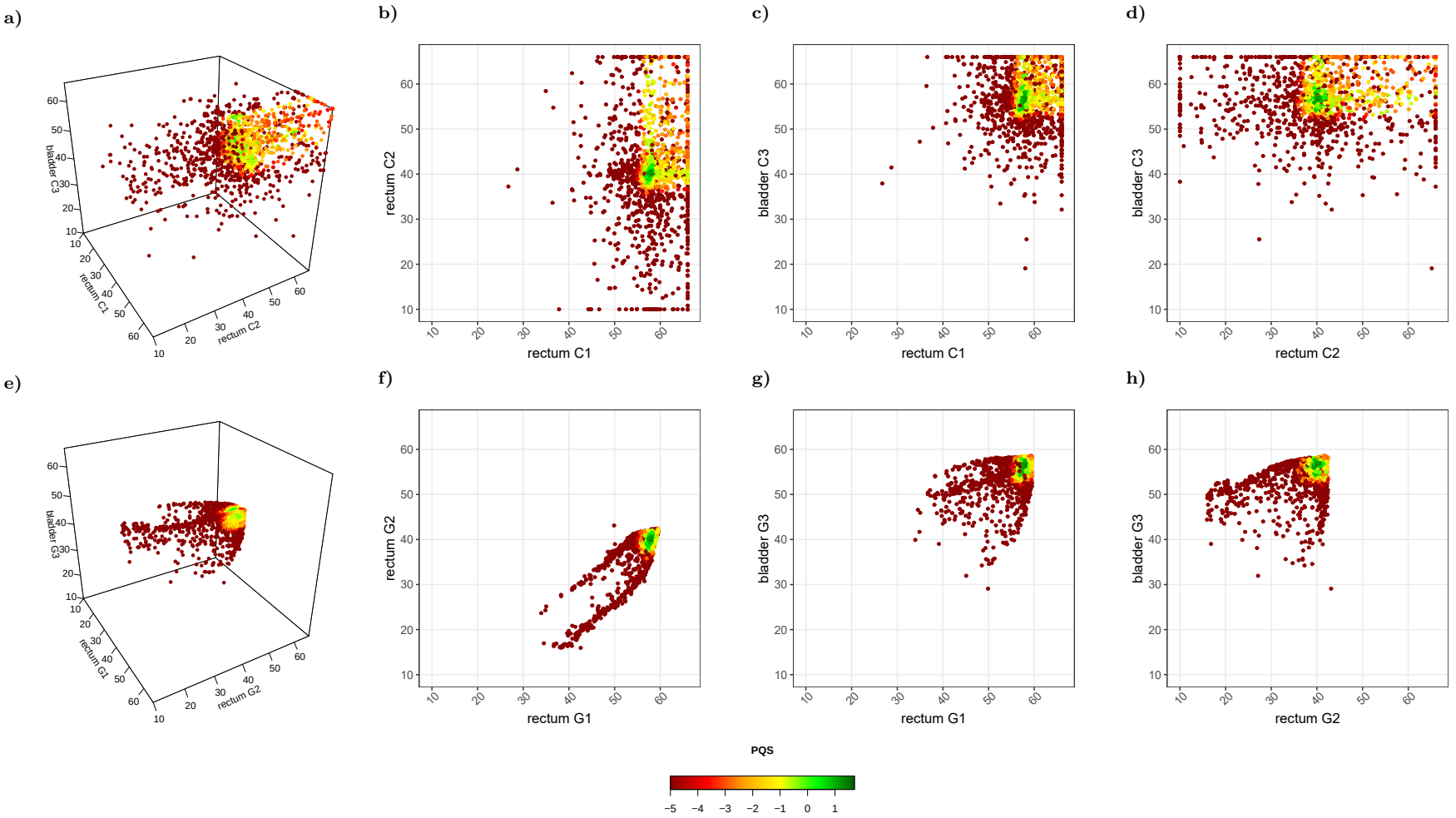

Figure 21: Positions visited in the search space for case PC03 in 3D and 2D plots. For sub-figures a) to d) position is defined by constraints C_j and for sub-figures e) to h) by reached dose-effects G_j.

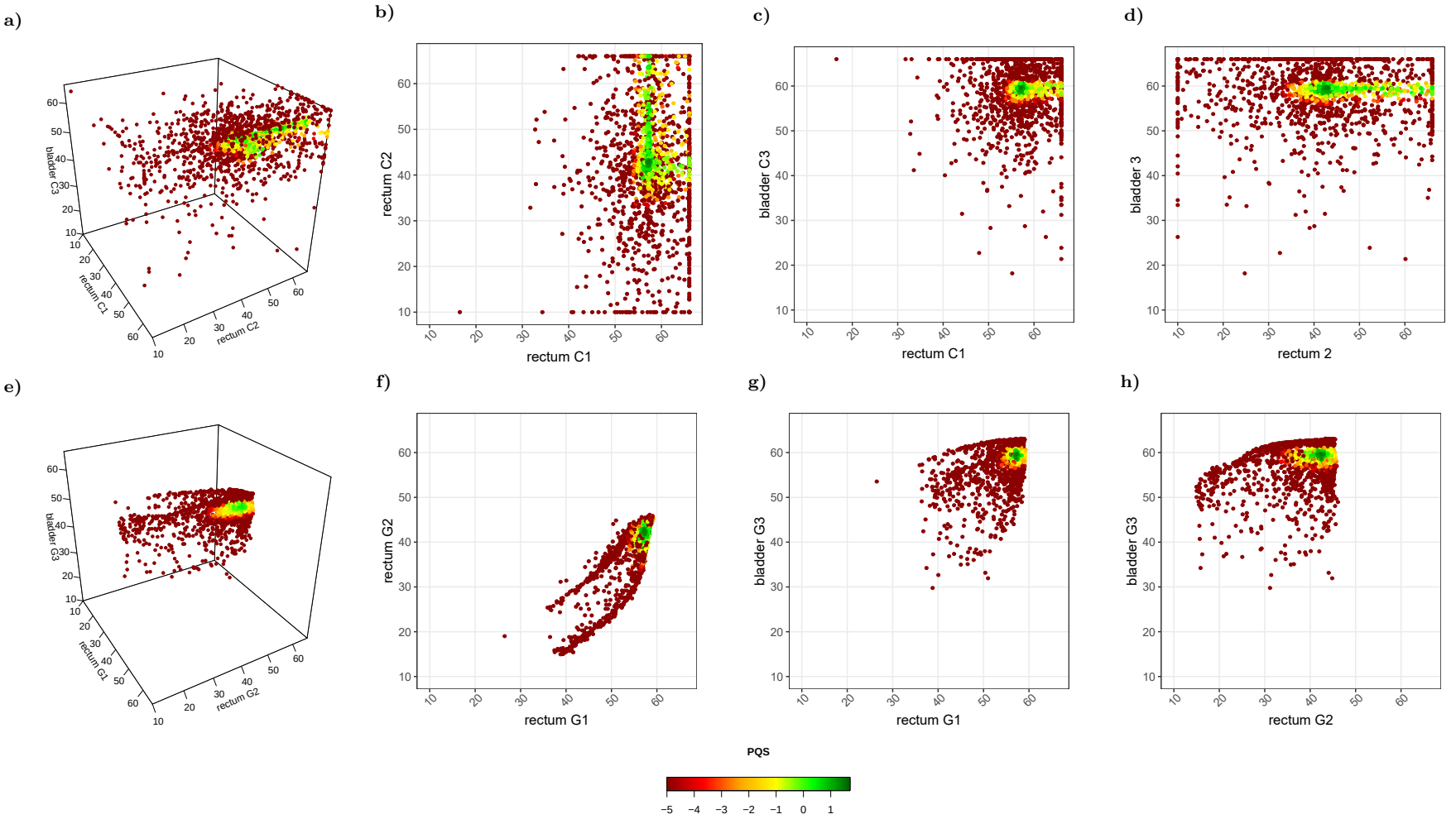

Figure 22: Positions visited in the search space for case PC08 in 3D and 2D plots. For sub-figures a) to d) position is defined by constraints C_j and for sub-figures e) to h) by reached dose-effects G_j.

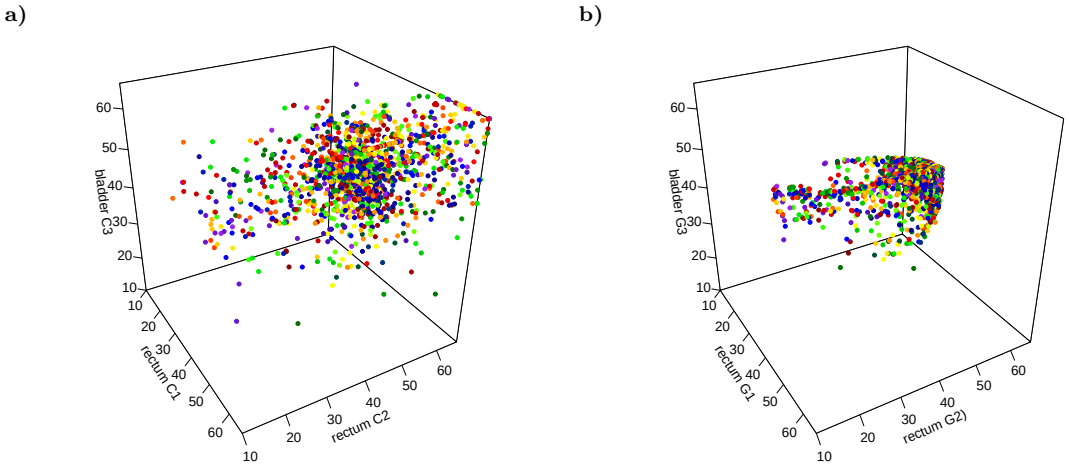

Figure 23: 3D plots of all positions visited in the search space during the course of PSO for PC03. The color distinguish the 30 different particles. In sub-figure a) positions are defined by constraints C_j and in b) by dose-effects G_j.

To further analyze the exploration ability, the search space was divided into eight sub-search spaces. All sub-search spaces had their origin at the final best position of the individual cases. A frequency polygon of the distances between all visited positions and the final best position is plotted in figure 24. As the distance between actual and final best position is relative, the information for all 10 cases can be combined in one plot. The frequency polygons for all 8 sub-search spaces followed the same behavior, the most frequent distance for all sub-search spaces was between 0.0 and 1.0 Gy or 1.0 and 2.0 Gy. After the peak, the frequencies dropped off immediately and the tail leveled out to the maximum distance. For all 8 sub-search spaces, there were more particles close to the final best position than far away, indicating a good exploitation. Nevertheless all sub-search spaces also presented higher distances, indicating particles far away from the optimum and therefore describing the exploration ability. The maximum distance in all search spaces was on average 44.70 Gy (range 31.92 - 52.65 Gy). The wide range of maximum distances was due to the different absolute sizes of the sub-search spaces, as the final best position was not in the center of the search space. In all 8 sub-search spaces positions close to the final best position were visited, as indicated by the average (range) minimum distance of 0.01,Gy (0.00 - 0.02 Gy). The average median distance was 3.96 Gy (1.51 - 5.46 Gy). As with increasing distance to the final best position the sub-search space gets wider, an average median distance of 3.96 Gy compared to the average maximum distance of 48.43 Gy indicates that more particles visited positions close to the final best position than far away. For details, see table 3. This is again an indicator for a good exploitation of the region around the final best position.

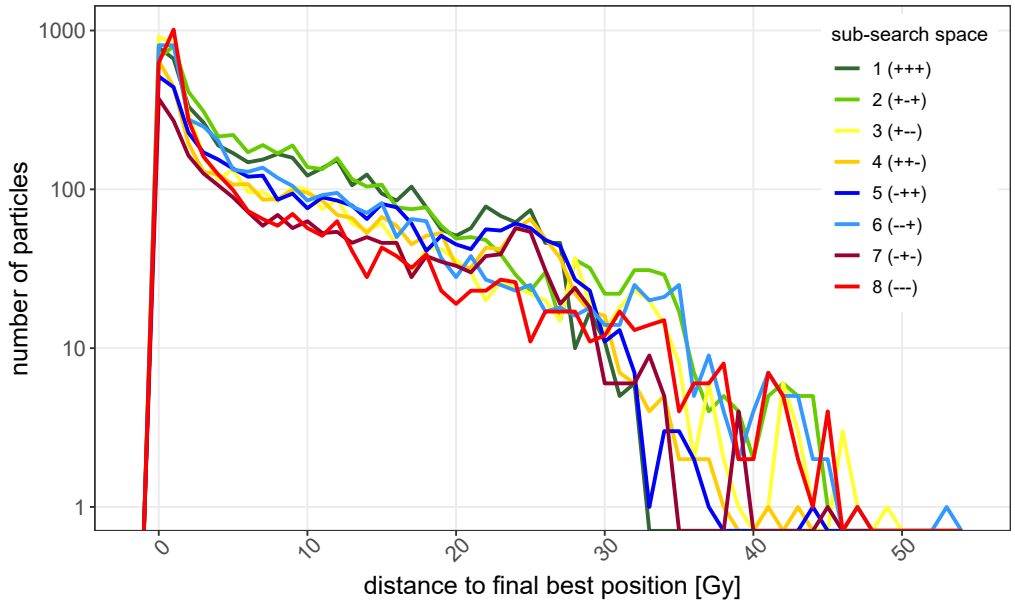

Figure 24: Frequency polygon of the distance between actual positions and final best position (note the logarithmic scaling). The search space is divided into 8 sub-search spaces, + means that the constraint defining the actual position is greater than the final best position, - indicates that it is lower. Therefor in sub-search space 1 (+++) all three constraints values are higher than the final best position. This represents the upper right front corner in the 3D plots in figure 21.

Table 3: Minimum, median, maximum and most frequent distance between final best position g_{best} and positions $x_{i,d}$ visited during course of PSO for the eight sub-search spaces over all 10 cases.

sub-search space	min [Gy]	median [Gy]	max [Gy]	most frequent [Gy]
1	0.00	4.97	31.92	1.0 - 2.0
2	0.01	4.77	44.54	1.0 - 2.0
3	0.01	1.99	49.40	1.0 - 2.0
4	0.01	4.59	42.80	1.0 - 2.0
5	0.01	5.46	44.19	1.0 - 2.0
6	0.01	3.09	52.65	1.0 - 2.0
7	0.01	5.31	45.12	1.0 - 2.0
8	0.02	1.51	46.96	1.0 - 2.0

The optimization parameter ω was decreased during optimization to promote a global search, i.e. exploration, in the beginning of PSO and a more local search, i.e. exploitation, during the end. This behavior is visualized in figure 25, where frequency polygons as a function of the distance to final best position for 10 groups of generations are shown. During generation 0 - 9, the frequency polygon is shallow and the most frequent distance is 8.0 - 9.0 Gy. Nevertheless there were also particles close to and far away from the final best position, as indicated by the minimum and maximum distances in table 4. Until generation 29 the particles seem to spread out, as the peak of the frequency polygon is shifted up to a distance of 12.0 - 13.0 Gy (see table 4). The maximum distance was also reached in the beginning of the PSO between generations 10 and 19. During the course of PSO, the most frequent distances in the frequency polygons are shifted towards smaller distances and at the same time the height of the peak increases. This is again an indication for exploration ability in the beginning of PSO, whereas during the course of PSO exploitation is becomes more important.

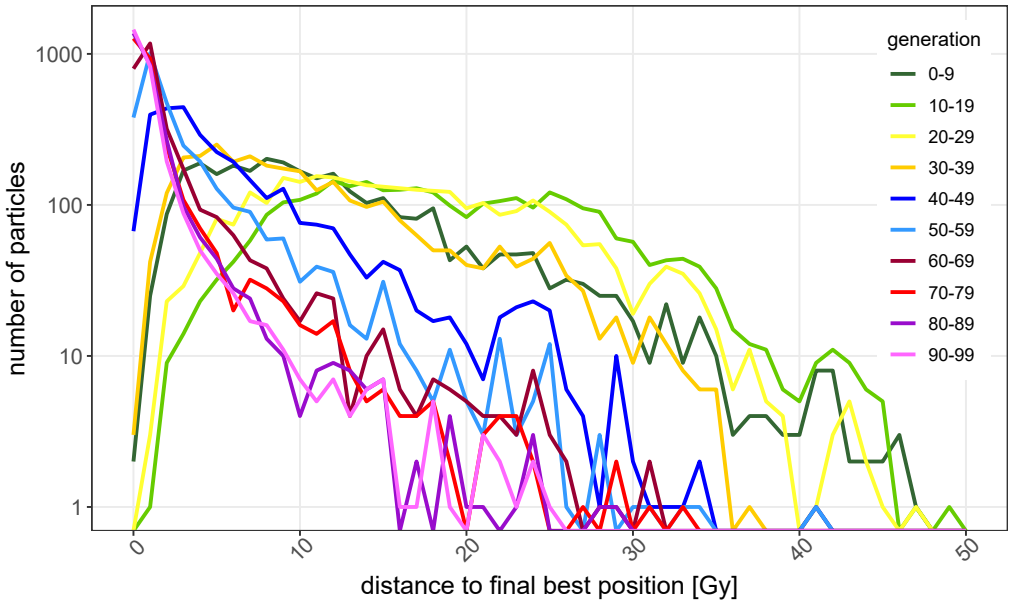

Figure 25: Frequency polygon of the distance between actual position and global best position over all 10 cases (note logarithmic scaling). The data is grouped by blocks of 10 succeeding generations.

Table 4: Minimum, median, maximum and most frequent distance between final best position g_{best} and positions $x_{i,d}$ visited during PSO over the generations.

generation	min [Gy]	median [Gy]	max [Gy]	most frequent [Gy]
0-9	0.32	10.18	46.96	8.0 - 9.0
10-19	1.46	18.05	52.65	12.0 - 13.0
20-29	0.79	15.52	47.02	11.0 - 12.0
30-39	0.20	8.99	41.14	5.0 - 6.0
40-49	0.17	3.93	40.57	3.0 - 4.0
50-59	0.00	1.66	41.02	1.0 - 2.0
60-69	0.00	0.95	31.05	1.0 - 2.0
70-79	0.00	0.61	33.08	0.0 - 1.0
80-89	0.00	0.52	28.60	0.0 - 1.0
90-99	0.00	0.47	25.40	0.0 - 1.0

3.3 Comparison of manual and PSO plans

PSO was able to propose treatment plans for all 10 cases. The PSO was considered successful if the particle's best position values stabilized after 100 generations.
9 out of 10 PSO plans were clinically applicable as proposed, one case (PC01) was of inferior quality. To assess the clinical applicability of the PSO plans, they were compared to manual plans. To test if PSO and manual plans showed significant differences, a Wilcoxon signed rank test with Bonferoni correction was carried out (for details see 2.5.2).
The median (range) PTV EUD was 65.4 Gy (64.7 - 66.0 Gy) in manual plans and 65.3 Gy (62.5 - 65.6 Gy, $p = 1$) in PSO plans. The near minimum dose $D_{98\%}$ was comparable for manual and PSO plans with 62.9 Gy (61.7 - 63.6 Gy) and 62.8 Gy (59.4 - 63.1 Gy, $p = 1$), respectively. Also near maximum dose $D_{2\%}$ did not show significant differences, with 67.7 Gy (67.4 - 68.0 Gy) for manual plans and 67.9 Gy (67.5 - 68.1 Gy, $p = 1$) for PSO plans. However, PSO plans presented significantly improved rectum high dose sparing by better respecting the limit for $D_{2\%}$ with 66.1 Gy (64.7 - 66.5 Gy) compared to 67.0 Gy (66.5 - 67.5 Gy, $p = 0.016$) for manual plans. For rectum $V_{60\text{Gy}}$ and $V_{40\text{Gy}}$ no significant differences between manual and PSO plans were reported. Manual plans reached median $V_{60\text{Gy}}$ of 22.7 % (12.0 - 34.7 %) and $V_{40\text{Gy}}$ of 47.6 % (38.5 - 63.5 %) and PSO plans median $V_{60\text{Gy}}$ of 22.4 % (13.0 - 33.4 %, $p = 1$) and $V_{40\text{Gy}}$ of 52.7 % (47.6 - 64.9 %, $p = 1$). Evaluated bladder dose-volume parameters were comparable with near maximum doses $D_{2\%}$ of 66.7 Gy (66.0 - 67.3 Gy) for manual plans vs. 66.7 Gy (63.3 - 67.2 Gy, $p = 1$) and $V_{60\text{Gy}}$ of 27.6 % (14.3 - 57.3 %) vs. 27.5 % (12.9 - 48 %, $p = 1$). A boxplot summarizing the evaluated DVH parameters is provided in figure 26. The resulting values for all evaluated parameters for manual and PSO plans are reported in table 5.

In total, 9 out of 10 PSO plans for postoperative treatments were clinically meaningful. In figure 27, PC03 is shown as example for successful PSO planning and is compared to the accepted manual RT treatment plan. Three representative slices showing coronal, sagittal and axial views of the dose-distribution are provided for the manual (figure 27a) and the PSO plan (figure 27b). At a first glance, the dose distributions do not differ strongly. Deviations are visible for the high-dose isolines at the interface between rectum and PTV, especially in the axial and sagittal views, which are more conformal in PSO plans, indicating better rectum sparing. As is clearly visible in all three views, bladder sparing was inferior for the PSO plan, with the high and intermediate isodoselines reaching further into the bladder. This is

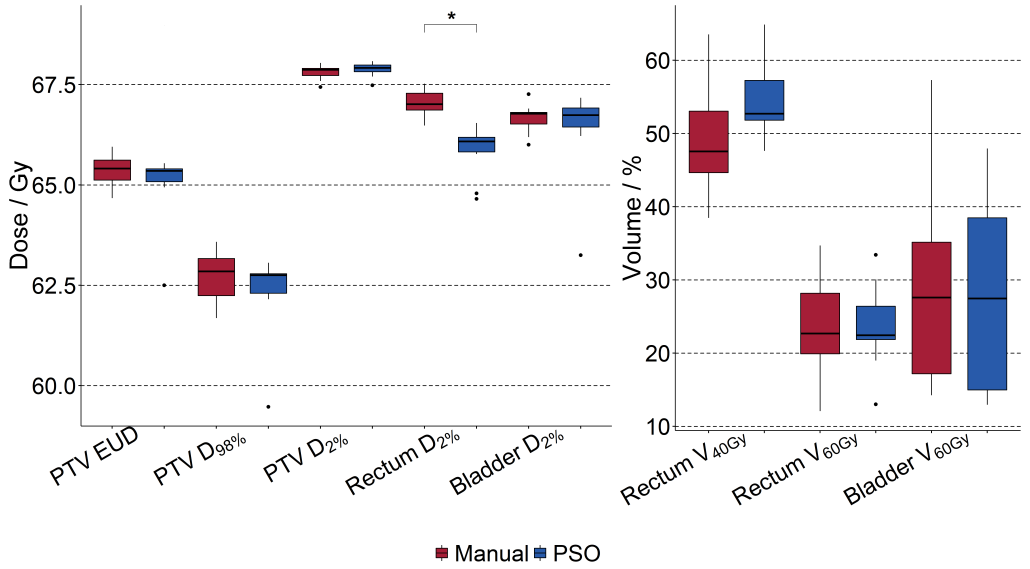

Figure 26: Boxplots showing the distribution of DVH parameters for the 10 cases (*p<0.05). *Reprinted from* [70] *with permission from Elsevier.*

also clearly visible in the DVH provided in figure 27 c). With 66.2 Gy the PSO plan nearly satisfied the preset of a rectum $D_{2\%}$ smaller than 66 Gy, but the manual plan did not adhere to this restriction ($D_{2\%} = 67.5$ Gy). To reach this limit, the bladder was exposed to a slightly higher dose, demonstrated by a $D_{2\%}$ of 66.8 Gy in manual plan vs. 67.2 Gy in the PSO plan and also in the volume parameter $V_{60\text{Gy}}$ where in the manual plan only 23.5 % of the bladder volume were exposed to 60,Gy, whereas for PSO $V_{60\text{Gy}}$ it was 28.6 %.

Figure 28 presents dose distributions for the manual and PSO plans of PC01. This was the only case where the resulting PSO plan was not clinically meaningful because of the poor target dose coverage. Figure 28 c) provides a DVH comparison clearly showing that the human planner decided to exceed the bladder $V_{60\text{Gy}}$ restriction ($V_{60\text{Gy}} < 50\,\%$) to fulfill the PTV prescription (c.f. to arrow). The PSO is restricted by the definition of the PQS, where exceeding of the pre-defined DVH parameters is strictly penalized. Therefore the PSO is unable to mimic this decision and hence the proposed plan is clinically not acceptable.

a) manual **b)** PSO

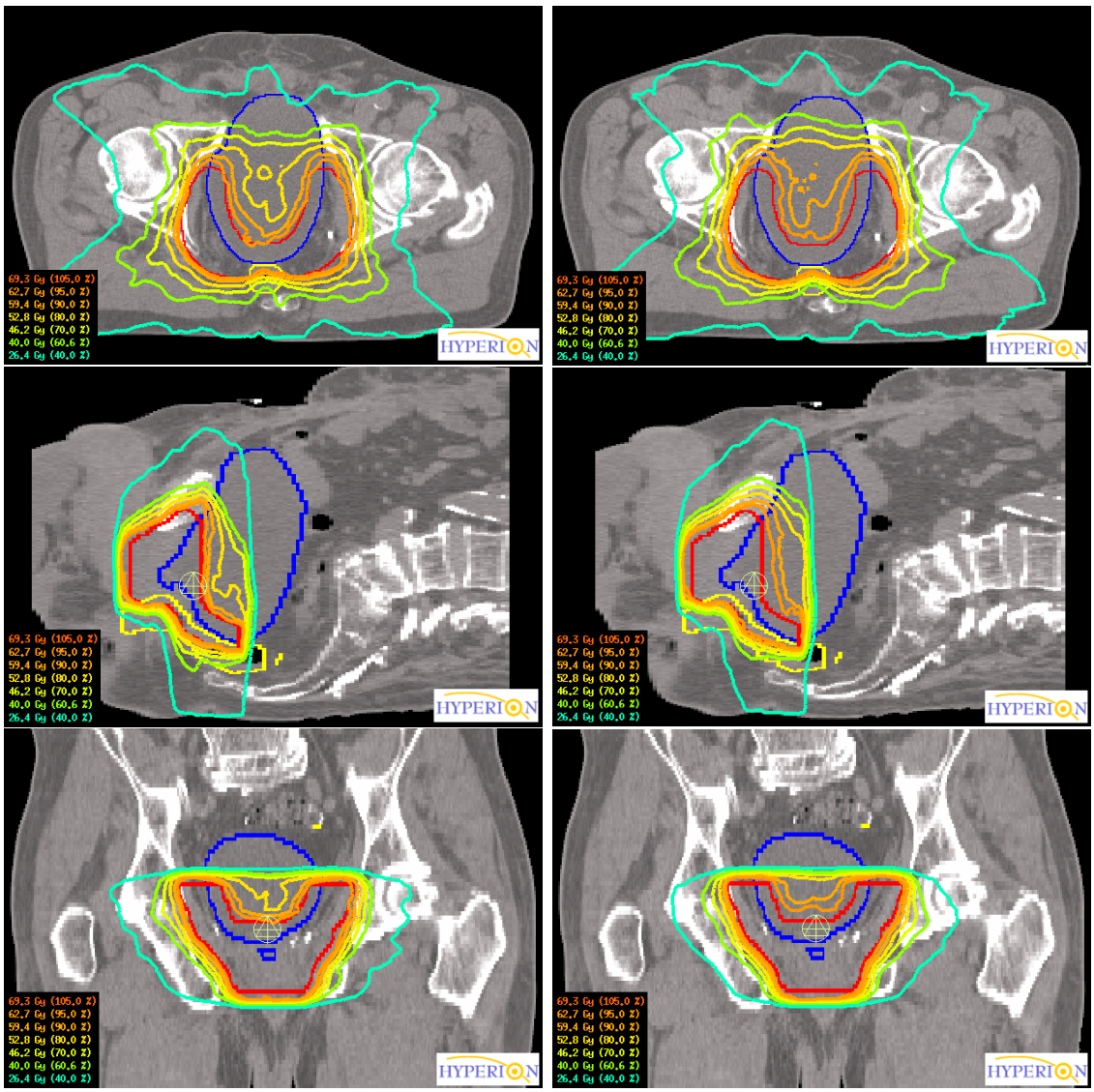

c) DVH comparision

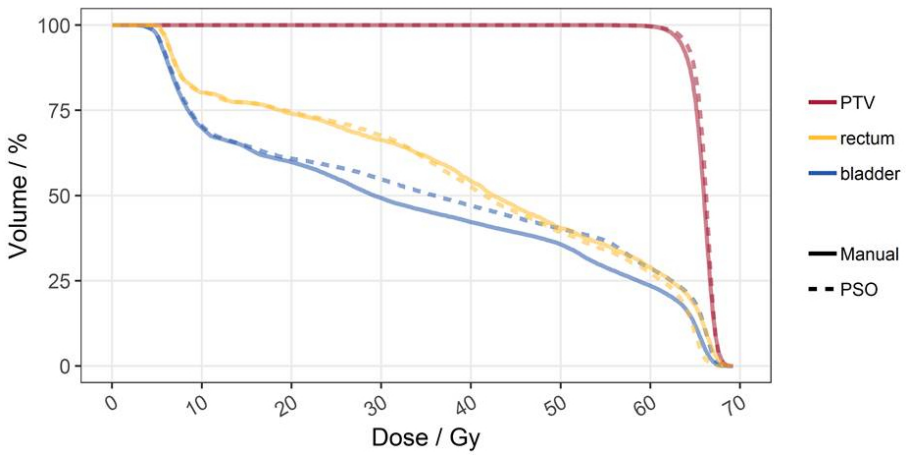

Figure 27: Case PC03 as representative example for the 9 successful cases: dose distribution in three representative slices of manual plan (a), PSO plan (b) and DVH comparison (c). For PC03, a better rectum high dose sparing could be reached while accepting slightly inferior bladder sparing. *Augmented from* [70].

a) manual **b)** PSO

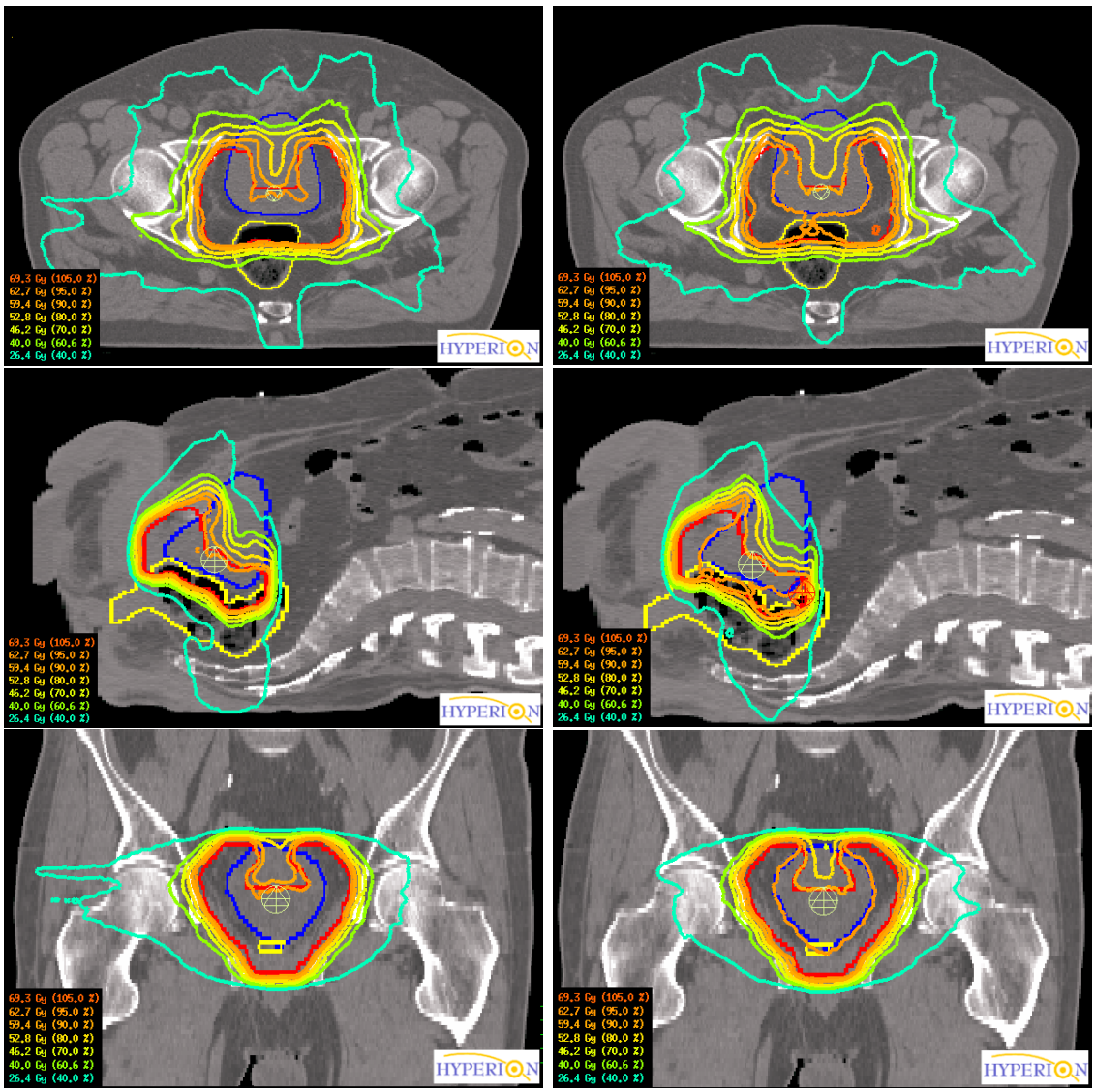

c) DVH comparision

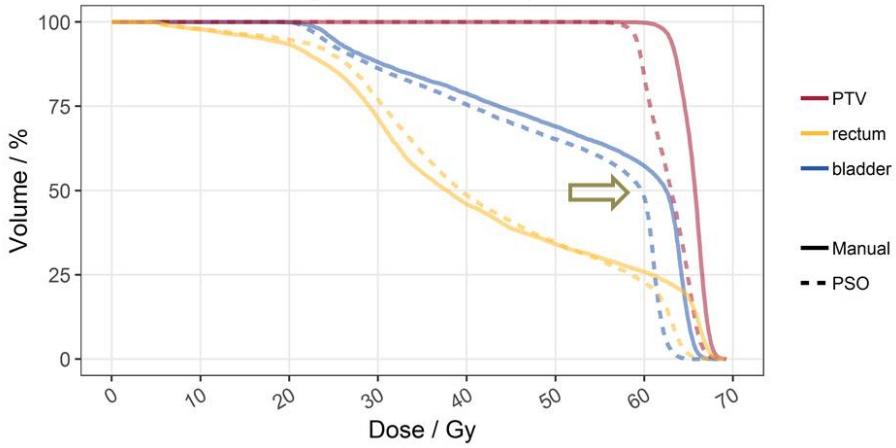

Figure 28: Dose distribution in three representative slices of manual a) and PSO b) plans and DVH comparison c) of case PC01. This is the only case where PSO could not propose a clinically acceptable plan. During manual planning, it was decided to violate the bladder $V_{60\mathrm{Gy}} < 50\,\%$ restriction to ensure dose coverage of the PTV (c.f. arrow). As PSO strictly respects the given restrictions, it is impossible to reflect this decision during automatic planning. *Augmented from* [70].

Table 5: Evaluated DVH parameters, MU and segments per plan and total score for all 10 cases for manual and PSO plans. If one of the plans adhered better to the pre-defined clinical goals, it is highlighted in bold. *Reprinted from* [70] *with permission from Elsevier.*

		PC01		PC02		PC03		PC04		PC05		PC06	
		Man	PSO	Man	PSO	Man	PSO	Man	PSO	Man	PSO	Man	PSO
PTV	EUD [Gy]	**64.8**	62.5	65.2	**65.3**	65.1	**65.3**	**65.6**	65.5	**65.9**	65.5	**65.8**	64.9
PTV	D98% [Gy]	**62.1**	59.5	62.3	**62.7**	62.2	**62.7**	**63.2**	63.1	**63.6**	62.8	**63.2**	62.2
PTV	D2% [Gy]	**67.9**	68.1	68.0	68.0	67.9	**67.8**	67.9	67.9	**67.8**	67.9	**67.7**	68.0
Rectum	D2% [Gy]	67.4	**64.8**	66.7	**66.1**	67.5	**66.2**	67.2	**66.4**	67.0	**66.1**	67.0	**65.8**
Rectum	V40Gy [%]	**45.9**	48.7	**44.2**	52.8	54.3	**52.7**	**46.9**	58.7	**49.5**	53.0	63.5	**60.3**
Rectum	V60Gy [%]	25.9	**22.8**	**19.2**	23.5	28.9	**27.4**	21.8	21.8	19.4	**19.0**	34.7	**33.4**
Bladder	D2% [Gy]	**66.0**	63.3	66.7	**66.4**	**66.8**	67.2	66.5	66.5	66.8	**66.6**	67.3	**66.2**
Bladder	V60Gy [%]	57.3	**48.0**	14.7	**12.9**	**23.5**	28.6	14.2	**13.9**	16.6	**13.2**	33.4	**26.3**
MU		585.3	553.7	507.4	606.3	606.8	536.3	486.1	485.1	421.2	500.4	434.8	579.1
Segments		185	186	183	207	190	194	182	182	164	193	166	195
Total PQS		-16.43	**-5.98**	-0.99	**1.23**	-0.61	**0.43**	0.56	**0.78**	0.06	**0.99**	-1.95	**1.07**

		PC07		PC08		PC09		PC10		manual		PSO	
		Man	PSO	Man	PSO	Man	PSO	Man	PSO	Median	Range	Median	Range
PTV	EUD [Gy]	**65.6**	65.4	64.7	**65.4**	**65.4**	65.0	**65.5**	65.4	65.4	64.7 - 66.0	65.3	62.5 - 65.5
PTV	D98% [Gy]	**63.3**	62.8	61.7	**62.8**	**62.7**	62.2	**63.0**	62.8	62.9	61.7 - 63.6	62.8	59.4 - 63.1
PTV	D2% [Gy]	**67.4**	67.5	68.0	**67.9**	**67.9**	68.0	**67.6**	67.7	67.7	67.4 - 68.0	67.9	67.5 - 68.1
Rectum	D2% [Gy]	66.9	**66.2**	67.3	**65.9**	66.6	**66.5**	66.5	**64.7**	67.0	66.5 - 67.5	66.1	64.7 - 66.5
Rectum	V40Gy [%]	58.2	**51.6**	**42.7**	52.5	48.2	**47.6**	**38.5**	64.9	47.6	38.5 - 63.5	52.7	47.6 - 64.9
Rectum	V60Gy [%]	23.6	**22.0**	**21.4**	22.0	30.5	**30.0**	**12.1**	13.0	22.7	12.0 - 34.7	22.4	13.0 - 33.4
Bladder	D2% [Gy]	**66.8**	66.9	**66.2**	67.0	66.9	66.9	**66.8**	66.9	66.8	66.0 - 67.3	66.7	63.3 - 67.2
Bladder	V60Gy [%]	**31.7**	38.0	**41.4**	45.6	19.0	**18.2**	**35.7**	38.6	27.6	14.3 - 57.3	27.5	12.9 - 48.0
MU		488.4	490.1	621.1	545.4	511.3	563.2	594.7	540.5	525.7	421.2 - 621.1	540.0	485.1 - 606.3
Segments		192	196	196	189	188	202	201	199	185	164 - 201	194	182 - 207
Total PQS		-0.65	**1.31**	-1.40	**6.25**	**-0.20**	-0.85	**1.08**	0.83	-0.82	-16.43 - 1.08	0.91	-5.98 - 6.25

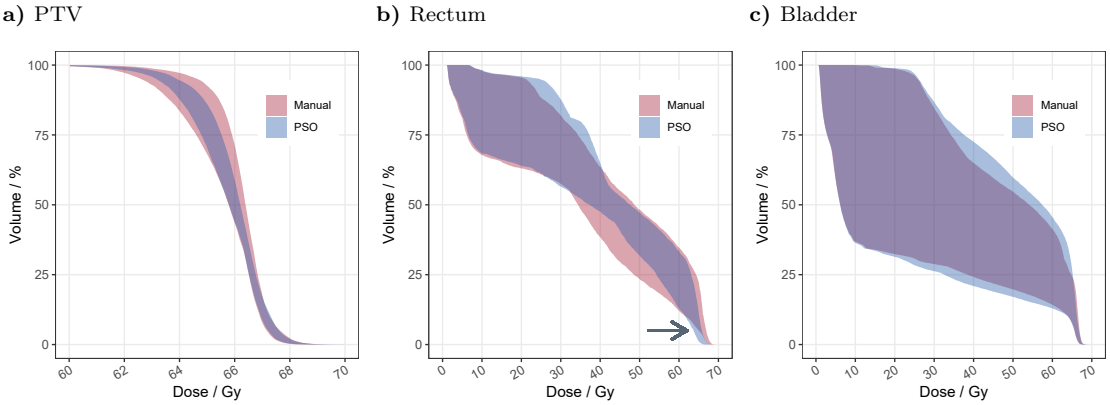

Figure 29: Comparison of the DVH spread for PTV a), rectum b) and bladder c) for cases PC02 - PC10. The colored DVH band comprises all individual DVHs of patients with clinically acceptable PSO plans (PC02 - PC10). The arrow in b) highlights the high dose region, where manual and PSO plans are clearly separated. *Augmented from* [70].

Figure 29 presents DVH comparisons for all 9 clinically acceptable plans (PC02 - PC10) for PTV, rectum and bladder. The clinically unacceptable plan for PC01 was excluded from this analysis. For a DVH analysis for this case, see the previous paragraph and figure 28 c). For figure 29, for each dose bin minimum and maximum volume fractions for all 9 individual DVHs were plotted. Therefore all individual DVHs are included in the shaded areas. An indication for the lower inter-plan variation in PSO plans is the narrower band, especially in the PTV DVH in figure 29 a) and in the rectum high dose region in b). This is also encouraged by the lower interquartile range for PTV parameters in the boxplot of figure 26. The DVH comparison also clearly shows the better rectum high-dose sparing in PSO plans, as in the high dose region the bands for PSO and manual plans are clearly separated (c.f. figure 29 b)). Patient individual bends in the PQS caused a broader range for volume parameters, such as $V_{40\mathrm{Gy}}$ and $V_{60\mathrm{Gy}}$. As the bladder filling extremely influences the possible dose sparing and hence reachable dose-volume constraints, this is even more pronounced in the dispersion of bladder DVHs (c.f. figure 29 c)). These points are also reflected in the boxplots in figure 26.

Figure 30 summarizes individual and total PQS for all 10 cases, supporting the presumption of comparable PTV EUDs for manual and PSO plans in most cases. Rectum $D_{2\%}$ always scored better in PSO plans than in manual plans, corresponding to better rectum high dose sparing. Rectum $V_{60\text{Gy}}$ also scored better in PSO plans, also indicating better rectum dose sparing in PSO plans. This is however partially reached due to inferior rectum $V_{40\text{Gy}}$ in PSO plans. But $V_{40\text{Gy}}$ is within the restriction defined by the SOP, whereas especially rectum near maximum dose ($D_{2\%}$) was normally exceeded in manual plans.
For 8 out of 10 cases, the total PQS was higher in PSO plans than in to manual plans, which was to be expected as the PSO uses the PQS directly as guidance for the optimization. Conversely, a human planner in principle knows the same limits, but does not receive direct feedback about the PQS during the trial-and-error planning process. The total PQS seems to be mainly driven by the rectum $D_{2\%}$ PQS. In cases where manual plans scored much worse than PSO plans, e.g. case PC01, PC06 and PC08 in figure 30, the total PQS was also divergent. In contrast, for cases where rectum high dose sparing was comparable, e.g. case PC09, the total PQS was also comparable.

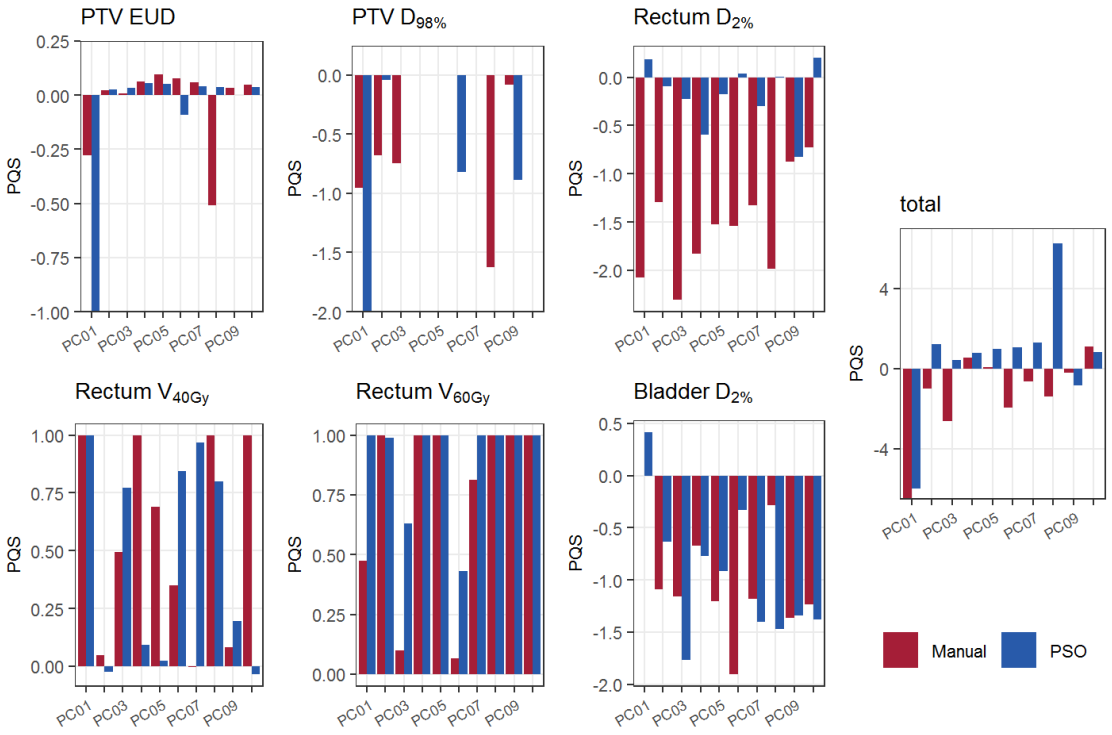

Figure 30: Overview of the individual scores for all 10 cases for manual and PSO plans. PTV $D_{2\%}$ is not presented as all cases fulfilled this parameter (PQS=0), bladder $V_{60\text{Gy}}$ is not presented as all cases obtained PQS=1, except for PC01:-14.60 manual and 0.41 PSO. *Reprinted from* [70] *with permission from Elsevier.*

4 Discussion

Modern RT treatment planning is an optimization problem, as the prescribed tumor dose needs to be reached, while OARs have to be spared from dose burden as much as possible. Inverse planning aims to achieve this by using constraints and objectives. A constraint is a prerequisite that has to be fulfilled, whereas an objective should be adhered to as much as possible. Depending on the patient's anatomy, individual trade-offs between constraints and objectives have to be defined. Therefore the formulation of the optimization problem is challenging, whereas the solution of the problem is well known. To find a good plan for each individual patient, the treatment planner has to try out different combinations of objectives and constraints. As this is a time consuming trial-and-error process, automatic planning has gained attention in recent years [1–7]. Although some of these approaches are already implemented in clinical practice, planning automation is still an active field of research. The usage of non-convex constraint functions and the increasing complexity of search spaces are particularly demanding. Statistical optimization techniques such as genetic algorithm (GA) and particle swarm optimization (PSO) entered into the field to address this requirements [58–64].

In the presented work, an automatic planning approach based on PSO was proposed and implemented. The plans were generated by using the TPS Hyperion, which uses constrained optimization to generate pareto-optimal plans. Nevertheless, the planner needs to balance the constraints to turn a pareto-optimal plan into a clinically acceptable plan by trying different combinations of planning constraints. This trial-and-error process can be seen as a manual exploration of the pareto-surface, which may however be ineffective and biased by the planner's experience. An automatic exploration of the pareto-surface was already introduced by Craft et al. [49, 50]. The automatic PSO planning approach proposed in this thesis can be seen as an efficient way to explore the pareto-surface, as it is able to automatically select an optimal, clinically acceptable plan for individual patients. Throughout this discussion the quality of the implementation is discussed (section 4.1), followed by a comparison to other automatic planning approaches in section 4.2. The section concludes with comments on the proof-of-principle study on n=10 post-operative prostate treatments.

4.1 Implementation of PSO for RT planning

Overall, the analysis of the PSO implementation for RT planning showed that the PSO is able to converge to a clinically meaningful position in the search space and that this position is a global optimum. A good balance between exploration in the beginning and exploitation of the global optimum throughout the PSO was also shown. Nevertheless, there is potential for future improvements, for example with regard to the implementation of the PSO as well as the PQS.
In section 3.2, it was mentioned that particles can be trapped at the boundary, because of how particles hitting the boundary are treated in the software. A particle that hits the boundary has a relocation vector pointing outside the search space. In the beginning, when the inertia weight is still high, it can take some generations until the attraction to the local and global optimum, pulling the particle back into the search space, can outweigh the inertia component. Hence, the particle will be trapped at the boundary for several generations. As the optimum PSO plan is not expected to lie on the boundary, this over-exploration of the boundary is unnecessary. To avoid this, the procedure for particles hitting the boundary should be changed. A potential solution to this may be to reflect the particle back into the search space. But this will cause a relocation vector which is not related to any attraction point, i.e. neither to the local nor global best position. Yet a simpler approach would be to stop the particle at the boundary, i.e. setting the relocation vector to 0 Gy. Then the local and global best positions will act as attraction points and will bring the particle back into the search space. While the inertia component would be irrelevant in this approach, it nonetheless seems rational given that the particle was facing outside the search space, i.e. into a clinically irrelevant region.
The 3D-plots of all positions visited in the search space (figure 21 and 22) clearly demonstrate that the exploration ability of the implemented PSO is good. The exploitation ability around the final best positions also seems to be sufficient. Nevertheless, in the plots of the positions defined by constraints there seem to be local optima, i.e. well scored positions close to the final best position, which are not further exploited. It could be shown, that this observation is a misinterpretation of particle position. Due to a feature of the TPS Hyperion for plans defined with non-binding constraints, the achieved dose-effect will be lowered thoroughly. Therefore a position definition by achieved dose-effects was additionally plotted in figures 21

and 22. With this improved position definition, it is evident that the PSO was able to find the global optimum. This difference in position definitions may however mislead the PSO, as it introduces a discrepancy between supposed position of a plan on the pareto-surface and the actual true position of the plan. As the actual position of a particle $x_{i,d}$, the particle's best achieved plan ($p_{best,i}$) and also the swarm's best position (g_{best}) are used to calculate the relocation for the subsequent generation this discrepancy could affect the position update. The improved position definition might be considered in a future implementation. By implementation of this updated position definition using dose-effects G_j instead of constraints C_j, the problem of particles sticking to the boundary can potentially also be solved, as these particles were all affected by tightening of non-binding constraints. This is shown in figures 21 and 22 d) to f), where no particles hit the boundary. But still this may only be sufficient with a reset of the inertia component of the relocation vector, because otherwise inertia would still point outside the search space. And as shown in the beginning of PSO where inertia is the driving force for relocation, this may cause the particle to be thrown back to the search space boundary. It should also be evaluated if the discrepancy between position definitions can mislead the optimization to a final best position with non-binding constraints. This should be done in conjunction with the definition of the PQS, because in general plans with non-binding constraints may contradict defined dose sparing for OARs, and therefore should be scored lower. Nevertheless, the plots with positions defined by constraints show that combinations with non-binding constraints also scored well, although they did not reach the best score.

Currently the search space is large, especially in the direction towards the lower boundary. However, it was shown that this huge search space is only explored during the first PSO generations and that in later generations, the optimization focused on the more promising region around the final best position. In terms of efficiency and convergence speed, it may be possible to shrink the search space from the beginning. But it is visible from the two rectum constraints that this shrinking need to be in close connection to the meaning of the constraints, as a constraint which controls the low or intermediate dose region in an OAR will take lower values than a high-dose constraint and may also show more intra-patient variation. It was also shown, that constraints are interacting with each other. Especially if two constraints control different regions of the DVH for the same OAR. Therefore it could be promising to restrict the search space to meaningful combinations of such constraints. In the example of two rectum constraints, where one restricts the high dose and one the intermediate dose region, it seems to be obvious that the intermediate dose constraint

should be set to a lower EUD level than the high dose constraint.
As described in section 3.1, the ability of the constraints to converge and the ability to meet the set convergence criterion of $\pm 0.1\,\%$ difference in mean constraint in subsequent generations and an interval of less than 1 Gy between maximum and minimum constraint differs over the three constraints. It is noticeable that the rectum constraint $C1$ converged in all cases whereas the interval criterion for the second rectum constraint $C2$ was never met and for the bladder constraint $C3$ only in 4 out of 10 cases. Nevertheless, it is notable that for some cases the termination criterion was nearly met. From the analysis it is not clear why this difference occurs. However, as the convergence was fully reached for one constraint, it is evident that this is not due to the implementation of the PSO. Instead, this probably arises from the definition of the PQS, which is critical for the success of the optimization. It should be further investigated if all constraints are depicted and balanced properly by the PQS.
The implementation used the Python random module, which is by default initialized by date and time of the server. The module gets reinitialized every time a Python script is called. As the implementation is constructed of several Python scripts (see section 2.1.2) which are controlled and iteratively executed by a bash script, the random module gets reinitialized several times. For an improved PSO implementation, the status of the random module should be tracked and then set with every recall of the Python script to fully utilize the random module.
Computation time is a key potential benefit off automatic planning approaches: preferably they should be faster than manual planners. Depending on the complexity of the intended treatment, an optimization time of 30 min for a simple prostate and up to several hours for complex head and neck VMAT treatments are realistic. Nevertheless the implemented automatic PSO planning is currently much slower. Currently, it takes around 3-5 min per plan to compute a plan on our server with 18 Intel® Xeon® Processors X5650. Thus, for a swarm of 30 particles executing 100 generations, the total computation time for 3000 plans is about 140 - 250 h, which at the moment impedes clinical application. As the implementation was not optimized for computation time for this study, time gain is probable with an enhanced implementation. As could be seen in the flowchart provided in figure 13, the computation of the individual plans per generation and the scoring are mutually independent. Therefore a straightforward way to speed up the PSO would be the parallelization of the plan computation within each generation. Computation on a graphics processing unit (GPU) is also not yet implemented for the TPS Hyperion and would boost the computation time per plan.

For the specific implementation, the choice of the inertia weight ω is crucial for the convergence ability and consequently influences the computation time for the entire PSO [74, 75]. As the inertia weight ω is intended to balance the exploration and exploitation ability of the swarm, a reduction seems to be reasonable. Currently, the inertia weight is reduced from 1.4 to 0.2 by 0.2 every 10th generation. A subject of further research should be the influence of different reduction schemes, such as linear functions of different steepness or other regimes promoting exploration or exploitation.

In the presented proof of principle study, post-operative prostate cancer cases were only planned using serial constraints. As serial constraints belong to the group of convex planning constraints, the search space was not expected to have local optima or discontinuities. This was verified by the plots in figures 21 and 22. Nevertheless, the full potential of a statistical optimization like PSO might only be visible for treatment planning problems with non-convex planning constraints. For a PSO implementation with non-convex constraints the search space might change tremendously and hence the number of particles I, the number of generations D and the inertia weight ω should be carefully chosen to ensure a good balance between exploration and exploitation and also to reach convergence to a global optimum.

4.2 Automatic PSO in comparison to other automatic planning approaches

In the past, different approaches to navigate the pareto-surface were explored. A first approach was introduced in 2006 by Craft et al. [49, 50]. They showed that by relying on a few pre-calculated pareto-optimal plans, the pareto-surface can be approximated by linear-combinations of these anchor points. The task of the manual planner is then to try out different linear-combinations. The planner thereby explores the pareto-surface manually. Afterwards, he or she has to decide which plan should be used for treatment. The calculation of the linear-combinations is fast and hence the planner can navigate the pareto-surface interactively. Another approach to calculate pareto-surfaces was recently introduced by van der Bijl et al. [54]. In this approach, the automatic planning approach iCycle [27] is used to compute 40 plans for cases in the training cohort. Afterwards, a super ellipsoid is used to fit the patient individual pareto-surface to this pre-calculated plans. By extracting anatomical features, a prediction model is developed, which has been successfully used to predict the pareto-surfaces for the cases in the validation cohort. The pareto-surface can then be evaluated by a human planner to explore planning trade-offs. The main difference between these two approaches and the presented automatic PSO planning in this thesis is that in the latter, the pareto-surface is explored automatically and quasi-continuously. The PSO approach therefor is far more expensive in terms of computational cost, which at the moment is around 150-200 h. Moreover, in the PSO approach the decision regarding the clinical plan is made by applying well-defined quality measures (PQS) and not by the subjective choice of a human planner. Another conceptual difference to the approach proposed by Craft et al [49, 50] is that the usage of linear-combinations of anchor points is inherently restricted to convex search spaces. The fit of an super ellipsoid in the approach of van der Bijl [54] is also restricted to a convex search space. In contrast, the statistical nature of the PSO is in principle capable of non-convex search spaces with local optima.

The Pinnacle AutoPlanning Module is already widely used in clinical routine planning for different treatment sites [19–25]. The approach uses voxel-based importance factors for sub-optimal regions of ROIs or DVH regions. These sub-optimal regions are automatically identified by comparing the actual case to a similar case in a database of previously treated patients. The quality of Pinnacle AutoPlanning is thus restricted by the quality of the plans in the database. The same inherent limitation applies all other automatic planning approaches which rely on a database

of previously treated patients, such as RapidPlan implemented for the TPS Eclipse. RapidPlan uses a model built from previously treated plans to predict feasible DVH constraints from the known patient individual anatomy [38].
Machine learning and deep learning also recently entered the field of automatic planning. With machine learning it is possible to predict single DVH points for individual patient anatomies, again on the basis of a model built form previously treated patients. As a DVH is not sufficient to judge plan quality and the 3D-dose distribution is equally important, deep learning is used to learn dose distributions for individual patients. Deep learning approaches showed promising solutions for the prediction of high dose regions around the PTV, but prediction of low dose regions and hence reliable prediction of OAR sparing is challenging [56, 57]. As plan quality is not only affected by the patients anatomy, but also by treatment accessories such as used machines or gantry angles, the solely usage of 3D-distributions may be insufficient. Deep learning may also identify dose distributions which are not applicable as at the moment only the final dose distribution is used as input for learning the model, whereas restrictions entered by the used LINAC are neglected.
A template based automatic planing approach is Erasmus iCycle, which uses predefined wishlists of hard and soft constraints [26, 27]. The whislist has a categorical order and defines the planning goals in descending priority. As the order and type of planning constraints are fixed, only the constraint value is altered patient specifically to meet as much of the planning goals as defined in the whislist. As described in section 1.4 the implemented 2-phase ϵ-constraint (2pϵc) optimization method has the hazard to be trapped at inferior objective combinations, where a small gain in a high prioritized OAR prevents a large dose sparing for a lower prioritized structure. This limitation is true for optimization techniques which rely on derivative information, but may be overcome by statistical optimization such as GA and the proposed PSO approach. In Erasmus iCycle this problem was solved by introducing the LRPM [36, 37] (for details see also 1.4). The LRPM uses tilted indifferent curves in the optimization space to define global trade-offs between conflicting objectives. In this manner, the method overcomes the trapping problem. However, it still uses derivative information and is therefore not applicable for non-convex objectives. Again, due to the statistical nature of the PSO, the optimization would in principle be capable to take non-convex functions into account, although this has not yet been demonstrated in practice. For the proof-of-principle study with post-operative prostate cases, only convex constraint functions were used.
Optimization with genetic algorithms (GA) belongs to the statistical nature-analogous optimization techniques, such as PSO. The approach implemented by Fiandra

et al. for automatic planning of prostate VMAT treatments using GA [58, 59] is conceptually similar to the presented automatic PSO planning. The GA optimizes the combination of rectum and bladder serial maximum constraints by adopting the natural concept of *survival of the fittest*. The implemented fitness function is straightforward:

$$FF = \sqrt{\frac{2(CI)^2 + 4(\frac{rAD}{PD})^2 + 2(\frac{bAD}{PD})^2 + (\frac{lfAD}{PD})^2 + (\frac{rfAD}{PD})^2}{10}} \tag{19}$$

CI and PD are conformity index and prescribed dose, whereas rAD, bAD, $lfAD$ and $rfAD$ are average doses of rectum, bladder and left and right femoral heads. Therefore, the fitness function is much simpler than the PQS used as fitness function for the PSO implemented in this study. But it should be mentioned that Fiandra et al. used a fitness function to score the option plans which evaluate PTV coverage and mean OAR doses, whereas in the optimization serial maximum constraints are used for rectum and bladder. Therefore, the fitness function evaluates a plan parameter which is only indirectly controlled during the plan optimization. Also the coverage of the target and mean OAR doses are not the sole criterion used to judge plan quality in clinical practice (see [59]). In contrast, the PQS used to evaluate plan quality in the PSO implementation is designed in a way to score all plan parameters which are evaluated clinically. This was done by adopting the institutional SOP in the PQS. Furthermore all the parameters included into the PQS were controlled by the optimization. For example the PSO optimized two rectum constraints. One for the high dose region, which is reflected by the individual PQS for near maximum dose $D_{2\%}$ and $V_{60\mathrm{Gy}}$. Whereas the second rectum constraint was to control mid dose constraint, which was reflected by the individual PQS for $V_{40\mathrm{Gy}}$. An interesting point in the fitness function proposed by Fiandra et al. is the normalization of the OAR mean doses to the prescribed tumor dose [58]. This makes the fitness function suitable for different prostate treatments with varying prescribed tumor doses. In contrast, the PQS in our PSO implementation is specifically designed for post-operative prostate treatments and the transferability to other prostate treatments is the subject of ongoing research. Another fundamental difference between GA and PSO is that GA is a statistical optimization which explores the search space at random: there is no interaction or sharing of knowledge about positions in the search space already visited. In contrast in PSO the sharing of knowledge is an inherent feature and the information regarding individual particles' best positions and swarm's global best position are directly taken into account to calculate position updates.
Some approaches for using PSO in the field of treatment planning have already been

proposed. The approach proposed by Yang et al. is similar to ours, as they used the PSO to set weighting factors in IMRT optimization [69]. Weighting factors and constraints are interchangeable objects in a multi-objective optimization. It is possible to define an optimization problem by setting the one ore the other and then the absent one is part of the solution. The principle idea is similar to the presented approach, a particle is considered a plan and the plan's position is then determined as a set of weighting factors or constraints. The position updates are computed by incorporating the information about particles' best and swarm's best positions in both approaches. Both approaches also use key points of the DVH as the basis of the evaluation function, called PQS in the presented approach. Nevertheless, the present approach uses one pre-defined PQS for the entire course of PSO, where the PTV coverage and the OAR sparing are considered concurrently. In contrast Yang et al. [69] use three different evaluation functions over the course of PSO: the first one should ensure PTV coverage. Once a satisfying plan is reached, the evaluation function is changed to evaluate high dose sparing for OARs and tries to minimize that dose burden, but at the same time the PTV coverage needs to be kept. The third evaluation function then evaluates the low dose sparing. They tested the implementation with 10 prostate cases, which were planned successfully. Comparison of DVHs showed that the manual planning and PSO planning reached similar solutions, if the same objective functions were used. Yang et al. enhanced the PSO implementation by integrating crossover and mutation strategies, known from GAs, mainly to avoid trapping at local optima [69]. Both PSO implementations showed that PSO is useful for automatic planning, nevertheless the crucial point is the evaluation of the candidate plans. Both implementations also presented successful evaluation strategies for simple prostate cases. However, the generalization for more complex planning tasks should be the focus of further research.

4.3 Proof of principle - PSO implementation for post-operative prostate RT

The automatic PSO planning was successfully implemented and tested for 10 post-operative prostate cancer cases. Manual planning relies on a trial-and-error process and therefore mainly on the planner's experience and time. In contrast, in automatic PSO planning even unlikely constraint combinations are explored by chance and the process is reproducible. In 9 out of 10 cases, PSO proposed a clinically acceptable plan. One case (PC01), where the proposed PSO plan offered insufficient PTV coverage, failed due to an unfavorable patient anatomy. The manual planner decided to exceed restriction of dose burden to the bladder to ensure the PTV dose. In difference to the manual planner, the PQS which guides the PSO is defined for a common clinical situation and reflects the criteria of the institutional SOP. Therefore, the PSO strictly adhered to the requested bladder $V_{60\mathrm{Gy}}$ specification and the PSO plan compromised the PTV dose to an unacceptable level of EUD=62.5 Gy. Sacrificing OAR restrictions to ensure PTV dose coverage is in the responsibility of the clinician and should be decided carefully and individually for each patient depending on the clinical situation. After discussion with the clinician, the planner can then alter planning constraints accordingly. Nevertheless, as this is a patient individual decision, it cannot be reflected in the definition of a common PQS.
For Pinnacle AutoPlanning and Erasmus iCycle gains for PTVs and OARs over all DVH regions were reported [1, 22, 24, 32]. In contrast, for the tested post-operative prostate cases planned with the automatic PSO approach only an superior rectum high-dose sparing was reported, compared to the manual plans. This reflects the conceptual difference of the strategy. The automatic PSO planning was implemented in conjunction with the TPS Hyperion, which provides pareto-optimal plans for all planning problems. To turn a pareto-optimal plan into a clinically favorable plan, competing constraints have to be well balanced and the used constraints need to reflect and probably control the clinical interests. For this study, the constraint types were not changed between manual plans and automatic PSO plans, moreover all plans were generated with TPS Hyperion and are hence considered as pareto-optimal. Therefore a gain for all DVH regions of PTV and OARs in the automatic PSO plan is not to be expected, as this would contradict the pareto-optimality of the manual plan. For the presented approach the superior rectum high-dose sparing comes at the cost of a slightly inferior bladder sparing, but this still adheres to the planning goals defined in the institutional SOP. The rectum dose sparing at the cost of bladder sparing is inherently due to the definition of the PQS, where

more dose-points are allocated to the rectum than to the bladder. This reflects the institutional standard, where rectum dose sparing is considered slightly more important than bladder dose sparing. Other compromises may also have been possible, depending on the implementation of PQS. Yang et al. implemented a similar PSO approach, yet using a different paradigm for the evaluation function. Nevertheless they also showed that if for manual and PSO plans the same constraint types are used, the resulting differences will be small [69]. This supports the assumption that large gains in dose sparing for OARs and PTVs are only reached due to different optimization or changed objective and constraint functions in manual and automatic planning.

For the presented automatic PSO planning approach, it is crucial to have a tool which independently measures the quality of treatment plans, which is needed for an objective comparison of inter- and intra-patient differences. During the manual planning process, planners are normally empirically affected by their experience and they do not have a clearly defined quality measure in mind. Furthermore there is no prompt feedback about plan quality during the trial-and-error process. In contrast, the automatic PSO planning uses the PQS for evaluation and is guided by this throughout the course of optimization. Hence, the definition of the PQS is crucial and needs to be done very carefully. The PQS is defined as treatment intent and treatment site specific class solution, which is referred to as a well-defined standard and should therefore reduce inter-patient variation. This was also shown for the PTV coverage of the presented post-operative prostate cases. Nevertheless, PQS is also able to account for individual patient anatomy, i.e. if a superior OAR sparing is possible without deteriorating PTV dose this compromise would be preferred, due to the increased PQS. The PQS was also customized for the planning goals which are highly related to patient anatomy, such as the volume parameters $V_{40\mathrm{Gy}}$ and $V_{60\mathrm{Gy}}$ for rectum and bladder. A further refinement of the PQS could be the prioritization of OAR structures: this might be even more important for more complex treatments where more different OARs will contribute to the total PQS. At the moment, all individual PQS for the different dose-points of different structures are set to the same maximum value, but in principle it would be possible to set different maximum contributions to the total PQS and thereby prioritize some planning goals over others. Nevertheless, this would not be a strict prioritization as in principle a less prioritized OAR can still outweigh a higher prioritized one, if a significantly better dose-sparing is reached, as PQS increases in this situation. For the presented post-operative prostate cases the PQS is relatively simple, nevertheless it is treatment site and intent specific. Even a PQS for other, more complex

prostate treatments probably needs to integrate additional OARs such as urethra, penile bulb or femoral heads. Currently, the PQS is solely based on DVH parameters, as these are clinically well-known measures of plan quality. But in principle, it should be possible to integrate further characteristics such as machine parameters or complex tumor control probability (TCP) and normal tissue complication probability (NTCP) models in a future implementation.

5 Conclusion

In this work, PSO was for the first time used as automatic treatment planning for RT VMAT treatments. The PSO was successfully implemented and integrated into the TPS Hyperion and used as an automatic VMAT treatment planning approach. The PSO implementation was analyzed concerning the balance of exploration and exploitation and the convergence ability. As intended, the implemented reduction scheme for the inertia weight ω steered the exploration in the beginning and promoted exploitation over the course of PSO. Nevertheless, other reduction schemes for the inertia weight may be worth investigation in the future. The stabilization of the mean constraint value over all particles in subsequent generations in combination with the distance between maximum and minimum constraint value was analyzed and identified as a potential convergence criterion for a future implementation. Concerning this criterion, the principle convergence ability of the PSO was proven. Nevertheless, the three used planning constraints converge in a different time frame and the convergence ability also differs between the cases. Therefore, in a future implementation such a convergence criterion could be used as the termination criterion for the PSO as it would save time for cases converging before the maximum number of generations is reached, whereas for other cases some more iterations of the PSO could have yielded a superior solution. Currently, the optimization time of several days would impede clinical application, but the implementation was not yet optimized for computation time. One straight-forward way would be to calculate all plans within one generation at the same time, i.e. a parallelization of the PSO.

With the implemented automatic PSO planning approach, 10 post-operative prostate cases were automatically planned and showed similar plan quality compared to manually optimized VMAT plans. The PQS was introduced as a measure of plan quality, which is based on well-defined DVH parameters which are widely used in clinical practice to judge plan quality. For 9 out of these 10 post-operative cases overall comparable PTV dosage was reached, whereas rectum is significantly better spared from high doses. This improved rectum sparing was reached by accepting inferior bladder dose sparing, but bladder dose parameters still fulfilled clinical requirements.

This different compromise between rectum and bladder dose is directly reflected by the PQS. In principle other compromises are possible, depending on the definition of the PQS. The PQS should be further refined and should integrate more complex plan quality measures such as normal tissue complication probability (NTCP) and tumor control probability (TCP) models.
Automatic treatment planning using PSO is technically feasible and highly promising for future clinical applications. Nevertheless, the implementation of the PSO and the definition should be further refined to use PSO for clinical RT treatment planning. The transferability to other treatment sites also needs further investigation. Additionally, further planning studies and comparative trials are needed to prove the clinical applicability of this approach.

6 Summary

All RT treatments need to be planned patient individually to ensure the best plan for each patient. For modern VMAT treatments inverse planning, where planning objectives and constraints are used to describe the dose prescribed to the target and the accepted dose burden to the surrounding healthy tissues, is state of the art. But depending on the patient anatomy, the dose burden that needs to be accepted to ensure target coverage with sufficient radiation dose may differ. Therefore, in manual planning different combinations of constraints and objectives need to be tested, which turns planning into a trial-and-error process which is highly related to the planner's experience and also to the available time. In this context automatic, planning gained attention in recent years and already showed its applicability and advantages in clinical practice [1–7]. Nevertheless, automatic approaches introduced thus far normally incorporate differential information to guide an optimization, which is only successful with convex constraint functions. Statistical optimization techniques are promising to overcome this problem, because they explore the search space randomly.

PSO is such a nature-analogous, statistical, iterative and collective optimization technique, which is inspired by the behavior of a swarm of fish or bird. A swarm is formed by particles, which explore a search space randomly. By sharing information regarding the quality of positions visited so far in the search space, each particle iteratively alters its position to approach the global optimum. In this work, an automatic planning approach based on PSO was implemented and successfully tested for post-operative prostate cases. For RT treatment planning, each particle equals a plan, with the position in the search space defined as a vector of planning constraints. PSO is used to manipulate these planning constraints iteratively and was implemented in this doctoral thesis in Python 2.7.3. Attached to the TPS Hyperion for plan generation, an automatic treatment planning approach was realized, analyzed and tested.

In the first part of this work, the implementation was tested by analyzing the exploration and exploitation ability. As intended by the inertia weight ω, the exploration dominates in the beginning and during the course of PSO exploitation is promoted.

Moreover, the convergence ability of the PSO was analyzed by monitoring the stabilization of the mean constraint values over all particles in subsequent generations and the distance between maximum and minimum constraint values. Overall, the implementation of the PSO is suitable for the usage as an RT planning approach. Nevertheless, the implementation should be further refined, especially to promote computation time.

The crucial point for all automatic planning approaches is the fair and reproducible comparison of competing plans. Especially for optimization algorithms, it is important to define what an optimal plan looks like, because this information is used by the algorithms to determine the further search direction. In this study, a plan quality score (PQS) based on well-known DVH parameters was introduced to measure plan quality. The DVH parameters were adapted from the institutional SOP and thereby our PQS reflects the clinical standard. In principle, the PQS rewards the adherence of the DVH criterion and penalizes its violation.

A PQS dedicated to post-operative prostate cases was implemented for this study. Using this PQS, 10 post-operative prostate cases were planned automatically with the implemented PSO and compared to manual plans in the second part of this work. Compared to manual plans, the automatic PSO plans were comparable in over-all plan quality. Nevertheless, PSO plans reached significantly better rectum high dose sparing, while accepting slightly inferior bladder dose sparing. This different compromise reflects the definition of the PQS. Other compromises would also have been possible.

In this work, the applicability of PSO as an automatic planning approach was proven. Nevertheless, as the PQS is defined treatment site and intent specific, the transferability to other prostate treatments and other treatment sites should be investigated in future studies.

7 Zusammenfassung

Strahlentherapeutische Behandlungen werden für jeden Patienten individuell geplant, um den bestmöglichen Plan zu gewährleisten. Moderne VMAT-Behandlungen werden heute standardmäßig invers geplant, dabei werden Planungszielvorgaben und -beschränkungen genutzt, um die Dosis im Zielvolumen und im umliegenden gesunden Gewebe zu charakterisieren. Je nach individueller Patientenanatomie muss unterschiedlich viel Dosis im gesunden Gewebe akzeptiert werden, um die Abdeckung des Tumors mit der benötigten Dosis zu gewährleisten. In der manuellen Planung müssen dafür unterschiedliche Kombinationen von Zielvorgaben und Beschränkungen erprobt werden. Damit hängt der Planungsprozess maßgeblich von der Erfahrung des Planers und der zur Verfügung stehenden Zeit ab. In den letzten Jahren wurden daher verschiedene automatische Planungsansätze vorgeschlagen, für die Anwendbarkeit und Nutzen bereits gezeigt wurden [1–7]. Alle bisher vorgeschlagenen Ansätze nutzen differentielle Informationen als Grundlage für die Optimierung, was ihre Anwendung auf einen Suchraum, der durch konvexe Beschränkungen beschrieben wird, begrenzt. Statistische Optimierungen stellen eine vielversprechende Möglichkeit dar, dieses Problem zu beheben, da sie den Suchraum zufällig erkunden.
Die Partikelschwarmoptimierung (PSO) ist ein solches naturanaloges, statistisches, iteratives und kollektives Optimierungsverfahren, welches sich am Verhalten von Vogelschwärmen oder Fischgruppen orientiert. Ein Schwarm setzt sich dabei aus Individuen, auch Partikel genannt, zusammen, welche den Suchraum zufällig erkunden. Indem die Partikel Informationen über die Güte der von ihnen besuchten Positionen austauschen, verändert jeder Partikel seine Position im Suchraum iterativ und versucht dabei, sich dem globalen Optimum anzunähern. In dieser Arbeit wurde ein automatischer Planungsansatz beruhend auf einer PSO implementiert und erfolgreich für post-operative Prostatakrebsfälle getestet. Für die strahlentherapeutische Planung entspricht dabei jeder Partikel einem Plan, dessen Position im Suchraum durch einen Vektor von Planungsbeschränkungen definiert wird. Die PSO verändert die Beschränkungen iterative. Dies wurde in dieser Doktorarbeit in Python 2.7.3 realisiert. In Verbindung mit dem Bestrahlungsplanungssystem Hyperion, das zur Planberechnung genutzt wurde, konnte ein automatischer Planungsansatz realisiert

und getestet werden.
Im ersten Teil der Arbeit wurde die Implementierung analysiert, dafür wurde die Fähigkeit des Algorithmus untersucht, den gesamten Suchraum zu erforschen und einen kleineren Suchraum genauer zu erkunden. Dies wurde durch die Wahl des Trägheitsgewicht ω umgesetzt. Weiterhin wurde das Konvergenzverhalten untersucht, wofür der mittlere Wert der drei Planungsbeschränkungen zwischen aufeinanderfolgenden Generation und der Abstand zwischen höchster und niedrigster Beschränkung untersucht wurden. Dabei zeigte sich, dass die Implementierung geeignet ist, um als automatischer Bestrahlungsplanungsansatz verwendet zu werden. Dennoch sollte die Implementierung in Zukunft weiter verbessert werden, vor allem in Hinblick auf die Rechenzeit.
Ein wichtiger Punkt für alle automatischen Planungsansätze ist der faire und reproduzierbare Vergleich von zwei konkurrierenden Plänen. Vor allem für Optimierungsalgorithmen ist es wichtig, einen optimalen Plan zu definieren, da diese Information genutzt wird, um die weitere Suchrichtung festzulegen. In dieser Arbeit wurde ein ‚plan quality score' (PQS) eingeführt, der auf bereits bekannten Dosis-Volumen-Histogramm (DVH)-Parametern beruht. Dafür wurden die DVH-Parameter, die in der hausinternen ‚standard operating procedure' (SOP) definiert sind, verwendet. Der PQS spiegelt damit den klinischen Standard wieder. Das Prinzip des PQS beruht darauf, die Einhaltung der DVH-Parameter zu belohnen und deren Verletzung zu bestrafen.
In der Studie wurde ein PQS für post-operative Prostatabestrahlungen implementiert. Dafür wurden 10 Fälle automatisch mit der implementierten PSO geplant und im zweiten Teil der Arbeit mit den manuell erstellten Plänen verglichen. Die manuellen und automatischen PSO-Pläne waren hinsichtlich ihrer allgemeinen Planqualität vergleichbar, aber die PSO-Pläne erreichten eine signifikant bessere Schonung des Rektums im Bereich hoher Dosen. Dafür musste eine etwas schlechtere Schonung der Blase akzeptiert werden. Dieser unterschiedliche Kompromiss zwischen Rektum- und Blasenschonung spiegelt die Definition des PQS wieder, es wären aber auch andere Kompromisse möglich.
Damit wurde in dieser Arbeit die Anwendbarkeit der PSO als automatischer Planungsansatz gezeigt. Da der PQS spezifisch für jede Tumorentität und das Behandlungskonzept definiert werden muss, muss die Übertragbarkeit auf weiter Prostatabestrahlungen und andere Tumorlokalisationen in zukünftigen Studien untersucht werden.

8 Publications related to the dissertation

Parts of the thesis are published in:

peer reviewed articles:
Künzel L.A., Leibfarth S., Dohm O.S., Müller A.-C., Zips D., Thorwarth D.: "Automatic VMAT planning for post-operative prostate cancer cases using particle swarm optimization: A proof of concept study", Physica Medica, Volume 69, January 2020, pp. 101-109, 2020. DOI: 10.1016/j.ejmp.2019.12.007

conference abstracts:
Jahrestagung der Deutschen Gesellschaft für Medizinsche Physik (DGMP) 2018:
Künzel L., Leibfarth S., Dohm O., Thorwarth D.: Automatic radiotherapy planning using particle swarm optimization, oral presentation

Annual Congress of the European SocieTy forRadiotherapy and Oncology (ESTRO) 2019:
Künzel L.A., Leibfarth S., Dohm O.S., Müller A.-C., Zips D., Thorwarth D.: PO-0919 Automatic radiotherapy treatment planning using Particle Swarm Optimization, Poster, Radiotherapy& Oncology, Volume 133 Supplement 1 (2019), Poster

Jahrestagung der Deutschen Gesellschaft für Medizinsche Physik (DGMP) 2019:
Künzel L.A., Leibfarth S., Dohm O.S., Müller A.-C., Zips D., Thorwarth D.: Partikelschwarmoptimierung zur automatische Bestrahlungsplanung, oral presentation

9 References

[1] M. Buschmann, A. W. M. Sharfo, J. Penninkhof, Y. Seppenwoolde, G. Goldner, D. Georg, S. Breedveld, B. J. M. Heijmen, Automated volumetric modulated arc therapy planning for whole pelvic prostate radiotherapy, Strahlentherapie und Onkologie. 194 (2017) pages 333–342, DOI: 10.1007/s00066-017-1246-2.

[2] L. E. Court, K. Kisling, R. McCarroll, L. Zhang, J. Yang, H. Simonds, M. du Toit, C. Trauernicht, H. Burger, J. Parkes, M. Mejia, M. Bojador, P. Balter, D. Branco, A. Steinmann, G. Baltz, S. Gay, B. Anderson, C. Cardenas, A. Jhingran, S. Shaitelman, O. Bogler, K. Schmeller, D. Followill, R. Howell, C. Nelson, C. Peterson, B. Beadle, Radiation Planning Assistant - A Streamlined, Fully Automated Radiotherapy Treatment Planning System, Journal of Visualized Experiments. (134) (2018) e57411–e57411, DOI: 10.3791/57411.

[3] J. Krayenbuehl, M. Zamburlini, S. Ghandour, M. Pachoud, S. Tol, M. Guckenberger, W. Verbakel, Planning comparison of five automated treatment planning solutions for locally advanced head and neck cancer, Radiation Oncology. 13 (170) (2018), DOI: 10.1186/s13014-018-1113-z.

[4] A. W. M. Sharfo, F. Stieler, O. Kupfer, B. J. M. Heijmen, M. L. P. Dirkx, S. Breedveld, F. Wenz, F. Lohr, J. Boda-Heggemann, D. Buergy, Automated VMAT planning for postoperative adjuvant treatment of advanced gastric cancer, Radiation Oncology. 13 (2018), DOI: 10.1186/s13014-018-1032-z.

[5] B. Vanderstraeten, B. Goddeeris, K. Vandecasteele, M. van Eijkeren, C. De Wagter, Y. Lievens, Automated Instead of Manual Treatment Planning? A Plan Comparison Based on Dose-Volume Statistics and Clinical Preference, International Journal of Radiation Oncology Biology Physics. 102 (2) (2018) pages 443–450, DOI: 10.1016/j.ijrobp.2018.05.063.

[6] J. Wang, Z. Chen, W. Li, W. Qian, X. Wang, W. Hu, A new strategy for volumetric-modulated arc therapy planning using AutoPlanning based multi-

criteria optimization for nasopharyngeal carcinoma, Radiation Oncology. 13 (2018) pages 1–10, DOI: 10.1186/s13014-018-1042-x.

[7] L. Rossi, A. Sharfo, S. Aluwini, M. Dirkx, S. Breedveld, B. Heijmen, First fully automated planning solution for robotic radiosurgery – comparison with automatically planned volumetric arc therapy for prostate cancer, Acta Oncologica. 0 (0) (2018) pages 1–9, DOI: 10.1080/0284186X.2018.1479068.

[8] G. N. Hounsfield, Computerized Transverse Axial Scanning (Tomography). 1. Description of System, British Journal of Radiology. 46 (552) (1973) pages 1016–1022, DOI: 10.1259/0007-1285-46-552-1016.

[9] A. Brahme, Optimization of stationary and moving beam radiation therapy techniques, Radiotherapy & Oncology. 12 (2) (1988) pages 129–140, DOI: 10.1016/0167-8140(88)90167-3.

[10] R. E. Drzymala, R. Mohan, L. Brewster, J. Chu, M. Goitein, W. Harms, M. Urie, Dose-volume histograms, International Journal of Radiation Oncology, Biology, Physics. 21 (1) (1991) pages 71–78, DOI: 10.1016/0360-3016(91)90168-4.

[11] T. Bortfeld, Optimized planning using physical objectives and constraints, Seminars in Radiation Oncology. 9 (1) (1999) pages 20–34, DOI: 10.1016/S1053-4296(99)80052-6.

[12] M. Alber, Normal tissue dose-effect models in biological dose optimisation, Zeitschrift für Medizinische Physik. 18 (2) (2008) pages 102–110, DOI: 10.1016/j.zemedi.2007.08.002.

[13] A. Niemierko, Reporting and analyzing dose distributions: A concept of equivalent uniform dose, Medical Physics. 24 (1) (1997) pages 103–110, DOI: 10.1118/1.598063.

[14] A. Niemierko, A generalized Concept of Equivalent Uniform Dose (EUD). 1999, URL: https://www.aapm.org/meetings/99AM/pdf/2682-56794.pdf (visited on 09/27/2019).

[15] C. Thieke, T. Bortfeld, A. Niemierko, S. Nill, From physical dose constraints to equivalent uniform dose constraints in inverse radiotherapy planning, Medical Physics. 30 (9) (2003) pages 2332–2339, DOI: 10.1118/1.1598852.

[16] M. Alber, F. Nüsslin, Ein Konzept zur Optimierung von klinischer IMRT, Zeitschrift für Medizinische Physik. 12 (2) (2002) pages 109–113, DOI: 10.1016/S0939-3889(15)70453-8.

[17] C. Cotrutz, L. Xing, IMRT dose shaping with regionally variable penalty scheme, Medical Physics. 30 (4) (2003) pages 544–551, DOI: 10.1118/1.1556610.

[18] I. Xhaferllari, E. Wong, K. Bzdusek, M. Lock, J. Chen, Automated IMRT planning with regional optimization using planning scripts, Journal of Applied Clinical Medical Physics. 14 (1) (2013) page 4052, DOI: 10.1120/jacmp.v14i1.4052.

[19] D. Gintz, K. Latifi, J. Caudell, B. Nelms, G. Zhang, E. Moros, V. Feygelman, Initial evaluation of automated treatment planning software, Journal of Applied Clinical Medical Physics. 17 (3) (2016) pages 331–346, DOI: 10.1120/jacmp.v17i3.6167.

[20] J. M. A. M. Kusters, K. Bzdusek, P. Kumar, P. G. M. van Kollenburg, M. C. Kunze-Busch, M. Wendling, T. Dijkema, J. H. A. M. Kaanders, Automated IMRT planning in Pinnacle, Strahlentherapie und Onkologie. 193 (12) (2017) pages 1031–1038, DOI: 10.1007/s00066-017-1187-9.

[21] I. Hazell, K. Bzdusek, P. Kumar, C. R. Hansen, A. Bertelsen, J. G. Eriksen, J. Johansen, C. Brink, Automatic planning of head and neck treatment plans, Journal of applied clinical medical physics. 17 (1) (2016) page 5901, DOI: 10.1120/jacmp.v17i1.5901.

[22] C. R. Hansen, A. Bertelsen, I. Hazell, R. Zukauskaite, N. Gyldenkerne, J. Johansen, J. G. Eriksen, C. Brink, Automatic treatment planning improves the clinical quality of head and neck cancer treatment plans, Clinical and Translational Radiation Oncology. 1 (2016) pages 2–8, DOI: 10.1016/j.ctro.2016.08.001.

[23] S. Clemente, C. Oliviero, G. Palma, V. D'Avino, R. Liuzzi, M. Conson, R. Pacelli, L. Cella, Auto- versus human-driven plan in mediastinal Hodgkin lymphoma radiation treatment, Radiation Oncology. 13 (2018) pages 1–10, DOI: 10.1186/s13014-018-1146-3.

[24] K. A. McConnell, T. Marston, B. E. Zehren, A. Lirani, D. N. Stanley, A. Bishop, R. Crownover, T. Eng, Z. Shi, Y. Li, D. Baacke, N. Kirby, K. Rasmussen, N. Papanikolaou, A. N. Gutierrez, Dosimetric evaluation of pinnacle's automated treatment planning software to manually planned treatments, Technology in Cancer Research and Treatment. 17 (2018) pages 1–7, DOI: 10.1177/1533033818780064.

[25] Y. Zhang, T. Li, H. Xiao, W. Ji, M. Guo, Z. Zeng, J. Zhang, A knowledge-based approach to automated planning for hepatocellular carcinoma, Journal of Applied Clinical Medical Physics. 19 (2017) pages 50–59, DOI: 10.1002/acm2.12219.

[26] S. Breedveld, P. R. M. Storchi, M. Keijzer, A. W. Heemink, B. J. M. Heijmen, A novel approach to multi-criteria inverse planning for IMRT. Physics in medicine and biology. 52 (20) (2007) pages 6339–53, DOI: 10.1088/0031-9155/52/20/016.

[27] S. Breedveld, P. R. M. Storchi, P. W. J. Voet, B. J. M. Heijmen, iCycle: Integrated, multicriterial beam angle, and profile optimization for generation of coplanar and noncoplanar IMRT plans. Medical physics. 39 (2) (2012) pages 951–63, DOI: 10.1118/1.3676689.

[28] P. W. J. Voet, S. Breedveld, M. L. P. Dirkx, P. C. Levendag, B. J. M. Heijmen, Integrated multicriterial optimization of beam angles and intensity profiles for coplanar and noncoplanar head and neck IMRT and implications for VMAT. Medical physics. 39 (8) (2012) pages 4858–65, DOI: 10.1118/1.4736803.

[29] P. W. J. Voet, M. L. P. Dirkx, S. Breedveld, D. Fransen, P. C. Levendag, B. J. M. Heijmen, Toward fully automated multicriterial plan generation: A prospective clinical study, International Journal of Radiation Oncology Biology Physics. 85 (3) (2013) pages 866–872, DOI: 10.1016/j.ijrobp.2012.04.015.

[30] P. W. J. Voet, M. L. P. Dirkx, S. Breedveld, B. J. M. Heijmen, Automated generation of IMRT treatment plans for prostate cancer patients with metal hip prostheses: Comparison of different planning strategies, Medical Physics. 40 (7) (2013), DOI: 10.1118/1.4808117.

[31] P. W. J. Voet, M. L. P. Dirkx, S. Breedveld, A. Al-Mamgani, L. Incrocci, B. J. M. Heijmen, Fully automated volumetric modulated arc therapy plan

generation for prostate cancer patients, International Journal of Radiation Oncology Biology Physics. 88 (5) (2014) pages 1175–1179, DOI: 10.1016/j.ijrobp.2013.12.046.

[32] A. W. M. Sharfo, M. L. Dirkx, R. G. Bijman, W. Schillemans, S. Breedveld, S. Aluwini, F. Pos, L. Incrocci, B. J. Heijmen, Late toxicity in the randomized multicenter HYPRO trial for prostate cancer analyzed with automated treatment planning, Radiotherapy and Oncology. 128 (2) (2018) pages 349–356, DOI: 10.1016/j.radonc.2018.05.028.

[33] B. Heijmen, P. Voet, D. Fransen, J. Penninkhof, M. Milder, H. Akhiat, P. Bonomo, M. Casati, D. Georg, G. Goldner, A. Henry, J. Lilley, F. Lohr, L. Marrazzo, S. Palotta, R. Pellegrini, Y. Seppenwoolde, G. Simontacchi, V. Steil, F. Stieler, S. Wilson, S. Breedveld, Fully automated, multi_criterial planning for Volumetric Modulated Arc Therapy - An international multi-center validation for prostate cancer, Radiotherapy and Oncology. 128 (2) (2018) pages 343–348, DOI: https://doi.org/10.1016/j.radonc.2018.06.023.

[34] A. W. M. Sharfo, P. W. Voet, S. Breedveld, J. W. M. Mens, M. S. Hoogeman, B. J. Heijmen, Comparison of VMAT and IMRT strategies for cervical cancer patients using automated planning, Radiotherapy and Oncology. 114 (3) (2015) pages 395–401, DOI: 10.1016/j.radonc.2015.02.006.

[35] A. W. M. Sharfo, S. Breedveld, P. W. Voet, S. T. Heijkoop, J. W. M. Mens, M. S. Hoogeman, B. J. Heijmen, Validation of fully automated VMAT plan generation for library-based plan-of-the-day cervical cancer radiotherapy, PLoS ONE. 11 (12) (2016) pages 1–13, DOI: 10.1371/journal.pone.0169202.

[36] R. van Haveren, S. Breedveld, M. Keijzer, P. Voet, B. Heijmen, W. Ogryczak, Lexicographic extension of the reference point method applied in radiation therapy treatment planning, European Journal of Operational Research. 263 (1) (2017) pages 247–257, DOI: 10.1016/j.ejor.2017.04.062.

[37] R. van Haveren, W. Ogryczak, G. M. Verduijn, M. Keijzer, B. J. M. Heijmen, S. Breedveld, Fast and fuzzy multi-objective radiotherapy treatment plan generation for head and neck cancer patients with the lexicographic reference point method (LRPM), Physics in medicine and biology. 62 (2017), DOI: 10.1088/1361-6560/62/11/4318.

[38] L. Yuan, Y. Ge, W. R. Lee, F. F. Yin, J. P. Kirkpatrick, Q. J. Wu, Quantitative analysis of the factors which affect the interpatient organ-at-risk dose sparing variation in IMRT plans, Medical Physics. 39 (11) (2012) pages 6868–6878, DOI: 10.1118/1.4757927.

[39] L. M. Appenzoller, J. M. Michalski, W. L. Thorstad, S. Mutic, K. L. Moore, Predicting dose-volume histograms for organs-at-risk in IMRT planning, Medical Physics. 39 (12) (2012) pages 7446–7461, DOI: 10.1118/1.4761864.

[40] J. P. Tol, A. R. Delaney, M. Dahele, B. J. Slotman, W. F. A. R. Verbakel, Evaluation of a knowledge-based planning solution for head and neck cancer, International Journal of Radiation Oncology Biology Physics. 91 (3) (2015) pages 612–620, DOI: 10.1016/j.ijrobp.2014.11.014.

[41] A. Fogliata, G. Nicolini, A. Clivio, E. Vanetti, S. Laksar, A. Tozzi, M. Scorsetti, L. Cozzi, A broad scope knowledge based model for optimization of VMAT in esophageal cancer: Validation and assessment of plan quality among different treatment centers, Radiation Oncology. 10 (2015) pages 1–11, DOI: 10.1186/s13014-015-0530-5.

[42] A. T. Chang, A. W. Hung, F. W. Cheung, M. C. Lee, O. S. Chan, H. Philips, Y. T. Cheng, W. T. Ng, Comparison of Planning Quality and Efficiency Between Conventional and Knowledge-based Algorithms in Nasopharyngeal Cancer Patients Using Intensity Modulated Radiation Therapy, International Journal of Radiation Oncology Biology Physics. 95 (3) (2016) pages 981–990, DOI: 10.1016/j.ijrobp.2016.02.017.

[43] C. Schubert, O. Waletzko, C. Weiss, D. Voelzke, S. Toperim, A. Roeser, S. Puccini, M. Piroth, C. Mehrens, J. D. Kueter, K. Hierholz, K. Gerull, A. Fogliata, A. Block, L. Cozzi, Intercenter validation of a knowledge based model for automated planning of volumetric modulated arc therapy for prostate cancer. The experience of the German RapidPlan Consortium, PLoS ONE. 12 (5) (2017) pages 1–13, DOI: 10.1371/journal.pone.0178034.

[44] K. Kubo, H. Monzen, K. Ishii, M. Tamura, R. Kawamorita, I. Sumida, H. Mizuno, Y. Nishimura, Dosimetric comparison of RapidPlan and manually optimized plans in volumetric modulated arc therapy for prostate cancer, Physica Medica. 44 (2017), DOI: 10.1016/j.ejmp.2017.06.026.

[45] A. Fogliata, G. Nicolini, C. Bourgier, A. Clivio, F. De Rose, P. Fenoglietto, F. Lobefalo, P. Mancosu, S. Tomatis, E. Vanetti, M. Scorsetti, L. Cozzi, Performance of a Knowledge-Based Model for Optimization of Volumetric Modulated Arc Therapy Plans for Single and Bilateral Breast Irradiation, PLoS ONE. 10 (12) (2015) pages 1–12, DOI: 10.1371/journal.pone.0145137.

[46] J. Wang, W. Hu, Z. Yang, X. Chen, Z. Wu, X. Yu, X. Guo, S. Lu, K. Li, G. Yu, Is it possible for knowledge-based planning to improve intensity modulated radiation therapy plan quality for planners with different planning experiences in left-sided breast cancer patients?, Radiation Oncology. 12 (2017) pages 1–8, DOI: 10.1186/s13014-017-0822-z.

[47] H. Wu, F. Jiang, H. Yue, S. Li, Y. Zhang, A dosimetric evaluation of knowledge-based VMAT planning with simultaneous integrated boosting for rectal cancer patients, Journal of Applied Clinical Medical Physics. 17 (6) (2016) pages 78–85, DOI: 10.1120/jacmp.v17i6.6410.

[48] G. Yu, Y. Li, Z. Feng, C. Tao, Z. Yu, B. Li, D. Li, Knowledge-based IMRT planning for individual liver cancer patients using a novel specific model, Radiation Oncology. 13 (2018) pages 1–8, DOI: 10.1186/s13014-018-0996-z.

[49] D. L. Craft, T. F. Halabi, H. A. Shih, T. R. Bortfeld, Approximating convex Pareto surfaces in multiobjective radiotherapy planning, Medical Physics. 33 (9) (2006) pages 3399–3407, DOI: 10.1118/1.2335486.

[50] D. Craft, M. Monz, Simultaneous navigation of multiple Pareto surfaces, with an application to multicriteria IMRT planning with multiple beam angle configurations, Medical Physics. 37 (2) (2010) pages 736–741, DOI: 10.1118/1.3292636.

[51] C. McIntosh, T. G. Purdie, Contextual Atlas Regression Forests: Multiple-Atlas-Based Automated Dose Prediction in Radiation Therapy, IEEE Transactions on Medical Imaging. 35 (4) (2016) pages 1000–1012, DOI: 10.1109/TMI.2015.2505188.

[52] C. McIntosh, M. Welch, A. McNiven, D. A. Jaffray, T. G. Purdie, Fully automated treatment planning for head and neck radiotherapy using voxel-based dose prediction and dose mimicking method, Physics in medicine and biology. 62 (15) (2017), DOI: 10.1088/1361-6560/aa71f8.

[53] C. McIntosh, T. G. Purdie, Voxel-based dose prediction with multi-patient atlas selection for automated radiotherapy treatment planning, Physics in Medicine and Biology. 62 (2) (2017), DOI: 10.1088/1361-6560/62/2/415.

[54] E. van der Bijl, Y. Wang, T. Janssen, S. Petit, Predicting patient specific Pareto fronts from patient anatomy only, Radiotherapy and Oncology. 150 (2020) pages 46–50, DOI: 10.1016/j.radonc.2020.05.050.

[55] V. Kearney, J. W. Chan, S. Haaf, M. Descovich, T. D. Solberg, DoseNet: a volumetric dose prediction algorithm using 3D fully-convolutional neural networks, Physics in Medicine & Biology. 63 (23) (2018), DOI: 10.1088/1361-6560/aaef74.

[56] X. Chen, K. Men, Y. Li, J. Yi, J. Dai, A feasibility study on an automated method to generate patient-specific dose distributions for radiotherapy using deep learning, Medical Physics. 46 (1) (2019) pages 56–64, DOI: 10.1002/mp.13262.

[57] J. Fan, J. Wang, Z. Chen, C. Hu, Z. Zhang, W. Hu, Automatic treatment planning based on three-dimensional dose distribution predicted from deep learning technique, Medical Physics. 46 (1) (2019) pages 370–381, DOI: 10.1002/mp.13271.

[58] C. Fiandra, A. Alparone, E. Gallio, C. Vecchi, G. Balestra, S. Bartoncini, S. Rosati, R. Ragona, U. Ricardi, Automated Heuristic Optimization of Prostate VMAT Treatment Planning, International Journal of Medical Physics, Clinical Engineering and Radiation Oncology. 7 (3) (2018) pages 414–425, DOI: 10.4236/ijmpcero.2018.73034.

[59] C. Fiandra, L. Rossi, A. Alparone, S. Zara, C. Vecchi, A. Sardo, S. Bartoncini, G. Loi, C. Pisani, E. Gino, M. Grazia Ruoredda, G. Marco Deotto, P. Tini, S. Comi, D. Zerini, G. Ametrano, V. Borzillo, L. Strigari, S. Strolin, A. Savini, A. Romeo, S. Reccanello, I. Abu Rumeileh, N. Ciscognetti, F. Guerrisi, G. Balestra, U. Ricardi, B. Heijmen, Automatic genetic planning for Volumetric Modulated Arc Therapy: a large multi-centre validation for prostate cancer, Radiotherapy and Oncology. 148 (2020) pages 126–132, DOI: 10.1016/j.radonc.2020.04.020.

[60] Y. Li, D. Yao, J. Yao, W. Chen, A particle swarm optimization algorithm for beam angle selection in intensity-modulated radiotherapy planning, Physics in

Medicine and Biology. 50 (15) (2005) pages 3491–3514, DOI: 10.1088/0031-9155/50/15/002.

[61] A. Modiri, X. Gu, A. Hagan, A. Sawant, Improved Swarm Intelligence Solution in Large Scale Radiation Therapy Inversie Planning, in: *2015 IEEE Great Lakes Biomedical Conference (GLBC), Milwaukee, WI.* 2015 pages 1–4, DOI: 10.1109/GLBC.2015.7158300.

[62] A. Modiri, X. Gu, A. Hagan, R. Bland, P. Iyengar, R. Timmerman, A. Sawant, Inverse 4D conformal planning for lung SBRT using particle swarm optimization, Physics in medicine and biology. 61 (10) (2016), DOI: 10.1088/0031-9155/61/16/6181.

[63] A. Modiri, X. Gu, A. M. Hagan, A. Sawant, Radiotherapy Planning Using an Improved Search Strategy in Particle Swarm Optimization, IEEE Transactions on Biomedical Engineering. 64 (5) (2017) pages 980–989, DOI: 10.1109/TBME.2016.2585114.

[64] D. Riofrio, S. Luan, J. Zhou, L. Ma, Particle swarm optimization for radiation therapy planning, BCB 2015 - 6th ACM Conference on Bioinformatics, Computational Biology, and Health Informatics. (2015) pages 250–257, DOI: 10.1145/2808719.2808745.

[65] W. Wisittipanich, P. Hengmeechai, Truck scheduling in multi-door cross docking terminal by modified particle swarm optimization, Computers and Industrial Engineering. 113 (2017) pages 793–802, DOI: 10.1016/j.cie.2017.01.004.

[66] P. N. Kechagiopoulos, G. N. Beligiannis, Solving the Urban Transit Routing Problem using a particle swarm optimization based algorithm, Applied Soft Computing Journal. 21 (2014), DOI: 10.1016/j.asoc.2014.04.005.

[67] M. Goodarzi, A. Fakharzadeh J., Shape and size determination of plasmonic nano particles using particle swarm optimization algorithm based absorption coefficient, Optik. 130 (2017) pages 44–49, DOI: 10.1016/j.ijleo.2016.11.041.

[68] C. H. Lee, K. S. Shih, C. C. Hsu, T. Cho, Simulation-based particle swarm optimization and mechanical validation of screw position and number for the fixation stability of a femoral locking compression plate, Medical Engineering

and Physics. 36 (1) (2014) pages 57–64, DOI: 10.1016/j.medengphy.2013.09.005.

[69] J. Yang, P. Zhang, L. Zhang, H. Shu, B. Li, Z. Gui, Particle swarm optimizer for weighting factor selection in intensity-modulated radiation therapy optimization algorithms, Physica Medica. 33 (2017) pages 136–145, DOI: 10.1016/j.ejmp.2016.12.021.

[70] L. A. Künzel, S. Leibfarth, O. S. Dohm, A.-C. Müller, D. Zips, D. Thorwarth, Automatic VMAT planning for post-operative prostate cancer cases using particle swarm optimization : A proof of concept study, Physica Medica. 69 (2020) pages 101–109, DOI: 10.1016/j.ejmp.2019.12.007.

[71] J. Kennedy, R. Eberhart, Particle swarm optimization, Neural Networks, 1995. Proceedings., IEEE International Conference on. 4 (1995) 1942–1948 vol.4, DOI: 10.1109/ICNN.1995.488968.

[72] Y. Shi, R. Eberhart, A Modified Particle Swarm Optimizer, Proceedings of the 1998 IEEE International Conference on Evolutionary Computation. IEEE World Congress on Computational Intelligence. (1998) pages 69–73, DOI: 10.1109/ICEC.1998.699146.

[73] Y. Shi, R. Eberhart, Empirical study of particle swarm optimization, Proceedings of the 1999 Congress on Evolutionary Computation. (1999) pages 1945–1950, DOI: 10.1109/CEC.1999.785511.

[74] J. C. Bansal, P. K. Singh, M. Saraswat, A. Verma, S. S. Jadon, A. Abraham, Inertia Weight Strategies in Particle Swarm Inertia Weight Strategies in Particle Swarm, in: *Third World Congress on Nature and Biologically Inspired Computing*. 2011 pages 633–640, DOI: 10.1109/NaBIC.2011.6089659.

[75] A. Nickabadi, M. M. Ebadzadeh, R. Safabakhsh, A novel particle swarm optimization algorithm with adaptive inertia weight, Applied Soft Computing Journal. 11 (4) (2011) pages 3658–3670, DOI: 10.1016/j.asoc.2011.01.037.

[76] M. Alber, R. Reemtsen, Intensity modulated radiotherapy treatment planning by use of a barrier-penalty multiplier method, Optimization Methods and Software. 22 (3) (2007) pages 391–411, DOI: 10.1080/10556780600604940.

[77] ICRU, Report 62: Prescribing, Recording and Reporting Photon Beam Therapy (Supplement to ICRU Report 50), Journal of the ICRU. 32 (1) (1999).

[78] ICRU, Report 83: Prescribing, Recording, and Reporting Photon-Beam Intensity-Modulated Radiation Therapy (IMRT), Journal of the ICRU. 10 (1) (2010).

[79] A. W. Pederson, J. Fricano, D. Correa, C. A. Pelizzari, S. L. Liauw, Late toxicity after intensity-modulated radiation therapy for localized prostate cancer: An exploration of dose-volume histogram parameters to limit genitourinary and gastrointestinal toxicity, International Journal of Radiation Oncology Biology Physics. 82 (1) (2012) pages 235–241, DOI: 10.1016/j.ijrobp.2010.09.058.

[80] S. L. Gulliford, K. Foo, R. C. Morgan, E. G. Aird, A. M. Bidmead, H. Critchley, P. M. Evans, S. Gianolini, W. P. Mayles, A. R. Moore, B. Sánchez-Nieto, M. Partridge, M. R. Sydes, S. Webb, D. P. Dearnaley, Dose-Volume Constraints to Reduce Rectal Side Effects From Prostate Radiotherapy: Evidence From MRC RT01 Trial ISRCTN 47772397, International Journal of Radiation Oncology Biology Physics. 76 (3) (2010) pages 747–754, DOI: 10.1016/j.ijrobp.2009.02.025.

[81] A. N. Viswanathan, E. D. Yorke, L. B. Marks, P. J. Eifel, W. U. Shipley, Radiation Dose-Volume Effects of the Urinary Bladder, International Journal of Radiation Oncology Biology Physics. 76 (3, Suppl.) (2010) pages 116–122, DOI: 10.1016/j.ijrobp.2009.02.090.

[82] R Core Team (2018), R: A language and Enviorment for Statistical Computing (), URL: hhtps://www.R-project.org/.

10 Statement on own contribution

I conducted the thesis in the section for Biomedical Physics at the Universityhospital for Radiationoncology Tübingen under supervision of Prof. Dr. rer. nat. Daniela Thorwarth.
The study was planned in collaboration with Prof. Dr. rer. nat. Daniela Thorwarth und Dr. rer. nat. Oliver Dohm.
Prof. Dr. med. Daniel Zips and PD Dr. Arndt-Christian Müller gave advise about medical issues and evaluated the generated treatment plans.
Dr. rer. nat. Sara Leibfarth supported me by discussing details about the implementation of the particle swarm optimization (PSO) in Python 2.7.3.
Parts of this thesis are published as conference abstracts and as a peer-reviewed paper, c.f. 8. All related manuscripts were written by me with supervision of Prof. Dr. rer. nat. Daniela Thorwarth and Dr. rer. nat. Sara Leibfarth. All other aforementioned persons are also co-authors of the publications and provided critical proofreading of the manuscripts.
The implementation of the PSO and the development of the plan quality score (PQS) was done by me. All used CT data and manual plans were taken from the clinical database. All analysis to evaluate the quality of the implementation and the detailed comparison of manual and PSO plans were conduced by me. The statistical analysis of the results was done by me.

Acknowledgments

Thank you to everyone who believed in me and this project, especially when I did not!

I want to express my gratitude to Prof. Daniela Thorwarth for here supervision and guidance thorough this demanding process. You accepted me as a doctoral candidate and with your help, enthusiasm and encouragement this project turned out as success. I also want to thank Prof. Zips for the opportunity to conduct this project at the Department for Radiation Oncology, University Hospital Tübingen and for his support to this project. Thanks are also due to Dr. Oliver Dohm for his support about computer problems and Prof. Arndt-Christian Müller for advising medical issues. I also owe a big thank you to Bettina Frey for sharing her knowledge about planning in Hyperion with me.
Stefan Pojtinger and Sara Leibfahrt introduced my to Particle Swam Optimization in one of our coffee breaks. It was totally in the right moment and right before I was giving up my doctoral project after a frustrating first year. I also want to thank all other former and present members of the research group: René, Jasmin, Marcel, Sebastian, Linda, Jairo, Pamela and David. Thank you for listening during lab meetings, for hilarious coffee and tea breaks and shared conferences.
Finally I owe a very special thank you to my cousin Eleni Dellas for accepting the challenge of proof reading this thesis.

This project received funding by Medical Faculty of the University Tübingen Fortüne Grant No. 2414-0-0.

Appendices

A Scripts

A.1 bash-script

A bash script called 'steuerung.sh' monitored the PSO and the interaction with the TPS Hyperion.

```
#!/bin/bash
###at the moment the number of constraints is fixed tp 3!

patient_name='...'
path='/....'
n_part=30  #number of particles
part_nr=0     #variable for counting active particle
i=0  #var for counting trials
i_max=30  #maximum number of trials
nr_const=3    #number of constraints

cd /home/hyperion/hyperion      #go to hyperion path

initialize particles
j=0
while [ "$j" -lt "$n_part" ]
    do
    if python /...initialize.py $path $patient_name $j $nr_const; then
        echo "initialize: sucess"
    else
        echo "initialize: failure"
        exit 1
    fi

    j=$(( $j + 1 ))
    done

#iterations
while [ "$i" -lt "$i_max" ]
    do
    #optimize with hyperion per particle
    part_nr=0
    while [ "$part_nr" -lt "$n_part" ]
        do
#         #check if the same plan was already calculated
#         if python /...check_existence.py $patient_name $path $part_nr $i; then
#             echo "existence: sucess"
#         else
#             echo "existence: failure"
#             exit 1
#         fi

        if [ "$i" -lt 10 ]
        then
            trial="${path}${patient_name}_${part_nr}/trial_00${i}"
        else
            trial="${path}${patient_name}_${part_nr}/trial_0${i}"
        fi

        if [ -d "$trial" ]
        then
            echo "true"
            #call get_pbest.py
            if python /...get_pbest.py $patient_name $path $part_nr $i $nr_const; then
                echo "get_pbest: sucess"
            else
                echo "get_pbest: failure"
                exit 1
            fi

        else
            #call hyperion
            hyp_path="${path}${patient_name}_${part_nr}/${patient_name}"
            export DISPLAY=:0 && timeout -k 20 1d /home/hyperion/hyperion/hyperion_LK $hyp_path

            #call scoring.py
            if python /...scoring.py $patient_name $path $part_nr $i; then
```

```
                echo "scoring: sucess"
            else
                echo "scoring: failure"
                exit 1
            fi

            #call get_pbest.py
            if python /...get_pbest.py $patient_name $path $part_nr $i $nr_const; then
                echo "get_pbest: sucess"
            else
                echo "get_pbest: failure"
                exit 1
            fi

#             #call evaluation.py
#             if python /...evaluation.py $patient_name $path $i $part_nr; then
#                 echo "evaluation: sucess"
#             else
#                 echo "evaluation: failure"
#                 exit 1
#             fi
        fi

        part_nr=$(( $part_nr + 1 ))
        done

    #call get_gbest.py
    if python /...get_gbest.py $patient_name $path $n_part $nr_const; then
        echo "get_gbest: sucess"
    else
        echo "get_gbest: failure"
        exit 1
    fi

    #call update_velo.py
    if python /...update_velo.py $patient_name $path $n_part $nr_const $i; then
        echo "update_velo: sucess"
    else
        echo "update_velo: failure"
        exit 1
    fi

    i=$(( $i +1 ))
    done
```

A.2 initialize.py

```
#!/usr/bin/env python
# coding: utf8
import os, sys, fileinput, os.path
from random import *
#initiliaze particles

path = str(sys.argv[1])
patient_name = str(sys.argv[2])
part_nr = int(sys.argv[3])
nr_const = int(sys.argv[4])


l_limit = [53.63,40.85,48.95]       #patient individual
u_limit = [63.63,50.85,58.95]
const = [0.0,0.0,0.0]
velos = [0.0,0.0,0.0]

particle_path = '%s%s_%i.txt' %(path,patient_name,part_nr)
with open(particle_path, 'a') as particle:
    particle.write('\n')
    i=0
    while i < nr_const:
        x = randint(int((l_limit[i])*100),int((u_limit[i])*100))
        #print(x)
        x = x/100.0
        v = random()
        p = random()
        if p < 0.5:
            v = v * -1.0
        particle.write('%.2f,%.2f,' %(x,v))
        const[i] = x
        velos[i] = v
        i+=1

CLN = os.path.join(path, '%s_%i/' %(patient_name,part_nr), '%s.CLN' %patient_name)

with open(CLN,  'r') as f:
        lineList = f.readlines()
        j=0
        while j < len(lineList):
            if 'isoconstraint' and 'var1' in lineList[j]:
                lineList[j] = lineList[j].replace('isoconstraint=var1', 'isoconstraint=%.2f' %const[0])
            elif 'isoconstraint' and 'var2' in lineList[j]:
                lineList[j] = lineList[j].replace('isoconstraint=var2', 'isoconstraint=%.2f' %const[1])
            elif 'isoconstraint' and 'var3' in lineList[j]:
                lineList[j] = lineList[j].replace('isoconstraint=var3', 'isoconstraint=%.2f' %const[2])
            j+=1

with open(CLN, 'w') as f:
    j=0
    while j < len(lineList):
        f.write('%s' %lineList[j])
        j+=1
```

A.3 scoring.py

```
#!/usr/bin/env python
# coding: utf8

###at the moment scoring only acepts EUD for PTV!!!!###

import os, sys, fileinput

def partition():
    return head,sep,tail

patient_name = str(sys.argv[1])
path = str(sys.argv[2])
part_nr = int(sys.argv[3])
history = int(sys.argv[4])

myfile2 = "%scombination.txt" %path

if history < 10:
    CLN = os.path.join(path,'%s_%i/' %(patient_name,part_nr),'trial_00%i/' %history, '%s.CLN'
    %patient_name)
    saved_path = os.path.join(path,'%s_%i' %(patient_name,part_nr),'trial_00%i/' %history)
else:
    CLN = os.path.join(path,'%s_%i/' %(patient_name,part_nr),'trial_0%i/' %history, '%s.CLN'
    %patient_name)
    saved_path = os.path.join(path,'%s_%i' %(patient_name,part_nr),'trial_0%i/' %history)

OAR = ['PTV66','PTV66','PTV66','Rektum','Rektum','Rektum','Blase','Blase']      #names must be
identical to structure set
typ = ['EUD','D,98','D,2','D,2','V,40','V,60','D,2','V,60']
limit = [65.00,63.7,70.6,66.0,80.0,40.0,66.0,50.00]         #patient individual
bend = [66.00,63.7,70.6,66.0,57.07,29.23,66.0,37.54]
vector=[]

i=0
while i < len(OAR):
    if typ[i] == 'EUD':
        mytest = open(CLN, "r")
        data = mytest.read()            #read data from CLN of last trial
        for text in data.split('\n\n'):         #getting names, types, weight, and isoeffects of all
        constraints
            if 'PTV' in text:
                for text2 in text.split('!END'):
                    if 'prescription' in text2:
                        for line in text2.split('\n'):
                            if 'isoeffect' in line:
                                head,sep,tail = line.partition('=')
                                vector.append(float(tail))
        mytest.close()    #close CLN

    else:
        myfile = os.path.join(saved_path, '%s_%s.dvh' %(patient_name,OAR[i]))
        data1 = open(myfile,'r')
        data2 = data1.read()
        data1.close()
  #definition von variablen

        pt,sep,tail = typ[i].partition(',')
        if pt == 'V':
            d = float(tail)
        else:
            volume = float(tail)

        dbigger = 100
        dsmaler = 0
        vbigger = 100
        vsmaler = 0
```

```
        for x in data2.split('\n'):

            if x and not x.isspace():
                head,sep,tail = x.partition(' ')
                dose = float(head)
                head,sep,tail = tail.partition(' ')
                vol = float(tail)
                if pt == 'V':
                    if dose > d and dose < dbigger:
                        vbigger = vol
                        dbigger = dose
                    elif dose < d and dose > dsmaler:
                        vsmaler = vol
                        dsmaler = dose
                else:
                    if vol > volume and vol <= vbigger:
                        vbigger = vol
                        dbigger = dose
                    elif vol < volume and vol >= vsmaler:
                        vsmaler = vol
                        dsmaler = dose

        if pt == 'V':
            a = (vbigger-vsmaler)/(dbigger-dsmaler)
            b = vsmaler-a*dsmaler
            v = d*a+b
            vector.append(v)
        else:
            a = (vbigger-vsmaler)/(dbigger-dsmaler)
            b = vsmaler-a*dsmaler
            dose = (volume-b)/a
            vector.append(dose)
    i+=1

actual_score = []
i=0
while i < len(OAR):
    if OAR[i] == OAR[1]:
        if typ[i] == 'EUD':
            if vector[i] < limit[i]:
                a=(0.0-(-1.0))/(limit[i] - 0.99*limit[i])
                b=-1.0-a*0.99*limit[i]
                actual_score.append(a*vector[i]+b)
            if (vector[i] >= limit[i] and vector[i] < bend[i]):
                a=(0.1-0.0)/(bend[i]-limit[i])
                b=0-a*limit[i]
                actual_score.append(a*vector[i]+b)
            if vector[i] >= bend[i]:
                actual_score.append(0.1)

        if typ[i] == 'D,98':
            if vector[i] < limit[i]:
                a=(0.0-(-1.0))/(limit[i]-limit[i]*0.99)
                b=-1.0-a*limit[i]*0.99
                actual_score.append(a*vector[i]+b)
            if vector[i] >= limit[i]:
                actual_score.append(0.0)

        if typ[i] == 'D,2':
            if vector[i] <= limit[i]:
                actual_score.append(0.0)
            if vector[i] > limit[i]:
                a=(-1.0-0.0)/(1.01*limit[i]-limit[i])
                b=0.0-a*limit[i]
                actual_score.append(a*vector[i]+b)

    else:
```

```
        if limit[i] == bend[i]:
            if vector[i] <= 0.9*limit[i]:
                actual_score.append(1.0)
            if (vector[i] > 0.9*limit[i] and vector[i] < limit[i]):
                a=(0.0-1.0)/(limit[i]-0.9*limit[i])
                b=1.0-a*0.9*limit[i]
                actual_score.append(a*vector[i]+b)
            if vector[i] >= limit[i]:
                a=(-1.0-0.0)/(1.01*limit[i]-limit[i])
                b=0.0-a*limit[i]
                actual_score.append(a*vector[i]+b)
        else:
            if vector[i] <= 0.9*bend[i]:
                actual_score.append(1.0)
            if (vector[i] > 0.9*bend[i] and vector[i] <= bend[i]):
                a=(0.0-1.0)/(bend[i]-0.9*bend[i])
                b=1.0-a*0.9*bend[i]
                actual_score.append(a*vector[i]+b)
            if (vector[i] > bend[i] and vector[i] <= limit[i]):
                a=(-0.1-0.0)/(limit[i]-bend[i])
                b=0.0-a*bend[i]
                actual_score.append(a*vector[i]+b)
            if vector[i] > limit[i]:
                a=(-1.0-(-0.1))/(1.01*limit[i]-limit[i])
                b=-0.1-a*limit[i]
                actual_score.append(a*vector[i]+b)
    i+=1

score = 0.0
if (actual_score[0] >= 0.0 and actual_score[1] >= 0.0 and actual_score[2] >= 0.0 and actual_score[3] >=
0.0 and actual_score[4] >= 0.0 and actual_score[5]>= 0.0):
    score = score + 5.0

if (actual_score[0] >= 0.0 and actual_score[1] >= 0.0 and actual_score[2] >= 0.0 and actual_score[6] >=
0.0 and actual_score[7] >= 0.0):
    score = score+5.0

results_score = os.path.join(path,'%s_%i_score.txt' %(patient_name,part_nr))
i=0
with open(results_score,'a') as f:
    f.write('\n')
    while i < len(OAR):
        f.write('%.4f,' %actual_score[i])
        score = score+actual_score[i]
        i+=1
    f.write('%.4f,' %score)

with open(myfile2, 'a') as f:           #add score to combination fileinpu
    f.write('%.4f,' %score)

results = os.path.join(path, '%s_%i.txt' %(patient_name,part_nr))
with open(results,'a') as f:
    f.write('%.4f,' %score)
```

A.4 get_pbest.py

```
#!/usr/bin/env python
# coding: utf8

import os, sys, fileinput

def partition():
    return head,sep,tail

patient_name = str(sys.argv[1])
path = str(sys.argv[2])
part_nr = int(sys.argv[3])
history = int(sys.argv[4])
nr_const = int(sys.argv[5])


OAR = []
typ = []
exponent = []
p = []
pbest = []
v = []

data = os.path.join(path, '%s_%i.txt' %(patient_name,part_nr))

with open(data,'r') as f:
    lineList=f.readlines()
    lastLine = lineList[len(lineList)-1]
    head,sep,tail = lastLine.partition(',')
    p.append(float(head))
    head,sep,tail = tail.partition(',')
    v.append(float(head))
    i=0
    while i < (nr_const-1):
        head,sep,tail = tail.partition(',')
        p.append(float(head))
        head,sep,tail = tail.partition(',')
        v.append(float(head))
        i+=1
    head,sep,tail = tail.partition(',')
    fitness = float(head)

    line = lineList[len(lineList)-2]
    head,sep,tail = line.partition(',')
    head,sep,tail = tail.partition(',')
    i=0
    while i < (nr_const-1):
        head,sep,tail = tail.partition(',')
        head,sep,tail = tail.partition(',')
        i+=1
    head,sep,tail = tail.partition(',')
    head,sep,tail = tail.partition(',')
    b_fitness = float(head)
    i=0
    while i < nr_const:
        head,sep,tail = tail.partition(',')
        pbest.append(float(head))
        i+=1


if fitness > b_fitness:

    b_fitness = fitness
    i=0
    while i < nr_const:
        pbest[i] = p[i]
        i+=1
```

```
if history == 0:                #after initilization the fitness should be set as best_fitness, to
prevent, that for negative scores 0 is set as best_score
    b_fitness = fitness
    i=0
    while i < nr_const:
        pbest[i] = p[i]
        i+=1

with open(data, 'a') as f:
    f.write('%.4f,' %b_fitness)
    i=0
    while i < nr_const:
        f.write('%.2f,' %pbest[i])
        i+=1
```

A.5 get_gbest.py

```
#!/usr/bin/env python
# coding: utf8
import os, sys, fileinput, os.path

def partition():
    return head,sep,tail

patient_name = str(sys.argv[1])
path = str(sys.argv[2])
n_part = int(sys.argv[3])
nr_const = int(sys.argv[4])

b_fitness = []
pbest = []

i=0
while i < n_part:
    with open('%s/%s_%i.txt' %(path,patient_name,i), 'r') as f:
        lineList = f.readlines()
        lastLine = lineList[len(lineList)-1]
        head,sep,tail = lastLine.partition(',')     #p1
        head,sep,tail = tail.partition(',')         #v1
        j=0
        while j < (nr_const-1):
            head,sep,tail = tail.partition(',')         #p2
            head,sep,tail = tail.partition(',')         #v2
            j+=1
        head,sep,tail = tail.partition(',')         #fitness
        head,sep,tail = tail.partition(',')         #b_fitness
        #print(tail)
        b_fitness.append(float(head))
        j=0
        while j < nr_const:
            head,sep,tail = tail.partition(',')         #pbest1
            pbest.append(head)
            j+=1
    i+=1

best = b_fitness.index(max(b_fitness))

with open('%sg_best.txt' %path, 'w') as f:
    f.write('%.4f,' %(b_fitness[best]))
    i=(best*nr_const)
    while i < ((best*nr_const)+nr_const):
        f.write('%s,' %pbest[i])
        i+=1
```

A.6 update_velo.py

```
#!/usr/bin/env python
# coding: utf8
import os, sys, fileinput, os.path
from random import *

def partition():
    return head,sep,tail

patient_name = str(sys.argv[1])
path = str(sys.argv[2])
n_part = int(sys.argv[3])
nr_const = int(sys.argv[4])
history = int(sys.argv[5])

#patient_name = 'PC02'
#path = '/IMRT_RESEARCH/Luise/autoplanning_data/PSO_scoring4/PC02_2/'
#nr_const = 3
#n_part = 30
#history = 0

if history <10:
    w=1.4
elif history >=10 and history <20:
    w=1.0
elif history >=20 and history <30:
    w=0.8
elif history >=30 and history <40:
    w=0.6
elif history >=40 and history <50:
    w=0.4
elif history >=50 and history <100:
    w=0.2

#print(w)

gbest = []

data_gbest = os.path.join(path, 'g_best.txt')

OAR = []
typ = []
exponent = []

constraints = os.path.join(path,'constraints.txt')
with open(constraints,'r') as f:
    LineList = f.readlines()
    i=0
    while i < len(LineList):
        line = LineList[i]
        head,sep,tail = line.partition(',')
        OAR.append(head)
        head,sep,tail = tail.partition(',')
        typ.append(head)
        exponent.append(tail.strip())
        i+=1

with open(data_gbest, 'r') as f:
    lineList = f.readlines()
    lastLine = lineList[len(lineList)-1]
    head,sep,tail = lastLine.partition(',')
    i=0
    while i < nr_const:
        head,sep,tail = tail.partition(',')
        gbest.append(head)
        i+=1

i=0
```

```
while i < n_part:
    const = []
    v = []
    pbest = []
    v_new = []
    v1_new = []
    v2_new = []
    v3_new = []
    const_new = []

    ###get v,pbest and present from particel file
    data = os.path.join(path, '%s_%i.txt' %(patient_name,i))
    data1 = os.path.join(path, 'velos_%i.txt' %(i))
    with open(data, 'r') as f:
        lineList = f.readlines()
        lastLine = lineList[len(lineList)-1]
        head,sep,tail = lastLine.partition(',')
        const.append(head)
        head,sep,tail = tail.partition(',')
        v.append(head)
        j=0
        while j < (nr_const-1):
            head,sep,tail = tail.partition(',')
            const.append(head)
            head,sep,tail = tail.partition(',')
            v.append(head)
            j+=1

        present,sep,tail = tail.partition(',')
        b_fitness,sep,tail = tail.partition(',')
        j=0
        while j < nr_const:
            head,sep,tail = tail.partition(',')
            pbest.append(head)
            j+=1

    #print(const)
    #print(v)
    #print(pbest)
    #print(gbest)

    j=0
    while j < nr_const:
        velo1 = float(v[j])*w
        velo2 = 2.0*random( ) * (float(pbest[j])-float(const[j]))
        velo3 = 2.0*random( ) * (float(gbest[j])-float(const[j]))
        velo = velo1 + velo2 + velo3
        v1_new.append(velo1)
        v2_new.append(velo2)
        v3_new.append(velo3)
        #velo = 2.0*random( ) * (float(pbest[j])-float(const[j])) + 2.0*random( ) * (float(gbest[j])-
float(const[j]))
        v_new.append(velo)
        new = float(const[j]) + v_new[j]
        if new < 10.0:
            const_new.append(10.00)
        elif new > 66.0:
            const_new.append(66.00)
        else:
            const_new.append(new)
        j+=1


    #print(v_new)
    #print(const_new)
    with open(data, 'a') as f:
        f.write('\n')
```

```
    j=0
    while j < nr_const:
        f.write('%.2f,%.2f,' %(const_new[j],v_new[j]))
        j+=1

with open(data1, 'a') as f:
    f.write('\n')
    j=0
    while j < nr_const:
        f.write('%.2f,%.2f,%.2f,%.2f,' %(v1_new[j],v2_new[j],v3_new[j],v_new[j]))
        j+=1

CLN = os.path.join(path, '%s_%i/' %(patient_name,i), '%s.CLN' %patient_name)

with open(CLN,  'r') as f:
    CLN_data = f.read()        #reading data from original CLN
    for text in CLN_data.split('\n\n'):
        j=0
        while j < nr_const:
            if OAR[j] in text:
                for text2 in text.split('!END'):
                    if typ[j] in text2:
                        if 'COSTFUNCTION' and 'exponent=%s' %exponent[j] in text2:
                            head,sep,tail = text2.partition('!COSTFUNCTION')
                            if exponent[j] in tail:
                                for line in tail.split('\n'):
                                    if 'isoconstraint' in line:
                                        head1,sep1,tail1 = line.partition('=')
                                        new = line.replace(tail1,'%.2f' %const_new[j])
                                        new = tail.replace(line,new)
                                        #print(new)
                                        new = text.replace(tail,new)
                                        #print('new: %s' %text)
                                        CLN_data = CLN_data.replace(text,new)
                                        text=new
            j+=1

#print(CLN_data)
with open(CLN, 'w') as f:
    f.write(CLN_data)

i+=1
```